

Identifying tidal divides, tidal subbasins
and tidal prisms in an exploratory model
of multi-inlet tidal systems

Master Thesis

L.C. Bogers

23-08-2019

Master Thesis in MSc Water Engineering and Management,
track River and Coastal Engineering
Faculty of Engineering Technology
University of Twente

Author: L.C. (Lisa) Bogers
Student number: S1889060

Graduation committee: Prof. dr. S.J.M.H. Hulscher
Dr. ir. P.C. Roos
Ir. K.R.G. Reef

Preface

This report is the final product of my master thesis for the MSc Civil Engineering and Management at the University of Twente, where I conducted my research at the Water Engineering and Management (WEM) department under the supervision of Prof. Dr. S.J.M.H. Hulscher, Dr. Ir. P.C. Roos and Ir. K.R.G. Reef.

Being a “mathematician” myself (I have a BSc in Mathematics), I very much appreciated the enthusiasm that Pieter Roos conveyed while teaching the course Mathematical Physics of Water Systems in the master programme. When the opportunity arose to execute the research of my master thesis in his field of work, I could not let it pass by. Now that it is (almost) finished, I can confirm that I have very much enjoyed studying this topic and I have certainly been challenged mathematically.

I would like to thank my supervisors, with in particular my daily supervisor Koen Reef for his explanations, weekly support and intermediate revisions of my work. Furthermore, I would like to thank my parents, brother and sister for their support during the entire process and especially my sister for taking some much-needed breaks with me during the long days of research and writing at the university. I would also like to thank my project teammates from the course Building with Nature; Marijn, Shawnee and Marsha, who were very cooperative in planning our project work alongside my thesis.

This work marks the end of my time as a student at the University of Twente. I have very much enjoyed the courses that I have followed during these two years and therefore I would like to express my sincere appreciation to all the staff involved in the master programme of Water Engineering and Management and in particular the track River and Coastal Engineering.

Finally, I just want to say that I hope you enjoy reading this report as much as I enjoyed writing it.

Abstract

Multi-inlet tidal systems typically consist of several barrier islands, separated by tidal inlets that connect a back-barrier basin to a sea or ocean. Hydraulic tidal divides, forming the boundaries between tidal subbasins corresponding to the inlets, can be identified based on the flow patterns in the back-barrier basin. In this study, these tidal divides are identified in the exploratory model by Roos et al. (2013). Furthermore, the model results are compared to the empirical O'Brien-Jarrett Law, which relates tidal prisms to the cross-sectional area of inlets, and a sensitivity analysis is performed with respect to the ocean conditions. From this, a relation between the tidal subbasin area and the cross-sectional area of an inlet is derived.

The model combines Escoffier's stability concept for tidal inlets with a hydrodynamic model. The evolution and stability of each tidal inlet depends on the balance between waves, transporting sediment into the inlet, and tidal currents, transporting sediment out of the inlets. Two possible methods of identifying tidal divides in the model by Roos et al. (2013) are compared. It is concluded that a method based on identifying lines of minimum flow velocity amplitude in the basin gives accurate results and can be used to divide the back-barrier basin into tidal subbasins for each open inlet, whereas the results of a method based on large phase differences in alongshore flow velocity amplitude cannot be used to calculate these tidal subbasin areas directly.

The tidal prism is defined as the water volume entering a tidal (sub)basin during a characteristic tidal cycle. It is approximated by multiplying the tidal range with the tidal (sub)basin area. The actual tidal prism resulting from the model is calculated by integrating the flow discharge through the inlet over half a tidal cycle. The result is a linear relationship between the tidal prism P and the inlet area Ω in the model. Comparing this to the empirical tidal prism - inlet area relationship of the form $\Omega = kP^\alpha$ called the O'Brien-Jarrett Law, the coefficient α is always equal to 1 when the system is in equilibrium and k only depends on the tidal frequency and the flow velocities in the inlets. From the approximated tidal prisms, it follows that the relationship between the subbasin area and inlet area in equilibrium depends on the equilibrium velocity, tidal range and tidal frequency.

A sensitivity analysis is performed in which the response of the system (number of inlets, tidal subbasin area, tidal prism(s) and inlet area per inlet and for the entire system) to changes in basin and ocean water depth, tidal amplitude and littoral drift is analysed. According to the model results, instant sea level rise results in fewer open inlets in equilibrium, but also a slight increase in the tidal basin areas and the inlet areas. The number of inlets in equilibrium and the total inlet area are directly proportional to the tidal amplitude. Both the inlet areas per inlet and the tidal prisms do not change significantly as the tidal amplitude changes, such that the relationship $\Omega = kP^\alpha$ is maintained with the same coefficients even when the tidal amplitude changes. An increase in littoral drift means an increase in sediment import and equilibrium velocity, which decreases the number of inlets and the total inlet area in equilibrium since more sediment is available to close the inlets. However, the tidal prisms increase, such that the tidal prism - inlet area relationship changes, which is expected as that relationship depends on the (equilibrium) flow velocity amplitude in the inlets.

Contents

Preface

Abstract

1. Introduction	1
1.1 Background	1
1.1.1 Tidal inlet systems and their stability	1
1.1.2 Modelling tidal inlet systems.....	3
1.1.3 Tidal divides, tidal subbasins and tidal prisms.....	4
1.2 Research objective.....	6
1.2.1 Knowledge gap and relevance	6
1.2.2 Objective and research questions	7
1.3 Reading guide	7
1.3.1 Outline of methodology	7
1.3.2 Outline of report	8
1.3.3 List of symbols.....	8
2. Model	9
2.1 Model set-up	9
2.1.1 Morphodynamics.....	9
2.1.2 Hydrodynamics	10
2.2 Solution method	11
2.3 Parameter values	13
3. Tidal divides	14
3.1 Identification methods	14
3.1.1 Method 1: Minimum flow velocity amplitudes	14
3.1.2 Method 2: Large phase differences.....	15
3.2 Results of identification.....	16
3.2.1 Two inlets	17
3.2.2 Three inlets.....	18
3.2.3 More than three inlets	20
3.3 Subconclusions.....	20
4. Tidal prism - inlet area relationship	22
4.1 Comparison method.....	22
4.1.1 Empirical O'Brien-Jarrett Law	22
4.1.2 Calculation of tidal prism	23
4.1.3 Calculation of coefficients.....	25
4.2 Results for different parameter sets	26
4.2.1 Wadden Sea runs	26

4.2.2 Atlantic coast runs	27
4.3 Accuracy of tidal prism approximation	29
4.4 Development over time.....	31
4.4.1 Open inlets	32
4.4.2 Closing inlets.....	35
4.5 Subconclusions.....	35
5. Sensitivity analysis.....	37
5.1 Water depth.....	37
5.2 Tidal amplitude	40
5.3 Littoral drift.....	42
5.4 Subconclusions.....	44
6. Discussion	46
6.1 Interpretation of tidal divides	46
6.2 Applicability of tidal prism - inlet area relationship	47
6.2.1 Single inlet vs. multiple inlets	47
6.2.2 Systems in equilibrium	48
6.2.3 Prediction of system's evolution	48
6.3 Relation between subbasin areas and inlet areas	49
7. Conclusion.....	51
8. Recommendations	52
Appendices.....	53
A. Example model run.....	53
B. Number of model runs for sensitivity analysis	55
C. Basin areas and inlet areas.....	57
References	58

1. Introduction

1.1 Background

1.1.1 Tidal inlet systems and their stability

Tidal inlet systems typically include barrier islands, tidal inlets and back-barrier basins and are therefore also called barrier coasts. They form about 10% of the coastlines around the world (e.g. Stutz and Pilkey, 2011). When more than one tidal inlet is included in the system, it is a multi-inlet tidal system. An example of such a system is the Wadden Sea. In general, a tidal inlet system is characterized by the presence of barrier islands, a back-barrier basin, inlet deltas (flood and ebb-tidal delta), tidal channel networks, tidal bars and meanders and the intertidal zone of tidal flats and salt marshes (De Swart and Zimmerman, 2009). These elements of a tidal system are schematically shown in Fig. 1.1. The tidal inlets connect the back-barrier basin to the sea or ocean, such that water and sediment can be exchanged between the basin and the outer sea.

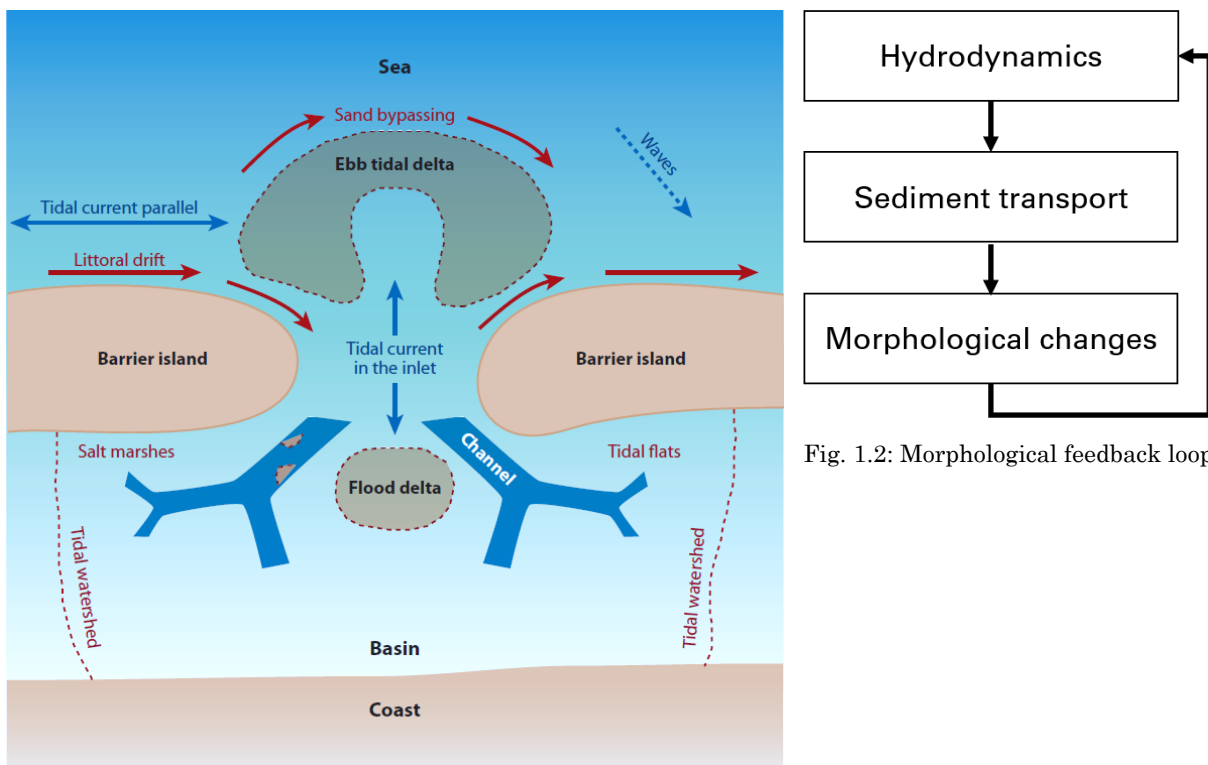


Fig. 1.1: Schematized overview of a tidal inlet system, including the different geomorphic elements and physical processes (De Swart and Zimmerman, 2009).

A tidal inlet system develops according to the morphological feedback loop, as shown in Fig. 1.2. The main hydrodynamic drivers that influence the development of a tidal inlet system are tidal currents and waves (e.g. Escoffier, 1940; De Swart and Zimmerman, 2009), also shown in Fig. 1.1. The hydrodynamics determine the sediment transport in the system, which in turn influences the morphological changes in the system. The changes in morphology again influence the hydrodynamics, forming a morphological feedback loop.

The hydrodynamic drivers that determine the sediment transport are waves and tidal currents. Waves that obliquely approach the shore generate longshore currents, also shown in Fig. 1.1. The combination of waves and longshore currents leads to longshore sediment transport, which is called the littoral drift (De Swart and Zimmerman, 2009). Part of the sediment in the littoral drift will pass the inlets, while another part of it will be transported into the inlets. This sediment is either deposited there or it is imported into the basin or out to the sea by the tidal currents. Hence, there is wave-driven sediment import into and tide-driven sediment export out of the inlets, so waves tend to close inlets while tidal currents keep them open. The competition between these two processes define the geometry and stability of the tidal inlets (De Swart & Zimmerman, 2009; Escoffier, 1940). Barrier islands and tidal inlets do not develop along tide-dominated coasts, while barrier islands along wave-dominated coasts tend to be long and narrow such that tidal inlets are spaced far apart (Hayes, 1979; Wang and Roberts Briggs, 2015). Besides the hydrodynamic drivers of tides and waves, also climate change, human interventions and storms can influence the system's evolution. Sea level rise and imposed and maintained basin geometries are examples of climate change and human interventions that influence multi-inlet tidal systems. Furthermore, storms may cause breaching of barrier islands, creating new tidal inlets. It is important to study the consequences of these mechanisms to successfully manage and protect tidal inlet systems like the Wadden Sea.

Stability

On a mesotidal coast, the stability and geometry of a tidal inlet mainly depends on the aforementioned two competing mechanisms: tidal currents, tending to keep the inlets open, and wind waves, tending to close the inlets. A tidal inlet is considered stable when it is in a stable equilibrium, which means that the cross-sectional area of the inlet returns to its equilibrium value after a small perturbation. According to Escoffier (1940), this depends on the ability of the waves and the tidal currents to transport the sediment, which in turn depends on the flow velocity amplitude in the inlet. Escoffier proposed that there is an equilibrium velocity $U = U_{eq}$ for the ebb-tidal flow velocity amplitude U in the inlet. When the flow velocity is larger than the equilibrium velocity ($U > U_{eq}$), the inlet erodes and its cross-sectional area will increase. When the flow velocity is smaller than the equilibrium velocity ($U < U_{eq}$), the inlet accretes and the cross-sectional area of the inlet will decrease.

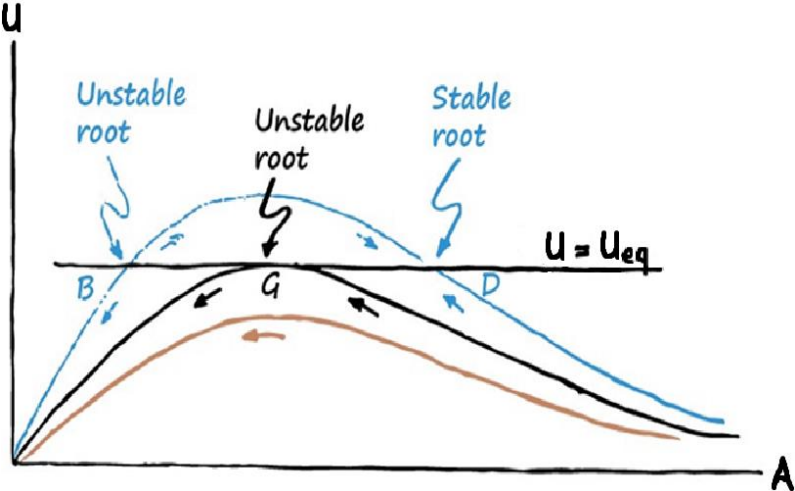


Fig. 1.3: Escoffier diagram (Escoffier, 1940), showing three possible closure curves, the equilibrium velocity U_{eq} and the stable and unstable roots resulting from intersections of the U -curves with the line $U = U_{eq}$.

For a single inlet system, the quantity U can be expressed as a function of the cross-section of the inlet, represented by A in Fig. 1.3. Three possible U -curves (also called closure curves) are

shown in Fig. 1.3. The intersections of the closure curve with the line of equilibrium velocity U_{eq} are the equilibria of the system, for which the inlet's cross-sectional area is stationary in size. However, the inlet is only stable when the equilibrium is stable, as is the case for root "D" in Fig. 1.3. For the other two possible closure curves shown in Fig. 1.3, no stable equilibrium exists and hence the tidal inlet will accrete and disappear ($A \rightarrow 0$). The equilibrium velocity U_{eq} is an empirical quantity that largely depends on sediment properties, such as grain size, and the magnitude of the littoral drift (Escoffier, 1940).

A multi-inlet tidal system is stable when it is in a stable equilibrium with more than one inlet open. The system is considered an unstable multi-inlet tidal system when only one inlet remains open, while all other inlets close. The stability of (multi-)inlet tidal systems can be studied using models. The closure curve used in Escoffier's stability concept is usually determined by solving the governing equations for the system's hydrodynamics. An assumption about the inlet's shape is also required. The concept of stability by Escoffier (1940) is still widely used in models of tidal inlet systems, such as the model used by Roos et al. (2013).

1.1.2 Modelling tidal inlet systems

For a single inlet system, Escoffier (1940) related the flow velocity in an inlet to the cross-sectional area of the inlet based on the balance between sediment import by waves and sediment export by tides. Van de Kreeke (1990) studied the stability of double-inlet tidal systems by extending Escoffier's approach to two inlets. He found no stable configurations for double-inlet tidal systems. Conversely, observations show that stable tidal systems with multiple inlets do exist. Several studies have since then identified options for processes that should be included in models of multi-inlet tidal systems to be able to find stable equilibria: topographic highs (Van de Kreeke et al., 2008), entrance/exit losses (Brouwer et al., 2012), spatial variations in basin water level and ocean amplitudes (Brouwer et al., 2008; Brouwer et al., 2013) and nonlinearities such as tidal distortion and residual flow patterns (Salles et al., 2005).

The models that are used to study the stability of tidal inlet systems can be classified into different types: empirical models, complex process-based models and idealized process-based, also called exploratory, models (Wang et al., 2012). Empirical models explicitly use empirical relations to define the morphological equilibrium of a tidal inlet system. An example of a semi-empirical model of tidal inlet systems is the ASMITA model, which is used for studying the long-term (decadal) behaviour of a tidal inlet, especially after human intervention and climate change (Kragtwijk, 2002; Wang et al., 2012). Alternatively, the aim of complex process-based modelling is to create the best possible description of the relevant processes, such that the models can be used for a detailed representation of the morphological changes. An example of a complex process-based model is the Delft3D model, which is used to simulate the morphological evolution of a tidal inlet (e.g. Tung et al., 2011). Idealized models are process-based models that use simplified physical and mathematical descriptions and schematized geometries to allow for efficient solutions. The difference with the complex process-based models is that the idealized models do not fully describe all processes, but only (a few) relevant processes (Wang et al., 2012). Idealized models can be used for exploring specific processes and phenomena and are therefore also called exploratory models, as is done by Murray (2003). Exploratory models are used when the aim is to discover what processes or interactions induce some poorly-understood phenomenon, usually without expecting quantitative accuracy (Murray, 2003). An example of an exploratory model is the model by Roos et al. (2013). In most models of tidal-inlet systems, process-based hydro- and morphodynamic models are combined with a (semi-)empirical relation for inlet stability, e.g. Escoffier's stability concept.

Roos et al. (2013) have been able to reproduce the observed existence of stable multi-inlet tidal systems with more than one inlet open, using an exploratory model that simulates the evolution of multi-inlet tidal systems. The model combines Escoffier’s stability concept with a process-based hydrodynamic model for depth-averaged tidal flow in the inlets, basin and ocean. As the model is exploratory, only the essential processes are taken into account and the geometry of the system is schematized, with the aim to qualitatively reproduce the evolution of multi-inlet tidal systems. Roos et al. (2013) state that natural phenomena such as tidal divides, inlet migration and alongshore variations in basin width are neglected in their model.

1.1.3 Tidal divides, tidal subbasins and tidal prisms

Tidal divides¹ are an important part of tidal inlet systems as they form the barriers or boundaries between tidal basins in the back-barrier basin of a multi-inlet tidal system, as shown in Fig. 1.1 and 1.4. A tidal subbasin can be interpreted as the “area of influence” of one tidal inlet, as the area of the back-barrier basin that is filled and emptied through a certain inlet belongs to the tidal subbasin corresponding to that inlet. A tidal divide can move, due to e.g. human interventions or sea level rise, changing the boundaries of the tidal subbasins. Changes in these areas of influence affect the morphological development of the subbasin in which it takes place, but also in the adjacent subbasins (Wang et al., 2011).

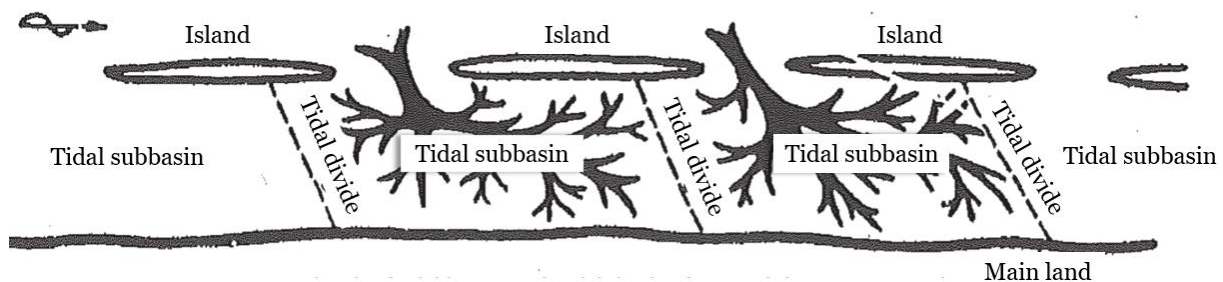


Fig. 1.4: Simplistic overview of tidal divides forming boundaries between tidal subbasins in a multi-inlet tidal system (Stive and Wang, 2003).

A distinction can be made between a hydraulic tidal divide and a morphological tidal divide (Wang et al., 2011). The hydraulic tidal divide is the line between two tidal subbasins in terms of drainage. Hence, the hydraulic tidal divide results from the flow field in the back-barrier basin. The hydraulic tidal divide can be defined as the location where flow velocity amplitudes are minimal. In their model of a tidal inlet system, Dastgheib et al. (2008) defined the hydraulic tidal divide as the line of minimum standard deviation over a tidal cycle of (depth-averaged) velocities.

The morphological tidal divide can be defined as the line between two adjacent tidal subbasins with the highest bed level elevation, so it can be seen as a physical barrier between tidal subbasins. The location of the morphological tidal divide does not necessarily have to coincide with the location of the hydraulic tidal divide. Morphological changes are happening over a longer time scale than hydraulic changes and therefore the morphological tidal divide is “slowly” moving towards the hydraulic tidal divide, as long as the system is not in equilibrium. In turn, the morphological tidal divide influences the location of the hydraulic tidal divide. However, even when no morphological tidal divides are present, hydraulic tidal divides can still be present as they result from flow patterns.

¹ In Fig. 1.1, other literature and hence in this report, tidal watershed is used as a synonym for tidal divide.

In Fig. 1.5, the approximate locations of tidal divides in the Dutch Wadden Sea are shown (e.g. Kragtwijk et al., 2004; Dastgheib et al., 2008; Wang et al., 2012). As can be seen in Fig. 1.5, it is found that most tidal divides behind the Wadden islands are approximately “straight” lines from a barrier island to the main land. On the other hand, the tidal divides behind Texel and Vlieland are shaped differently, as two tidal divides seem to converge into one. An example of a large human intervention in the Wadden Sea is the closure dam separating the Zuiderzee from the Wadden Sea (Kragtwijk et al., 2004), also shown in Fig 1.5. Such interventions have affected the location and shape of the tidal divides and with that the size and shape of the tidal subbasins, influencing the morphology of the entire Wadden Sea (Kragtwijk et al., 2004). Therefore, it is important to study the occurrence, position and shape of tidal divides and thereby the tidal subbasins.

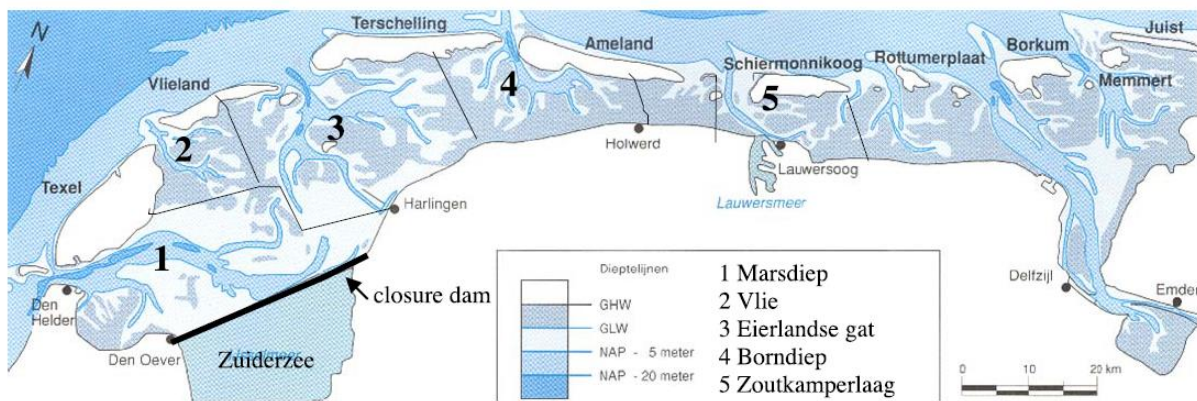


Fig. 1.5: The (approximate) tidal divides and tidal subbasins in the Wadden Sea (Kragtwijk et al., 2004).

Tidal prism - inlet area relationship

Throughout the years, several attempts have been made to determine an empirical relationship between the total water volume entering a tidal (sub)basin during a characteristic tidal cycle, which is called the tidal prism, and the cross-sectional area of a tidal inlet. Such empirical relationships couple tidal hydrodynamic and morphodynamic processes and they can be used to predict the long-term morphological evolution of tidal inlet systems, e.g. in response to forcings affecting the tidal prism. In a modelling context, they can also be used to validate models of tidal inlet systems.

The first attempts to actually determine an empirical relationship between the inlet’s cross-sectional area, Ω , and the tidal prism, P , were by O’Brien (1931, 1969). He proposed an empirical tidal prism - inlet area relationship of the form

$$\Omega = kP^\alpha \quad (1.1)$$

where Ω is the minimum cross-sectional area (m^2 or ft^2) of the tidal inlet, i.e. below mean water level, P is the tidal prism (m^3 or ft^3) based on the spring tidal range and α (–) and k ($m^{2-3\alpha}$) are coefficients that can be determined empirically, for inlets that are assumed to be in equilibrium. Jarrett (1976) attempted to test this empirical P - Ω relationship by considering a large number of tidal inlets in North America, and determining the coefficients k and α through regression analysis (D’Alpaos et al., 2009).

Eq. (1.1) with the coefficients k and α that are empirically determined by Jarrett (1976) is called the O’Brien-Jarrett Law, which is a well-established empirical relationship. Dieckmann et al. (1988) have analysed the tidal prism - inlet area relationship for the Wadden Sea and have also determined the coefficients k and α .

To be able to analyse the coefficients k and α , the inlet's cross-sectional area Ω and the tidal prism P should be computed using data or a model. Several different methods can be used to calculate the tidal prism, defined as the total water volume entering a tidal basin within each tidal cycle. One method of calculating the tidal prism, used by e.g. Krishnamurthy (1977), is based on a given velocity profile along any vertical in the basin, which is integrated along the inlet's cross-section to obtain the flow discharge through the inlet. This is then integrated over half a tidal cycle to obtain the tidal prism:

$$P_{exact} = \frac{1}{2} \int_0^T |BU(t)D(t)| dt \quad (1.2)$$

where B is the width of the rectangular cross-sectional area of the inlet with uniform flow, U is the local depth-averaged flow velocity and D is the flow depth at the inlet caused by a sinusoidal tidal forcing with period T (Krishnamurthy, 1977).

If the size of the tidal basin is assumed to be small compared to the tidal wave length, which is a correct assumption for e.g. the Wadden Sea according to Kragtwijk (2002), spatial variation in water level can be neglected and the tidal prism can be estimated as

$$P_{approx} = H \cdot A_b \quad (1.3)$$

where A_b is the surface area of the tidal (sub)basin and H is the tidal range.

1.2 Research objective

1.2.1 Knowledge gap and relevance

For the management and protection of multi-inlet tidal systems such as the Wadden Sea system, knowledge on the morphodynamic development of multi-inlet tidal systems is essential. The morphodynamic development of such systems is influenced by waves and tidal currents and hence also by sea level rise and storms, as well as by human interferences. However, according to Wang et al. (2012), our present knowledge of multi-inlet tidal systems is not sufficient to predict the effects of human interferences under different climate change scenarios in sufficient detail and accuracy.

The positions of the tidal inlets cannot be seen separately from the tidal divides, so understanding the movement of the tidal divides is important for the prediction of the development of a multi-inlet tidal system. Nevertheless, the knowledge about the processes involved in the movement of tidal divides is still insufficient. The exploratory model by Roos et al. (2013) can be used to study the long-term development of multi-inlet tidal systems, but tidal divides do not pre-exist in the model. Roos et al. (2013) have stated that tidal divides can be interpreted as resulting from the flow patterns in the model. While this may be true, the identification of tidal divides in the model has not yet been specified. Identification of tidal divides in the model is important for the usability of the model for studying the movement of tidal divides due to e.g. sea level rise or human interventions.

It is still unknown whether the model by Roos et al. (2013) complies with the empirical relationship between tidal prisms and cross-sectional areas of the inlets as shown in Eq. (1.1). This O'Brien-Jarrett Law might be used as validation of the model results, but the applicability of such empirical relationships in models of multi-inlet tidal systems can also be tested. When tidal divides in the model are identified, the basin areas of tidal subbasins can be determined, after which the tidal prism can be calculated in two different ways and the model results can be compared to the empirical O'Brien-Jarrett Law.

External changes such as sea level rise and human interventions in the basin are still absent in the model by Roos et al. (2013). To investigate the sensitivity of the system to these processes, parameters such as water depths, tidal amplitude and littoral drift can be varied in the model by Roos et al. (2013). Furthermore, the model can be used to study the effect of such changes on the tidal prism - inlet area relationship.

1.2.2 Objective and research questions

The aim of this research is to extend the possibilities of the model by Roos et al. (2013) and to study to what extent the model results match empirical laws and observations. To this end, identification methods for tidal divides in models of multi-inlet tidal systems are studied and applied to the model by Roos et al. (2013). Also, the model results are compared with an empirical tidal prism - inlet area relationship, the O'Brien-Jarrett Law. The objective is to draw conclusions about the applicability of such empirical relationships for different situations and about the model's performance. Furthermore, we want to study the effects of changing outer sea or ocean conditions, e.g. sea level rise, on the development and stability of multi-inlet tidal systems and the tidal prism - inlet area relationship.

The model that is used in this research is the model by Roos et al. (2013). The research questions that are answered are the following:

- 1) How can hydraulic tidal divides be identified in models of multi-inlet tidal systems without topographic highs?
- 2) To what extent do the model results agree with the empirical tidal prism - inlet area relationships?
- 3) How will changes in ocean conditions affect the stability of multi-inlet tidal systems and the tidal prism - inlet area relationship?

1.3 Reading guide

1.3.1 Outline of methodology

Several methods are developed and applied to answer the research questions, using the model by Roos et al. (2013). The goal of the first research question is to actually develop an identification method for tidal divides in the model by Roos et al. (2013). Therefore, possible methods are explored and two identification methods are applied to the model. It is important that the tidal divide identification method can be used to calculate surface areas of tidal subbasins corresponding to open inlets, such that these subbasin areas can be used to calculate the approximate tidal prisms for the second research question.

For that second question, first the empirically determined values of the coefficients of the O'Brien-Jarrett Law are studied. Then, the tidal prisms and inlet areas are calculated from the model results, after which a function is fit to the model data and the coefficients of that function are compared to the empirical values. The tidal prisms are calculated using the two different methods that are introduced in Section 1.1.3, of which one calculates the exact tidal prisms and the other method gives approximated tidal prisms. Plotting the approximated tidal prisms against the exact tidal prisms gives insight into the accuracy of the tidal prism approximation under different circumstances. Furthermore, the temporal development of the tidal prisms and inlet areas over a model run is investigated, such that the applicability of the tidal prism - inlet area relationship for systems that are not (yet) in equilibrium can be studied.

For the last research question, the ocean and basin water depths, the tidal amplitude and the littoral drift are modified in the model. The sensitivity of the equilibrium number of inlets, tidal subbasin areas, tidal prisms and inlet areas to these changes is studied by constructing boxplots of the model results, in order to determine the effect of such external changes on the stability of the system and on the tidal prism - inlet area relationship.

1.3.2 Outline of report

The model by Roos et al. (2013) that is used in this research is explained in Chapter 2, including the model set-up, the solution method and the parameter values that will be used. The methodology, results and subconclusions for the first research question concerning the identification of tidal divides are presented in Chapter 3. In Chapter 4, the empirical coefficients of the O'Brien-Jarrett Law are presented, after which the model results are compared to the empirical law. The accuracy of the tidal prism approximation and the development of the system over time are also discussed. The sensitivity analysis that is performed with respect to the ocean conditions is presented in Chapter 5. In Chapter 6, the overall discussion is presented in which the results are interpreted, their significance is discussed and they are compared to previous studies. Then in Chapter 7, overall conclusions are drawn. Lastly, recommendations for future research are made in Chapter 8.

1.3.3 List of symbols

An overview of the symbols that are used in this report is presented in Table 1.1. All model parameters are introduced and explained in Section 2.1 and 2.2, so they will not be shown in Table 1.1 unless they are explicitly used in the methods or results in Chapter 3, 4 and 5. Furthermore, the values and meanings of the input parameters of the model are presented separately in Table 2.1. Therefore, only the symbols that are not (input) model parameters, but will be used in the remaining part of the report are presented in Table 1.1.

Symbol	Meaning
U or U_j (m/s)	Flow velocity amplitude (in inlet j)
U_{eq} (m/s)	Equilibrium flow velocity amplitude
Ω or Ω_j (m ²)	Inlet cross-sectional area (of inlet j) in the tidal prism - inlet area relationship
k (m ^{1-2α})	Coefficient in the tidal prism - inlet area relationship $\Omega = kP^\alpha$
α (-)	Coefficient in the tidal prism - inlet area relationship $\Omega = kP^\alpha$
P_{exact} or $P_{j,exact}$ (m ³)	Exact tidal prism (corresponding to inlet j)
P_{approx} or $P_{j,approx}$ (m ³)	Approximated tidal prism (corresponding to inlet j)
H (m)	Tidal range (= $2Z$, where Z is the tidal amplitude)
A_b or $A_{b,j}$ (m ²)	Surface area of tidal subbasin (corresponding to inlet j)
A_j (m ²)	Inlet cross-sectional area (of inlet j) in the model equation
\hat{u}_b and \hat{v}_b (m/s)	Complex flow velocity amplitudes in the basin, in respectively the cross-shore x - and the alongshore y -direction
ϕ (rad)	Phase angle of the flow velocity in the y -direction in the basin
b_j (m)	Width of inlet j
λ (m)	Tidal wave length
R^2 (-)	Coefficient of determination

Table 1.1: Overview of the symbols used in this report, their dimensions and meanings.

2. Model

The model that is used is the exploratory model introduced by Roos et al. (2013). In Sections 2.1 and 2.2, the model set-up and the solution method are explained. Then in Section 2.3, the parameter values that are used for modelling different locations are presented.

2.1 Model set-up

The model consists of a hydrodynamic and a morphodynamic part. Escoffier's stability concept is used to simulate the morphological evolution of the inlets. The hydrodynamic model simulates the water motion, described by the linearized shallow water equations, in the outer sea, the tidal inlets and the tidal basin. The model domain is a simplified barrier coast consisting of a multi-inlet tidal system with J inlets that connect a single rectangular basin to a semi-infinite outer sea, as shown in Fig. 2.1. Both the tidal basin and the outer sea are assumed to be of uniform depth. Similar to Roos et al. (2013), all simulations start with an initial (large) number of inlets.

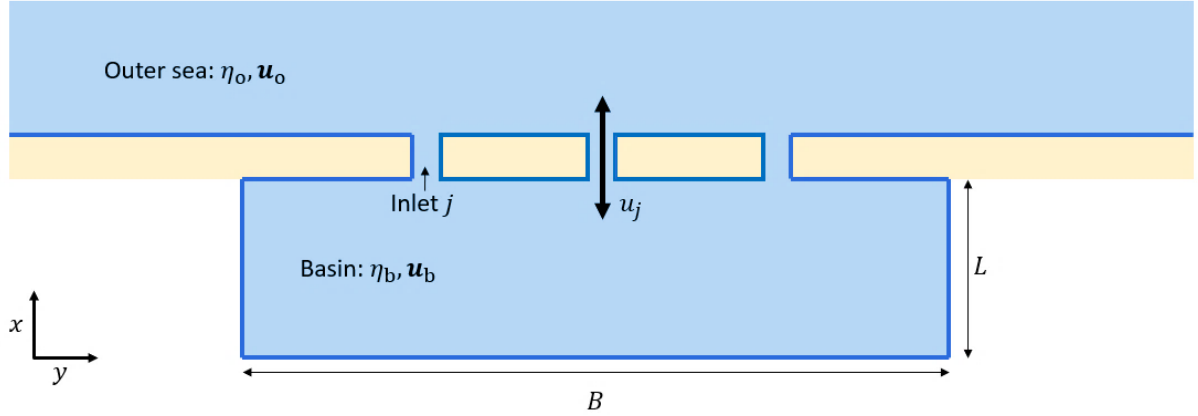


Fig. 2.1: Model geometry of a multi-inlet tidal system consisting of the outer sea that is connected to a basin by J ($J = 3$ in this example) tidal inlets, where the arrow u_j denotes the flow velocity of the inflow and outflow of water through the inlets.

2.1.1 Morphodynamics

For the morphodynamics, it is assumed that each inlet j has a rectangular cross-section, with width b_j , depth h_j , and area $A_j = b_j h_j$. The evolution of the cross-sectional area of each inlet over time depends on the volumetric import M_j and export X_j of sediment. It is assumed that this is uniformly distributed along the inlet channel, such that

$$l_j \frac{dA_j}{dt} = X_j - M_j \quad (2.1)$$

where l_j is the length of the inlet. Similar to Escoffier (1940), it is assumed that (i) the tide-driven sediment export X_j is proportional to the velocity amplitude of a sinusoidal tide in the inlet, U_j , cubed: $X_j = \kappa U_j^3$, with a constant κ , and (ii) the wave-driven sediment import M_j is externally imposed and hence an equilibrium velocity U_{eq} can be derived for which the sediment import and export are equal, satisfying $M_j = \kappa U_{eq}^3$. Eq. (2.1) can then be rewritten as

$$\frac{dA_j}{dt} = \frac{M}{l_j} \left(\left(\frac{U_j}{U_{eq}} \right)^3 - 1 \right) \quad (2.2)$$

The parameters l_j , U_{eq} and hence M are assumed to be identical for each inlet. From Eq. (2.2), the change in cross-sectional area of the inlets can be computed, given the velocity scale U_j in the inlet. This velocity scale U_j is determined using a hydrodynamic model, to be presented in Section 2.1.2.

Eq. (2.2) tells us that the cross-sectional area of an inlet increases if $U_j > U_{eq}$, decreases if $U_j < U_{eq}$ and remains the same if $U_j = U_{eq}$. An assumption regarding the cross-section of the inlet is needed in order to translate the evolution of an inlet's cross-sectional area $A_j = b_j h_j$ into the evolution of inlet width b_j and depth h_j . As is done in many previous studies, it is assumed that the cross-sectional area is shape-preserving, such that the aspect ratio (i.e. shape factor) $\gamma_j^2 = h_j/b_j$ is kept constant.

The inlets' geometries are considered to be fixed on the time scale of the hydrodynamics. This is justified by the large difference between the timescales of the hydrodynamics (order of a day) and morphodynamics (order of years).

2.1.2 Hydrodynamics

The hydrodynamic model simulates the hydrodynamics in the outer sea, the tidal inlets and the tidal basin. The model is forced by a tidal wave at the outer sea, resulting in radiating waves in the outer sea, flow of water through the tidal inlets, and oscillations in the tidal basin. Let $u_j(t)$ denote the cross-sectionally averaged flow velocity in inlet j as a function of time t . For each inlet j , the momentum equation reads

$$\frac{\partial u_j}{\partial t} + \frac{r_j u_j}{h_j} = -g \frac{\langle \eta_o \rangle_j - \langle \eta_b \rangle_j}{l_j} \quad (2.3)$$

where u_j is the flow velocity, assumed to be uniform over the length of the inlet channel, η_o is the water level in the outer sea, η_b is the water level in the tidal basin, l_j is the length of the inlet channel and r_j is a linear bottom friction coefficient (to be specified in Eq. (2.14)). The angle brackets denote lateral averaging over the inlet mouth, such that

$$\langle \eta_o \rangle_j = b_j^{-1} \int_{y_j - b_j/2}^{y_j + b_j/2} \eta_o(0, y) dy$$

at the outer sea side, where b_j is the width of the basin and y_j is the location of the middle of the basin, and

$$\langle \eta_b \rangle_j = b_j^{-1} \int_{y_j - b_j/2}^{y_j + b_j/2} \eta_b(-l, y) dy$$

at the basin side.

The solutions in the outer sea and basin satisfy the linear shallow water equations. In the outer sea, denoted with subscript 'o', bottom friction and Coriolis acceleration are neglected. The linearized model equations are

$$\frac{\partial \mathbf{u}_o}{\partial t} = -g \nabla \eta_o, \quad \frac{\partial \eta_o}{\partial t} + h_o (\nabla \cdot \mathbf{u}_o) = 0 \quad (2.4)$$

where h_o is the water depth in the outer sea, $\nabla = (\partial/\partial x, \partial/\partial y)$ is the nabla operator and $\mathbf{u}_o = (u_o, v_o)$ is the depth-averaged flow velocity in the outer sea with components in the x - and y -direction, respectively.

In the basin, Coriolis acceleration is also neglected, but linearized bottom friction is included. The linearized model equation for the basin, denoted with subscript ‘b’, are the following:

$$\frac{\partial \mathbf{u}_b}{\partial t} + \frac{r_b \mathbf{u}_b}{h_b} = -g \nabla \eta_b, \quad \frac{\partial \eta_b}{\partial t} + h_b (\nabla \cdot \mathbf{u}_b) = 0 \quad (2.5)$$

where h_b is the water depth in the basin, $\mathbf{u}_b = (u_b, v_b)$ is the depth-averaged flow velocity in the basin with components in the x - and y -direction and r_b is the linearized friction coefficient. At the closed boundaries of the basin and the outer sea, the normal velocity vanishes. At the open boundaries between the inlet and the basin, as well as the inlet and the outer sea, continuity of surface elevation and continuity of transport of water is required. The continuity of surface elevation is implied in the momentum equation in Eq. (2.3). The continuity of transport of water implies

$$h_o \langle u_o \rangle_j = h_j u_j = h_b \langle u_b \rangle_j \quad (2.6)$$

where h is the water depth, $\langle u \rangle$ is the width-averaged flow velocity and the subscripts ‘o’, ‘j’ and ‘b’ represent outer sea, inlet j and basin, respectively.

2.2 Solution method

The equations introduced in Section 2.1 describe the hydrodynamics and morphodynamics in the outer sea, the tidal inlets and the back-barrier basin. The morphodynamic evolution is analysed using Forward Euler discretisation of the time derivative in Eq. (2.2) with time step Δt . The hydrodynamic model is solved analytically and yields flow velocities and water levels in the outer sea, the tidal inlets and the basin.

To solve the hydrodynamic part of the model, the water levels and flow velocities are expressed as the product of complex amplitudes and a time-periodic part:

$$(\eta_o, u_o, v_o) = \Re\{(\hat{\eta}_o, \hat{u}_o, \hat{v}_o) \exp(i\omega t)\} \quad (2.7)$$

$$(\eta_b, u_b, v_b) = \Re\{(\hat{\eta}_b, \hat{u}_b, \hat{v}_b) \exp(i\omega t)\} \quad (2.8)$$

$$u_j = \Re\{\hat{u}_j \exp(i\omega t)\} \quad (2.9)$$

where \Re means the real part and \hat{u}_j , $(\hat{\eta}_b, \hat{u}_b, \hat{v}_b)$ and $(\hat{\eta}_o, \hat{u}_o, \hat{v}_o)$ are complex amplitudes. Furthermore, $\omega = 1.405 \times 10^{-4}$ rad/s is the angular frequency (in this case that of the semi-diurnal M_2 tide) and k_o is the shallow water wave number in the outer sea or ocean. The elevation in the outer sea is viewed as a superposition of the incoming tidal wave and waves radiating from all inlets, which implies

$$\eta_o(t, x, y) = Z \cos(\omega t + k_o y) + \sum_q \eta_{oq}(t, x, y) \quad (2.10)$$

where Z is the elevation amplitude of the incoming tide. The elevation at the basin side of the inlet is the superposition of radiating waves from the inlets and waves reflecting against the coasts:

$$\eta_b(t, x, y) = \sum_q \eta_{bq}(t, x, y) \quad (2.11)$$

Combining the expressions in Eq. (2.7) – (2.11) and the momentum equation (Eq. (2.3)) gives the momentum equation for an inlet j :

$$i\omega \mu_j^2 \hat{u}_j = -\frac{g}{l} \left(Z \langle \exp(ik_o y) \rangle_j + \sum_q \langle \hat{\eta}_{oq} \rangle_j - \sum_q \langle \hat{\eta}_{bq} \rangle_j \right) \quad (2.12)$$

where $\mu_j^2 = 1 - ir_j/(\omega h_j)$ is a complex frictional correction factor. The term $Z\langle \exp(ik_0 y) \rangle_j$ is the forcing term, representing the elevation due to the tidal wave in the outer sea. The second term on the right-hand side is the elevation due to radiating waves in the outer sea and the third term is the elevation in the basin. Hence, the flow velocity in the inlets is expressed in terms of elevation in the outer sea (tidal wave and radiating waves) and the basin. Expressing the second and third term on the right-hand side in terms of \hat{u}_j gives

$$\langle \hat{\eta}_{0q} \rangle_j = z_{0jq} \hat{u}_q, \quad \langle \hat{\eta}_{bq} \rangle_j = z_{bjq} \hat{u}_q \quad (2.13)$$

Here, z_{0jq} is the outer sea impedance and z_{bjq} is the basin impedance, expressing the influence of flow through inlet q on the elevation at inlet j . Derivation of the impedances will result in a linear system that can be written in matrix form according to $\mathbf{A}\mathbf{u} = \mathbf{f}$, where $\mathbf{u} = (\hat{u}_1, \dots, \hat{u}_J)$ for J inlets. The forcing term \mathbf{f} represents the incoming tidal wave. This system is then solved for the unknown velocity amplitudes \hat{u}_j in the inlets.

It is important to emphasize the flow solution's dependency on the friction coefficients r_j and r_b . The bottom friction coefficients r_j (in the inlets) and r_b (in the basins) are chosen according to Lorentz' linearization, such that

$$r_j = \frac{8}{3\pi} c_d U_j, \quad r_b = \frac{8}{3\pi} c_d U_b \quad (2.14)$$

where c_d is the drag coefficient $c_d = 2.5 \times 10^{-3}$ and U_j and U_b are the velocity scales representative of the inlets and basin, respectively. The velocity scale in the inlets is defined as $U_j = |\hat{u}_j|$, where \hat{u}_j is the amplitude of the velocity in the inlet for a sinusoidal tide. The velocity scale in the basin is the average velocity in the basin, which is defined as

$$U_b^2 = \frac{1}{BL} \int_0^B \int_0^L (|\hat{u}_b|^2 + |\hat{v}_b|^2) dx dy \quad (2.15)$$

The velocity scales U_j in the inlet and U_b in the basin are both inputs and output of the model, so an initial guess is used as first input and the actual velocity scales are determined iteratively. The initial guess is $U_j = Z/\sqrt{gh_j}$ and $U_b = 0$. The values of $U_j = |\hat{u}_j|$ and U_b resulting from this solution are then used in Eq. (2.14) to obtain new values of the friction coefficients r_j and r_b , leading again to new solutions for U_j and U_b . The velocity scales are updated iteratively by applying an underrelaxation procedure until the input and output velocity scales are approximately equal (using a maximum error tolerance of 10^{-10}).

The system of equations in Section 2.1 can also be solved for the elevation amplitude $\hat{\eta}_b$ and flow velocity amplitude $\hat{\mathbf{u}}_b$ in the basin. The model equations for the basin in Eq. (2.5) can be combined with the expression in terms of complex amplitudes ($\hat{\eta}_b, \hat{u}_b, \hat{v}_b$) in Eq. (2.8) to get

$$\nabla^2 \hat{\eta}_b + \mu_b^2 k_b^2 \hat{\eta}_b = 0, \quad \hat{\mathbf{u}}_b = \frac{gi}{\mu_b^2 \omega} \nabla \hat{\eta}_b \quad (2.16)$$

with frictional correction factor $\mu_b^2 = 1 - ir_b/(\omega h_b)$ and shallow water wave number $k_b = \omega/\sqrt{gh_b}$ for the basin. Using Green's function to determine the co-oscillating basin solution $\hat{\eta}_{bq}$ due to inlet q , the following expression for the surface elevation in the basin due to inlet q is found:

$$\hat{\eta}_{bq}(x - l - L, y) = \frac{ib_q h_q \hat{u}_q}{\omega} \sum_{m=n=1}^{M,N} c_{mnq} \psi_{mn}(x, y), \quad c_{mnq} = \frac{\langle f_q \psi_{mn} \rangle_q}{1 - \mu_b^{-2} k_b^{-2} k_{mn}^2} \quad (2.17)$$

Here, ψ_{mn} are the normalized eigenmodes of the closed basin, with in this research $M = 50$ in the cross-shore x -direction and $N = 50$ in the alongshore y -direction, and

$$k_{mn} = \sqrt{(m\pi/L)^2 + (n\pi/B)^2} \quad (2.18)$$

are the corresponding eigenvalues. The eigenmodes are given by

$$\psi_{mn}(x, y) = a_{mn} \cos(m\pi x/L) \cos(n\pi y/B) / \sqrt{BL} \quad (2.19)$$

with $a_{00} = 1$, $a_{m0} = a_{0n} = \sqrt{2}$ and $a_{mn} = 2$ for $m \neq 0$ and $n \neq 0$.

Since the elevation $\hat{\eta}_b$ and the flow velocity amplitude $\hat{\mathbf{u}}_b$ are a superposition of the contributions of all the open inlets q , we obtain

$$\hat{\eta}_b = \frac{i\omega\mu_b^2}{g} \sum_{m=n=1}^{M,N} \tilde{c}_{mn} \psi_{mn}(x, y), \quad \hat{\mathbf{u}}_b = - \sum_{m=n=1}^{M,N} \tilde{c}_{mn} \nabla \psi_{mn}(x, y) \quad (2.20)$$

where

$$\tilde{c}_{mn} = \frac{1}{\mu_b^2 k_b^2 h_b} \sum_q b_q h_q \hat{u}_q c_{mnq}$$

Hence, we now have an expression for the flow velocity amplitude $\hat{\mathbf{u}}_b = (\hat{u}_b, \hat{v}_b)$ in the basin, with \hat{u}_b and \hat{v}_b the complex flow velocity amplitudes in the cross-shore x - and alongshore y -direction:

$$\hat{u}_b = - \sum_{m=n=1}^{M,N} \tilde{c}_{mn} \frac{\partial \psi_{mn}(x, y)}{\partial x}, \quad \hat{v}_b = - \sum_{m=n=1}^{M,N} \tilde{c}_{mn} \frac{\partial \psi_{mn}(x, y)}{\partial y} \quad (2.21)$$

2.3 Parameter values

The parameter values in Table 2.1 represent the locations Georgia Bight on the Atlantic Coast and the Wadden Sea on the Northern European coast (Roos et al., 2013). The initial values for the inlet widths and depths in Table 2.1 are mean values. The individual widths are randomized around the value presented in Table 2.1 (by $(0.2 \cdot \text{rand}(0,1) + 0.9)b_j$, where $\text{rand}(0,1)$ is a random value between 0 and 1), after which they are multiplied with the constant shape factor to calculate the corresponding inlet depths.

Parameter	Symbol & unit	Value (Wadden Sea)	Value (Georgia Bight)
Tidal amplitude	Z (m)	1	1
Tidal frequency	ω (rad/s)	1.41×10^{-4}	1.41×10^{-4}
Basin width	B (m)	100×10^3	100×10^3
Basin length	L (m)	10×10^3	2×10^3
Basin depth	h_b (m)	5	2
Ocean depth	h_o (m)	20	30
Wave number	k_o (rad/m)	8.2×10^{-6}	0
Inlet length	l_j (m)	5×10^3	1×10^3
Initial inlet depth	h_j (m)	5	2
Initial inlet width	b_j (m)	1.0×10^3	0.4×10^3
Inlet shape factor	γ_j^2 (-)	0.005	0.005
Drag coefficient in inlet and basin	c_d (-)	0.0025	0.0025
Initial nr. of inlets	J (-)	40	40
Equilibrium flow velocity	U_{eq} (m/s)	1.0	1.0
Sediment import	M	1.0×10^6	1.0×10^5
Time step	Δt (year)	1	0.5

Table 2.1: Parameter values used in this study for the Wadden Sea and Georgia Bight (on the Atlantic coast) (Roos et al., 2013).

3. Tidal divides

How can hydraulic tidal divides be identified in models of multi-inlet tidal systems without topographic highs?

The objective of the first research question is to determine how tidal divides can be identified in the exploratory model by Roos et al. (2013) presented in Chapter 2. Morphological tidal divides are not included in the model, but hydraulic tidal divides can be interpreted as resulting from the flow field. Two different methods will be applied to locate the tidal divides and these methods are introduced in Section 3.1. In Section 3.2, the results of applying the identification methods are presented for systems with two inlets, three inlets and more than three inlets. In Section 3.3, the results are discussed and conclusions about the applicability of the methods are drawn in Section 3.4.

3.1 Identification methods

The first identification method of tidal divides makes use of the definition of tidal divide by Dastgheib et al. (2008): the line of minimum standard deviation over a tidal cycle of (depth-averaged) velocities is the tidal divide. Since our modelling approach yields the complex amplitude of the flow velocity in the basin, the time factor of the tidal cycle does not have to be taken into account. Therefore, the first definition of tidal divide that will be used is the following: the line of minimum amplitude of (depth-averaged) flow velocities. The second method relates to the fact that the hydraulic tidal divide is the boundary between adjacent tidal basins, i.e. tidal waves entering the back-barrier basin through two adjacent tidal inlets are “meeting” each other at the hydraulic tidal divide. Consequently, there will be a relatively large phase difference in alongshore flow velocity at the tidal divide.

Hence, the hydraulic tidal divides will be located using two different methods: (1) locating minimum amplitudes of (depth-averaged) flow velocities, and (2) locating large phase differences in the alongshore velocity (in the alongshore y -direction). Both methods make use of the (complex) tidal flow velocity amplitude in the basin.

3.1.1 Method 1: Minimum flow velocity amplitudes

The definition of the tidal divide that is used in this method is the line of minimum amplitude of the (depth-averaged) flow velocities. Usually, the local minima of the flow velocity amplitudes can be located by setting the (spatial) derivative equal to zero. However, the current approach yields complex vectors of the flow velocity amplitude, with spatial components \hat{u}_b and \hat{v}_b , and therefore finding the minima by taking the derivative is not as straightforward. Furthermore, the complex flow velocity amplitudes are discretized and calculated on what can be interpreted as a “spatial grid” and hence their derivatives are discretized and most likely nowhere exactly equal to zero. Therefore, the minimum flow velocity amplitudes have to be located without using derivatives. This is done by assuming that a tidal divide is located between every pair of adjacent tidal inlets, such that local minima in a certain range of x - and y -coordinates can be found. Furthermore, it is assumed that a tidal divide starts directly behind a barrier island. Hence, the minimum flow velocity amplitude directly behind every barrier island has to be located. Then, the seemingly continuous line of minimum flow velocity amplitudes towards the main land forms the tidal divide. Using this method, bifurcations cannot appear in one tidal divide, but adjacent tidal divides may converge.

To apply this method, firstly the open inlets have to be located. The inlet morphology is updated in the model at every time step, until an equilibrium is reached. Hence, the locations of the open inlets and thus of the barrier islands are known for every time step. The model yields the complex flow velocity amplitude $\hat{\mathbf{u}}_b$, so the norm $\|\hat{\mathbf{u}}_b\|$ of this complex vector will be considered to find the minimum values:

$$\|\hat{\mathbf{u}}_b\| = \sqrt{\hat{u}_b \overline{\hat{u}}_b + \hat{v}_b \overline{\hat{v}}_b} \quad (3.1)$$

where $\overline{\hat{u}}_b$ and $\overline{\hat{v}}_b$ are the complex conjugates of \hat{u}_b and \hat{v}_b , respectively. Combining the expressions for \hat{u}_b and \hat{v}_b in Eq. (2.21) with $\psi_{mn}(x,y)$ in Eq. (2.19) gives the following expressions for the complex (depth-averaged) flow velocity amplitude in the cross-shore x -direction:

$$\hat{u}_b = - \sum_{m=n=1}^{M,N} \tilde{c}_{mn} \frac{\partial \psi_{mn}(x,y)}{\partial x} = - \sum_{m=n=1}^{M,N} \tilde{c}_{mn} \frac{-\frac{a_{mn} m \pi}{L} \sin\left(\frac{m \pi x}{L}\right) \cos\left(\frac{n \pi y}{B}\right)}{\sqrt{BL}} \quad (3.2)$$

and in the alongshore y -direction:

$$\hat{v}_b = - \sum_{m=n=1}^{M,N} \tilde{c}_{mn} \frac{\partial \psi_{mn}(x,y)}{\partial y} = - \sum_{m=n=1}^{M,N} \tilde{c}_{mn} \frac{-\frac{a_{mn} n \pi}{B} \cos\left(\frac{m \pi x}{L}\right) \sin\left(\frac{n \pi y}{B}\right)}{\sqrt{BL}} \quad (3.3)$$

where $M = N = 50$. Note that \tilde{c}_{mn} varies over (morphodynamic) time, while $\psi_{mn}(x,y)$ varies over the locations (x,y) . Hence, \hat{u}_b and \hat{v}_b and their complex conjugates $\overline{\hat{u}}_b$ and $\overline{\hat{v}}_b$ can be calculated for every timestep and every location. From that, $\|\hat{\mathbf{u}}_b\|$ can be determined according to Eq. (3.1).

By the definition of a hydraulic tidal divide, the line where norm $\|\hat{\mathbf{u}}_b\|$ of the complex flow velocity amplitude $\hat{\mathbf{u}}_b$ is minimal forms the tidal divide. In this method, it is assumed that a tidal divide appears on the basin side of every barrier island located between a pair of adjacent open inlets. Hence, after the open inlets have been located, the lines of minimum flow velocity amplitude can be identified. Note that $\|\hat{\mathbf{u}}_b\|$ is discretized spatially. The desired number of data points in the cross-shore x -direction and the alongshore y -direction can be implemented in the model.

3.1.2 Method 2: Large phase differences

At a hydraulic tidal divide, tidal waves entering the back-barrier basin through two adjacent tidal inlets are “meeting” each other. Consequently, at that location there will most likely be a large phase difference in the alongshore y -component of the flow velocity, v_b . Recall that v_b is written as $v_b = \Re(\hat{v}_b \exp(i\omega t))$ in Eq. (2.8), where \hat{v}_b is the complex amplitude. An advantage of this complex representation is that the amplitude A and the phase angle ϕ of the alongshore flow velocity v_b are combined into the single complex amplitude \hat{v}_b , which can be written as

$$\hat{v}_b = A e^{i\phi} \quad (3.4)$$

where A is the magnitude and ϕ is the argument of \hat{v}_b . The magnitude A of the complex amplitude \hat{v}_b is the amplitude of the flow velocity v_b , while the argument ϕ of \hat{v}_b is the phase angle of the flow velocity v_b . Hence, the phase angle ϕ of the flow velocity in the y -direction can easily be determined:

$$\phi = \text{Arg}(\hat{v}_b) = \text{Arg}(a + bi) = \text{atan2}(b, a) \quad (3.5)$$

where a is the real part and b is the imaginary part of the complex amplitude \hat{v}_b (such that $\hat{v}_b = a + bi$), Arg stands for argument (of a complex number) and atan2 is a function that can

be used to calculate the argument of a complex number. It is assumed that the phase differences at the tidal divides are significantly larger than anywhere else and that they are approximately π rad (or 180° degrees). The condition for locating tidal divides is then a phase change from below π rad to above π rad, in the positive longshore y -direction. It is important to note that phase changes from above π rad to below π rad occur in the middle of open inlets.

3.2 Results of identification

In this section, the results of the identification methods from Section 3.1 will be presented. The algorithms for identifying tidal divides are run without morphological changes, so there is no evolution of inlets. To evaluate the applicability of the identification methods for different inlet morphologies, six cases with either two or three inlets are considered. Expectations about the approximate location(s) of the tidal divide(s) are presented in Table 3.1. The qualitative expectations will be compared to the results of the two methods, as the objective is to evaluate the correctness of the results and the applicability of the methods for different geometries. The results for the two identification methods are shown in surface plots, alongside a plan view of the geometry showing the locations and widths of the inlets. The parameter values that are used in the model simulations are those representing the Wadden Sea (see Table 2.1), where the number of inlets and the inlet widths (and hence depths) are modified to simulate the cases presented in Table 3.1.

Case	Inlets	Expected tidal divide(s)
1	Two, equally-sized ($b_1 = b_2$)	One, in the middle between the two open inlets
2	Two, differently-sized ($b_1 < b_2$)	One, closer to the smaller inlet than to the wider inlet
3	Three, equally-sized ($b_1 = b_2 = b_3$)	Two, in the middle between each pair of adjacent open inlets
4	Three, differently-sized ($b_2 < b_1 = b_3$)	Two, closer to the smaller inlet and, in case the middle inlet is significantly small, converging into one tidal divide towards the coast
5	Three, differently-sized ($b_2 > b_1 = b_3$)	Two, closer to the smaller inlets and, when the outer inlets are significantly small, deflecting towards the outer inlets
6	Three, differently-sized ($b_1 < b_2 < b_3$)	Two, closer to the smaller inlets and, when the smaller inlets are significantly small, deflecting towards the smaller outlets

Table 3.1: The six cases that are studied and a description of the tidal divides that are expected to be found. The exact locations and widths of the inlets are specified in Table 3.2 and 3.3.

To check whether symmetry is captured correctly by the tidal divide identification methods, the first case we study is one where both tidal inlets are of equal size and at equal distance from the sides of the basin. We expect that the tidal divide is a line straight down the middle between the two open inlets. The second case we consider again consists of two open inlets, but different in size. It is expected that a larger tidal inlet acquires a larger “area of influence”. Hence, no symmetry is expected as the hydraulic tidal should be closer to the smaller inlet. For three equally-sized inlets (Case 3), two straight tidal divides are expected to occur in the middle between the two pairs of adjacent open inlets, as again the situation in the basin should be symmetric. For the cases with three differently-sized inlets (Cases 4, 5 and 6), the tidal divides should be closer to and deflect towards the smaller inlet(s). For Case 4, where the middle inlet is smaller than the outer two, the tidal divides are even expected to converge into one tidal divide when the middle inlet is significantly smaller than its neighbouring inlets (Kragtwijk et al., 2004).

3.2.1 Two inlets

In a tidal inlet system with two inlets, only one tidal divide should occur. The cases that are considered are the case with two equally-sized inlets and two differently-sized inlets. The widths and locations of the tidal divides studied for the different cases are shown in Table 3.2.

Case	Inlets	b_1 (m)	b_2 (m)	y_1 (m)	y_2 (m)
1	Two, equally-sized ($b_1 = b_2$)	7,000	7,000	25,000	75,000
2	Two, differently-sized ($b_1 < b_2$)	3,000	10,000	25,000	75,000

Table 3.2: Inlet widths and locations for the cases with two open inlets.

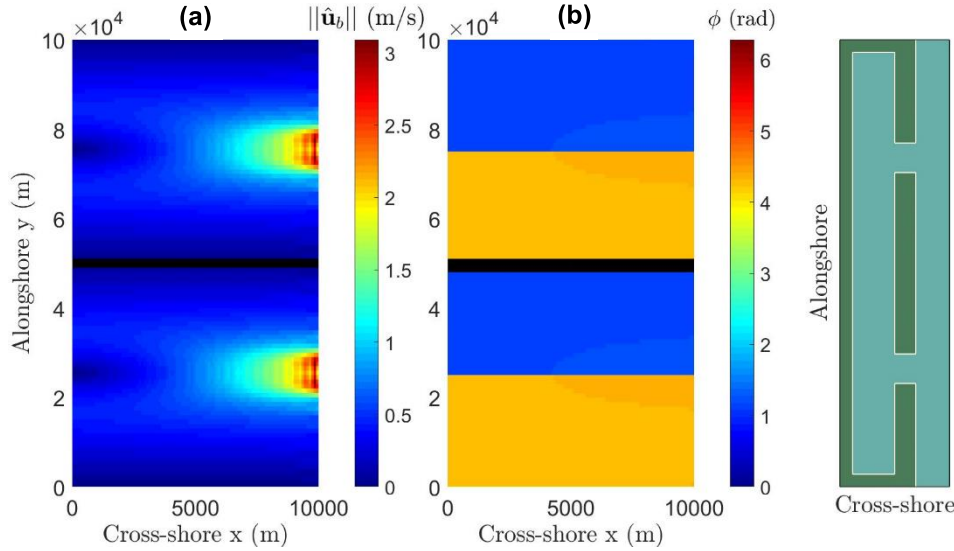


Fig. 3.1: Surface plots of (a) $\|\hat{\mathbf{u}}_b\|$ and (b) ϕ , showing the tidal divide (in black) according to (a) method 1 and (b) method 2, with two open inlets of inlet width 7 km (so equally-sized) at $y = 25$ km and $y = 75$ km.

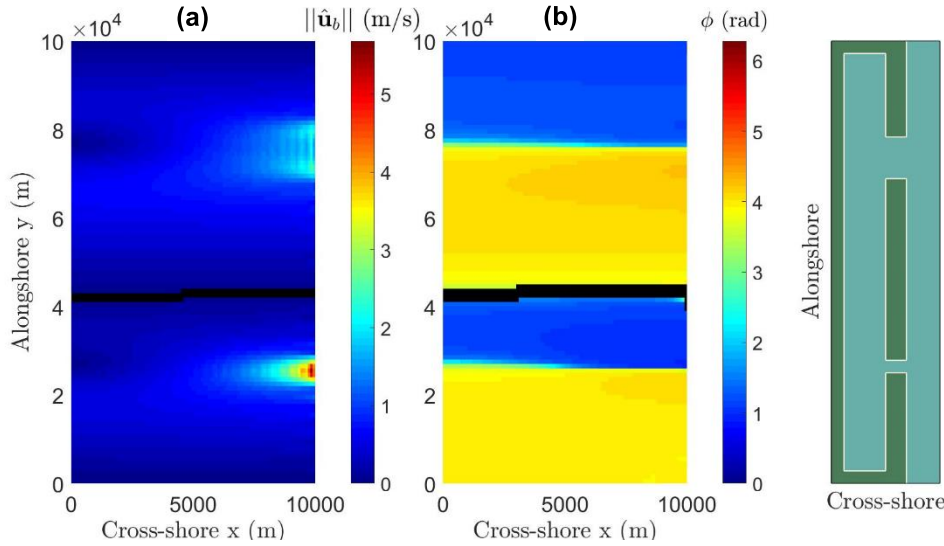


Fig. 3.2: Surface plots of (a) $\|\hat{\mathbf{u}}_b\|$ and (b) ϕ , showing the tidal divide (in black) according to (a) method 1 and (b) method 2, with two open inlets of inlet width 3 km and 10 km (so differently-sized) at $y = 25$ km and $y = 75$ km.

For two equally-sized inlets (Fig. 3.1), the result is a straight tidal divide in the middle between the two inlets. For two differently-sized inlets (Fig. 3.2), the tidal divide is located closer to the smaller inlet. Furthermore, in Fig. 3.2 a slight deflection of the tidal divide towards the smaller inlet can be seen.

3.2.2 Three inlets

When three tidal inlets are included in the multi-inlet tidal system, two tidal divides are expected to occur. Furthermore, it is expected that the tidal divide(s) will be closer to and deflect towards narrower inlets. The four cases that are considered for three tidal inlets are presented in Table 3.3 and the results are shown in Fig. 3.3, 3.4, 3.5 and 3.6.

Case	Inlets	b_1 (m)	b_2 (m)	b_3 (m)	y_1 (m)	y_2 (m)	y_3 (m)
3	Three, equally-sized ($b_1 = b_2 = b_3$)	7,000	7,000	7,000	25,000	50,000	75,000
4	Three, differently-sized ($b_2 < b_1 = b_3$)	10,000	2,000	10,000	25,000	50,000	75,000
5	Three, differently-sized ($b_2 > b_1 = b_3$)	5,000	10,000	5,000	25,000	50,000	75,000
6	Three, differently-sized ($b_1 < b_2 < b_3$)	3,000	5,000	10,000	25,000	50,000	75,000

Table 3.3: Inlet widths and locations for the cases with three open inlets.

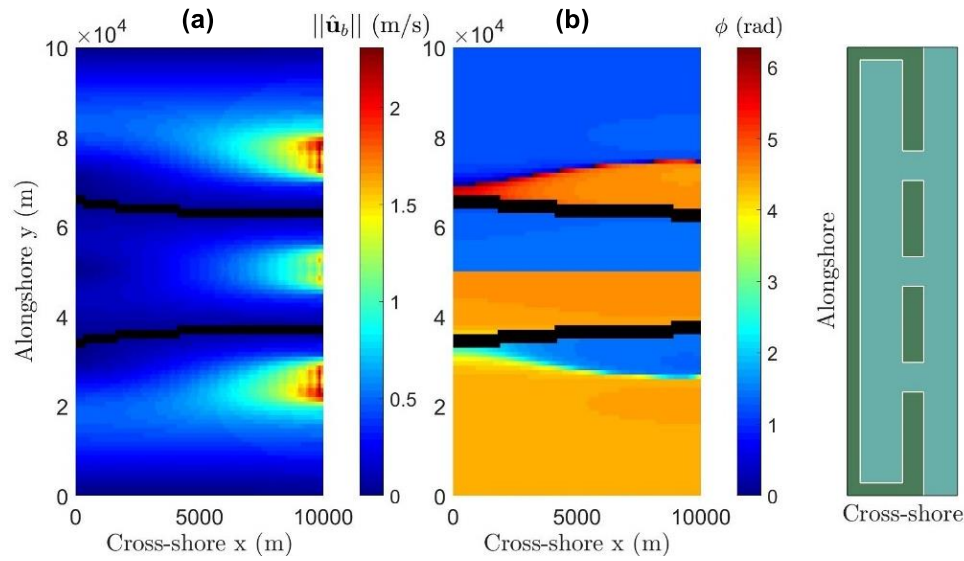


Fig. 3.3: Surface plots of (a) $\|\hat{\mathbf{u}}_b\|$ and (b) ϕ , showing the tidal divide (in black) according to (a) method 1 and (b) method 2, with three open inlets of inlet width 7 km (so equally-sized) at $y = 25$ km, $y = 50$ km and $y = 75$ km.

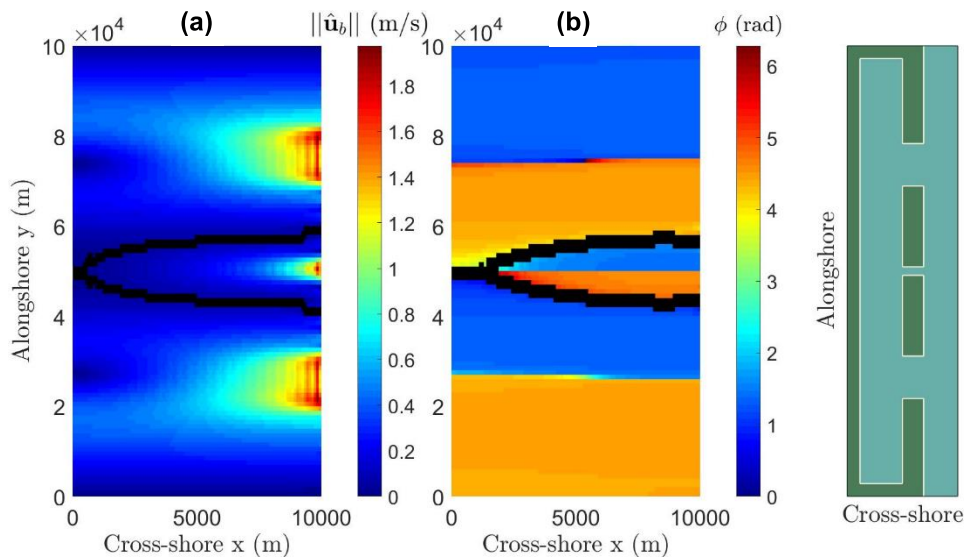


Fig. 3.4: Surface plots of (a) $\|\hat{\mathbf{u}}_b\|$ and (b) ϕ , showing the tidal divide (in black) according to (a) method 1 and (b) method 2, with three open inlets of inlet width 10 km, 2 km and 10 km (so differently-sized) at $y = 25$ km, $y = 50$ km and $y = 75$ km.

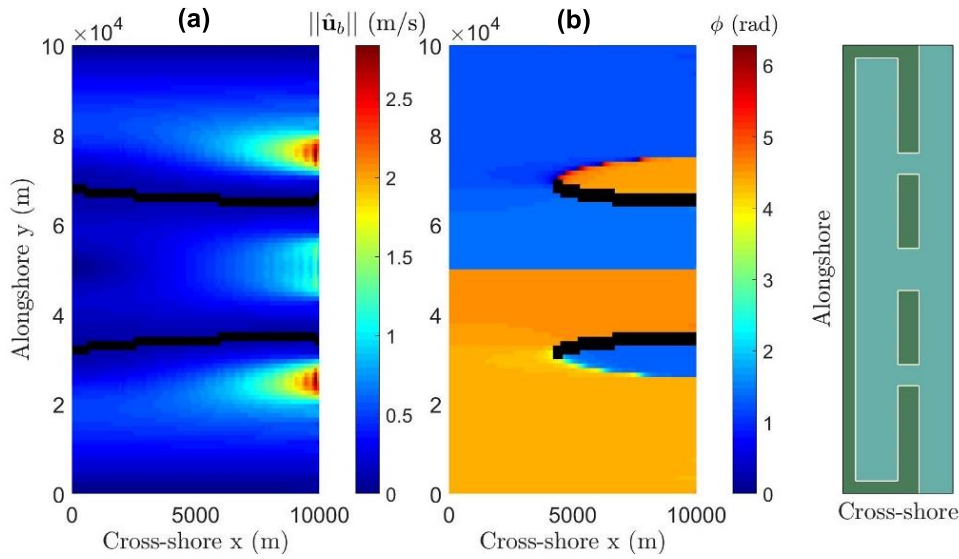


Fig. 3.5: Surface plots of (a) $||\hat{\mathbf{u}}_b||$ and (b) ϕ , showing the tidal divide (in black) according to (a) method 1 and (b) method 2, with three open inlets of inlet width 5 km, 10 km and 5 km (so differently-sized) at $y = 25$ km, $y = 50$ km and $y = 75$ km.

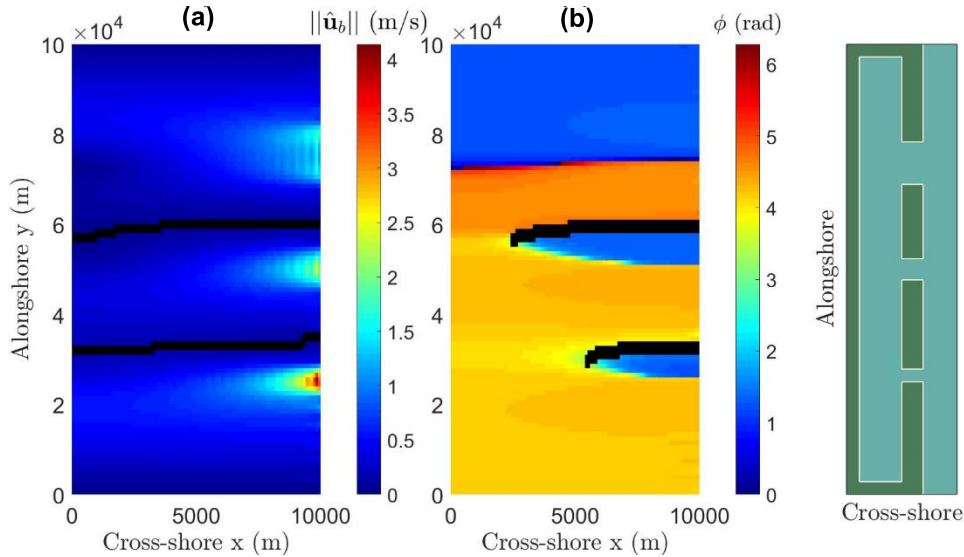


Fig. 3.6: Surface plots of (a) $||\hat{\mathbf{u}}_b||$ and (b) ϕ , showing the tidal divide (in black) according to (a) method 1 and (b) method 2, with three open inlets of inlet width 3 km, 5 km and 10 km (so differently-sized) at $y = 25$ km, $y = 50$ km and $y = 75$ km.

For three equally-sized inlets, two tidal divides are located in the middle between two adjacent inlets, but they are not straight as they deflect slightly towards the sides of the basin (Fig. 3.3). For differently-sized inlets, the tidal divides are located closer to the smaller inlet(s) and they also deflect slightly to those inlets (Fig 3.4, 3.5 and 3.6). As can be seen in Fig. 3.4, it is also possible that adjacent tidal divides converge into one tidal divide, when the middle open inlet in the middle is sufficiently small. Comparing Fig. 3.4(a) to Fig. 3.4(b), there is a slight difference between the locations where this convergence occurs according to the two identification methods. However, we do not know which result is more accurate, as there are no data available to assess these qualitative results.

3.2.3 More than three inlets

To analyse the applicability of both tidal divide identification methods for situations with more than three inlets, an equilibrium situation resulting from a model run with the Wadden Sea parameters (see Table 2.1) is used.

It can be seen that the first identification method (Fig. 3.7(a)) always yields tidal divides that reach all the way to the main land, while the second method (Fig. 3.7(b)) does not.

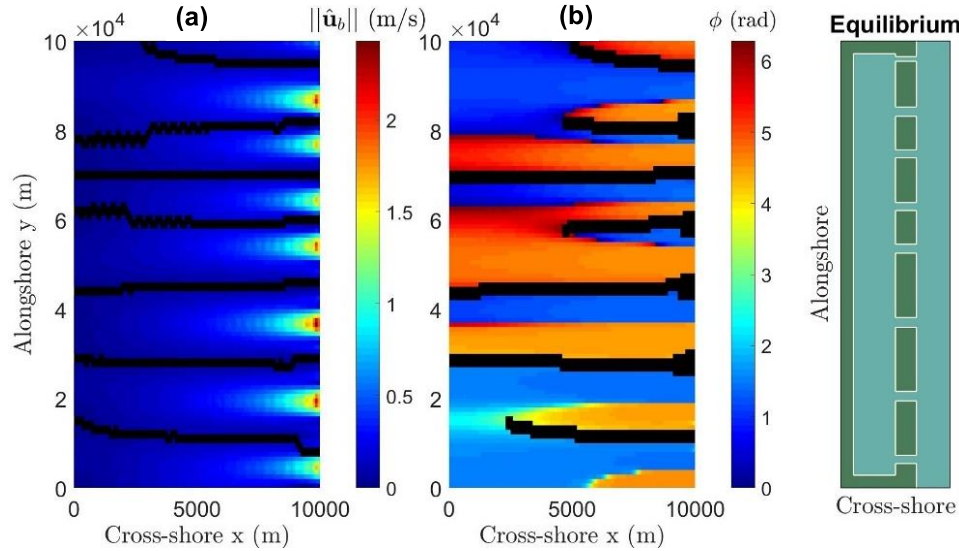


Fig. 3.7: Surface plots of (a) $\|\hat{\mathbf{u}}_b\|$ and (b) ϕ , showing the tidal divide (in black) for (a) method 1 and (b) method 2, for an equilibrium situation for the Wadden Sea parameter values, as shown in the most right figure (see Table 2.1).

3.3 Subconclusions

Two possible methods of identifying hydraulic tidal divides are studied, which both make use of the complex amplitude of the flow velocity in the back-barrier basin. The first method uses the definition of tidal divides as lines of minimum flow velocity amplitude (Dastgheib et al., 2008). It is assumed that such a line is located between every barrier island and the main land. The second method makes use of large phase differences in the alongshore flow velocity, as hydraulic tidal divides are locations where the tidal waves through two (adjacent) open inlets “meet” each other and hence a large phase difference in alongshore flow velocity occurs there. The results of both methods for different cases are shown in Table 3.4.

From the results of both identification methods, it is evident that the tidal divides are located closer to smaller inlets and they deflect towards the smaller inlets as they approach the main land. Consequently, the tidal divides converge towards each other when an inlet is much smaller than its two neighbouring inlets. When the middle inlet is significantly small, its adjacent tidal divides converge into one tidal divide. An important feature of identification methods for tidal divides is whether they are able to reproduce such tidal divides, as they also occur in nature when one tidal inlet is significantly small with respect to two adjacent inlets (Kragtwijk et al., 2004). Both methods are capable of reproducing these tidal divides and it is difficult to state which result is more accurate, as there are no data or observations to which the results can be compared.

The results for both methods are similar, but in the first method the assumption is made that the tidal divide is a line over the entire distance between a barrier island and the main land. Hence, the results of the first method of course show seemingly continuous lines all the way

from the barrier island to the main land. Consequently, tidal subbasin areas can be calculated directly from the results of that identification method. This is not the case for the second method, as such an assumption is not included in that method. This can of course be solved by assuming and imposing that the tidal divide continues from the “end” of the identified tidal divide towards the main land in one straight line. Unfortunately, this would undoubtedly reduce the accuracy of the method that is based on large phase differences. This is undesirable and probably unnecessary, as the first identification method seems to provide a respectable alternative to identify the tidal divides towards the main land that is actually based on the model results, namely the minimum flow velocity amplitudes in the basin. Therefore, the method that locates the lines of minimum flow velocity amplitudes in the basin will be used in the remaining part of this research to identify tidal divides and subsequently calculate the surface areas of tidal subbasins. The method can also be applied over time during a model simulation, if the objective is to study the development of tidal subbasin areas over time.

Case	Inlets	Expected tidal divide(s)	Method 1	Method 2
1	Two, equally-sized ($b_1 = b_2$)	One, in the middle between the two open inlets	Yes, a straight line	Yes, a straight line
2	Two, differently-sized ($b_1 < b_2$)	One, closer to the smaller inlet than to the wider inlet	Yes	Yes
3	Three, equally-sized ($b_1 = b_2 = b_3$)	Two, in the middle between each pair of adjacent open inlets	Yes, not a straight line	Yes, not a straight line
4	Three, differently-sized ($b_2 < b_1 = b_3$)	Two, closer to the smaller inlet and, in case the middle inlet is significantly small, converging into one tidal divide towards the coast	Yes	Yes
5	Three, differently-sized ($b_2 > b_1 = b_3$)	Two, closer to the smaller inlets and, in case the outer inlets are significantly small, deflecting towards the outer inlets	Yes	Yes, but not reaching the main land
6	Three, differently-sized ($b_1 < b_2 < b_3$)	Two, closer to the smaller inlets and, in case the smaller inlets are significantly small, deflecting towards the smaller outlets	Yes	Yes, but not reaching the main land

Table 3.4: Expected tidal divides for the different cases that are considered, and an indication of whether the results from the two methods agree with the expectations.

4. Tidal prism - inlet area relationship

To what extent do the model results agree with the empirical tidal prism - inlet area relationships?

The objective of this research question is to compare the model results with the O'Brien-Jarrett Law, which is an empirical relationship between tidal prisms and inlets' cross-sectional areas (P - Ω relationship). The methodology that is applied is introduced in Section 4.1, including the calculation methods of tidal prisms. In Section 4.2, the results of the comparison are shown for parameter sets representing the Wadden Sea and the Georgia Bight (Atlantic coast). In Section 4.3, the accuracy of the tidal prism approximation is discussed. Then in Section 4.4, the temporal development of the tidal prism - inlet area relationship during the system's evolution is investigated. A discussion of the results and the subconclusions are presented in Section 4.5.

4.1 Comparison method

To enable us to compare the model results to the empirical tidal prism - inlet area relationship that was introduced in Section 1.1.3, the coefficients of that empirical O'Brien-Jarrett Law have to be known. They are presented in Section 4.1.1. Then, the tidal prisms resulting from the model have to be calculated (Section 4.1.2) in order to determine the coefficients according to the model (Section 4.1.3). These coefficients according to the model can then be compared to the empirically determined coefficients, which is done in Section 4.2.

4.1.1 Empirical O'Brien-Jarrett Law

Empirical relationships between the tidal prism and the cross-sectional area of a tidal inlet can be used to predict the long-term morphological equilibrium and hence development of tidal inlet systems. In a modelling context, they can also be used to validate models of tidal inlet systems. The first attempts to actually determine an empirical relationship between the inlet's cross-sectional area, Ω , and the tidal prism, P , were by O'Brien (1931, 1969). He proposed an empirical relationship of the form

$$\Omega = kP^\alpha \quad (4.1)$$

where Ω is the minimum cross-sectional area of the tidal inlet, i.e. below mean water level, P is the tidal prism based on the spring tidal range, $\alpha = 0.85$ and $k = 4.69 \times 10^{-4}$, where Ω is in ft^2 and P is in ft^3 . Later, Jarrett (1976) attempted to validate this empirical relationship by considering a large number of tidal inlets in North America, and determining the coefficients k and α through regression analysis. The results of his analysis are shown in Fig. 4.1 and presented in Table 4.1.

Jarrett (1976) distinguished between various groups of inlets. He used data from inlets in North-America, where he distinguished between the Atlantic coast, the Pacific coast and the Gulf of Mexico and whether no jetties, one jetty or two jetties were present at the studied location. A similar trend as found by Jarrett (1976) also emerged from the model experiments of Mayor-Mora (1973) and Seabergh et al. (2001) that were carried out under controlled conditions including wave actions (D'Alpaos et al., 2009). Byrne et al. (1981) also performed model experiments, but for smaller inlets. The results of all these experiments are also shown in Fig. 4.1. The systems for which the empirical relationship is determined are assumed to be in equilibrium, so for now it is assumed that the O'Brien-Jarrett Law holds (only) for tidal inlet systems that are in equilibrium. Note that in Section 4.4, the tidal prism - inlet area relationship for systems that are not yet in equilibrium is studied.

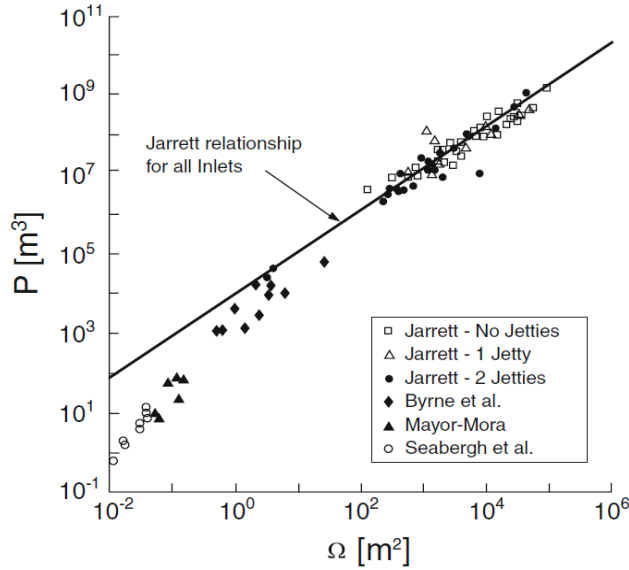


Fig. 4.1: Tidal prism P vs. equilibrium cross-sectional area Ω , for field and laboratory data (D'Alpaos et al., 2009).

Location	No. of jetties	k ($m^{2-3\alpha}$)	α (-)	95% CI k	95% CI α	No. of data points
Atlantic	0,1,2	7.75×10^{-6}	1.05	$7.14 \times 10^{-6} - 8.41 \times 10^{-6}$	0.99 - 1.12	79
	0,1	5.37×10^{-6}	1.07	$4.86 \times 10^{-6} - 5.92 \times 10^{-6}$	0.99 - 1.16	50
	2	5.77×10^{-5}	0.95	$4.98 \times 10^{-5} - 6.69 \times 10^{-5}$	0.81 - 1.09	29
Pacific	0,1,2	1.19×10^{-4}	0.91	$1.07 \times 10^{-4} - 1.32 \times 10^{-4}$	0.86 - 0.97	47
	0,1	1.91×10^{-6}	1.03	$1.57 \times 10^{-6} - 2.32 \times 10^{-6}$	0.99 - 1.21	16
	2	5.28×10^{-4}	0.85	$4.96 \times 10^{-4} - 5.23 \times 10^{-4}$	0.81 - 0.88	31
Gulf of Mexico	0,2	5.02×10^{-4}	0.84	$4.25 \times 10^{-4} - 5.93 \times 10^{-4}$	0.73 - 0.95	36
	0	3.51×10^{-4}	0.86	$2.97 \times 10^{-4} - 4.16 \times 10^{-4}$	0.73 - 0.99	30
All data	0,1,2	5.74×10^{-5}	0.95	$5.36 \times 10^{-5} - 6.13 \times 10^{-5}$	0.91 - 1.00	162
	0,1	1.04×10^{-5}	1.03	$9.47 \times 10^{-6} - 1.13 \times 10^{-5}$	0.97 - 1.10	96
	2	3.76×10^{-4}	0.86	$3.44 \times 10^{-4} - 4.11 \times 10^{-4}$	0.91 - 0.92	66

Table 4.1: Results of the regression analysis by Jarrett (1976) for coefficients k and α , where inlet area Ω is in ft^2 and tidal prism P is in ft^3 .

Dieckmann et al. (1988) have analysed the tidal prism - inlet area relationship $\Omega = kP^\alpha$ for the Wadden Sea and they have determined the coefficients k and α . They used the data from 26 from a total of 28 tidal inlets and 11 inlet-type structures along the coast of the “German Bight” between Den Helder in the Netherlands and Skallingen in Denmark. It turned out that all data points lie within the 95% confidence limits and are very close to the regression curve found by Jarrett (1976). With Ω and P in metric units, the results for the German Bight inlets (Dieckmann et al., 1988) and the American inlets (Jarrett, 1976) are presented in Table 4.2.

Location	k	α
German Bight (Wadden Sea)	3.720×10^{-4}	0.915
Atlantic coast	3.039×10^{-5}	1.050
Gulf coast	9.311×10^{-4}	0.840
Pacific coast	2.833×10^{-4}	0.910

Table 4.2: Results of the analyses by Dieckmann et al. (1988) and Jarrett (1976), where inlet area Ω is in m^2 and tidal prism P is in m^3 .

4.1.2 Calculation of tidal prism

To compare the empirical O'Brien-Jarrett Law to the model results, the tidal prism P resulting from the model has to be calculated. The tidal prism P is defined as the volume of water entering a tidal basin during flood tide and leaving the basin again during ebb tide.

As introduced in Section 1.1.3, there are different ways of calculating the tidal prism, differing in their complexity and hence accuracy. The first method we will consider is used by e.g. Krishnamurthy (1977) and it is based on obtaining the flow discharge through the inlet by multiplying the flow velocity with the width and depth of the inlet, and integrating over half the tidal cycle to obtain the tidal prism. This yields the exact tidal prism for the model that is used in this study, which can be calculated as

$$P_{j,exact} = \frac{1}{2} \int_0^T |BU(t)D(t)| dt = \frac{1}{2} b_j h_j \int_0^T |u_j(t)| dt \quad (4.2)$$

where B is the width of the rectangular cross-section of tidal inlet j , U is the local depth-averaged velocity and D is the instantaneous flow depth at the inlet caused by a sinusoidal tidal forcing with period T ($= 2\pi/\omega$, where ω is the tidal frequency) (Krishnamurthy, 1977). Since the inlet geometry does not change on the time scale of the hydrodynamics, the width B of the cross-section of the tidal inlet is b_j . Similarly, $D(t)$ can be written as h_j . The local depth-averaged velocity at the inlet is $u_j(t)$, which can be written as $u_j(t) = \Re\{\hat{u}_j \exp(i\omega t)\}$, where we know that $U_j = |\hat{u}_j|$. Hence, this gives the following expression for the tidal prism in Eq. (4.2):

$$\begin{aligned} P_{j,exact} &= \frac{1}{2} b_j h_j \int_0^T |u_j(t)| dt = \frac{1}{2} b_j h_j \int_0^T |\Re\{\hat{u}_j \exp(i\omega t)\}| dt = \frac{1}{2} b_j h_j \int_0^T |U_j \cos(\omega t)| dt \\ &= \frac{1}{2} b_j h_j \left(\int_{3T/4}^T U_j \cos(\omega t) dt + \int_{T/4}^{3T/4} -U_j \cos(\omega t) dt + \int_0^{T/4} U_j \cos(\omega t) dt \right) \\ &= \frac{1}{2} b_j h_j \left(\left[\frac{U_j}{\omega} \sin(\omega t) \right]_{3T/4}^T + \left[-\frac{U_j}{\omega} \sin(\omega t) \right]_{T/4}^{3T/4} + \left[\frac{U_j}{\omega} \sin(\omega t) \right]_0^{T/4} \right) \\ &= \frac{1}{2} b_j h_j \frac{U_j}{\omega} (1 + 2 + 1) = 2b_j h_j U_j / \omega \end{aligned} \quad (4.3)$$

where b_j and h_j are the width (m) and depth (m) of open inlet j respectively, U_j is the flow velocity amplitude (m/s) in open inlet j and ω is the tidal frequency (rad/s) of the outer sea.

The cross-sectional areas of the inlets, i.e. inlet areas, are given by

$$\Omega_j = h_j \cdot b_j \quad (4.4)$$

where Ω_j is the minimum (below mean sea-level) cross-sectional area (m²) of inlet j and h_j and b_j are the inlet depth (m) and width (m), respectively. Hence, Eq. (4.3) can be written as

$$P_{j,exact} = 2\Omega_j U_j / \omega \quad (4.5)$$

which is then the actual tidal prism resulting from the model.

The second calculation method is an approximation of the tidal prism, which is only valid when the size of the tidal basin is sufficiently small compared to the tidal wave length, such that the spatial variation in water level in the basin can be neglected (Kragtwijk, 2002). Thus, this method assumes a uniform water level throughout the basin, such that

$$P_{j,approx} = H \cdot A_{b,j} \quad (4.6)$$

where $P_{j,approx}$ is the approximation of the tidal prism (m³) corresponding to open inlet j , H is the tidal range (m) and $A_{b,j}$ is the surface area of the tidal subbasin (m²) corresponding to open inlet j . This is also the method of calculating the tidal prism proposed by Bruun (1978), who calculated the tidal prism as the ‘‘watershed area’’ (tidal (sub)basin area) times twice the tidal amplitude. Hughes (2002) also observed that the tidal prism can be approximated as $P = \varphi 2aS$,

where φ is an empirical factor accounting for the effects of non-sinusoidal tides, a is the amplitude of the tidal forcing and S is the surface area of the tidal basin. Hence, for sinusoidal tides, the method used by Hughes (2002) is the same as the methods used by e.g. Bruun (1978) and Kragtwijk (2002).

To approximate the tidal prism from the model results, the tidal divides have to be located first. They form the boundaries between the tidal basins, so their locations are required to calculate the tidal subbasin areas $A_{b,j}$. Therefore, the tidal divides are located using the first method described in Section 3.1.1. The area between two neighbouring (in the alongshore direction) tidal divides is then the basin area $A_{b,j}$. The tidal range H is twice the tidal amplitude Z , which is an input parameter of the model depending on the location that is considered.

4.1.3 Calculation of coefficients

To validate whether the model results comply with the O'Brien-Jarrett Law, the model is run several times, where it is assumed that 50 model runs is sufficient to determine the coefficients k and α . The input of the model are the parameter values shown in Table 2.1 for the different locations. The development of the inlets and hence the model output is different for every model run, because the initial inlet widths and depths that are implemented in the model are actually mean values. The individual inlet widths are randomized around the values shown in Table 2.1, after which the initial inlet depths are calculated using the constant shape factor. Subsequently, the model output is used to calculate the inlet areas Ω_j and the corresponding tidal prisms P_j for every inlet j (see Eq. (4.5) and (4.6)). The O'Brien-Jarrett Law is empirically determined for tidal inlet systems that are assumed to be in equilibrium (D'Alpaos et al., 2009), so the model is run until an equilibrium situation is reached and only the resulting inlets' cross-sectional areas and tidal prisms are used in the analysis. The values of Ω_j and P_j are plotted in a similar loglog-plot as Fig. 4.1 (with the same value ranges on the axes to allow us to also compare visually) and the coefficients k and α of the relationship $\Omega = kP^\alpha$ are determined. To this end, a function that complies with the O'Brien-Jarrett Law is fitted to the data. This function is a first degree polynomial of the form

$$\ln \Omega = \alpha \cdot \ln P + \ln k \quad (4.7)$$

such that the coefficients of the polynomial are α and $\ln k$. Hence, the values of the coefficients k and α are determined using the polynomial coefficients of this fitted polynomial curve. Finally, the resulting values of k and α are compared to the coefficient values in Table 4.2.

The expression in Eq. (4.5) is a linear relation between Ω_j and P_j . Therefore, for this model we would expect a linear relation between Ω_j and P_j (so $\alpha = 1$ in Eq. (4.1)). As the O'Brien-Jarrett Law is based on observations of systems that are assumed to be in equilibrium, the law is applicable in equilibrium situations. The flow velocity U_j in the inlet is then equal to the equilibrium flow velocity U_{eq} . Hence, the relationship between the cross-sectional areas of the inlets and the tidal prisms in the model largely depends on the equilibrium flow velocity, as from Eq. (4.5) it follows that

$$k = \frac{\omega}{2U_{eq}}, \quad \alpha = 1 \quad (4.8)$$

in Eq. (4.1). Thus, for this model we expect a relationship between the exact tidal prisms $P_{j,exact}$ and inlet areas Ω_j of the form $\Omega = kP^\alpha$ (see Eq. (4.1)), where k and α are given by Eq. (4.8).

4.2 Results for different parameter sets

The parameter sets that are used for the runs for different locations, representing the Wadden Sea and Georgia Bight, are presented in Table 2.1. The model is run 50 times with the same set of parameter values, each run giving different results due to the slight difference in initial inlet size. Once the system is in equilibrium, the tidal prisms and cross-sectional inlet areas are calculated. Herein, $P_{j,approx}$, is calculated using the tidal basin area (see Eq. (4.6)), while $P_{j,exact}$ depends on the flow velocity in the inlet and the inlet area (see Eq. (4.5)). From a plot of the tidal prisms P_j against the inlet areas Ω_j , the coefficients k and α of the tidal prism cross-sectional area relationship in Eq. (4.1) are calculated and compared to the values found by Jarrett (1976) and Dieckmann et al. (1988).

4.2.1 Wadden Sea runs

The parameter values for the Wadden Sea (see Table 2.1) are implemented in the model, which is run 50 times until it is in equilibrium each time. The tidal prisms $P_{j,exact}$ are calculated according to Eq. (4.5) and inlet areas Ω_j according to Eq. (4.4) for every open inlet j . The results of this are plotted in Fig. 4.2.

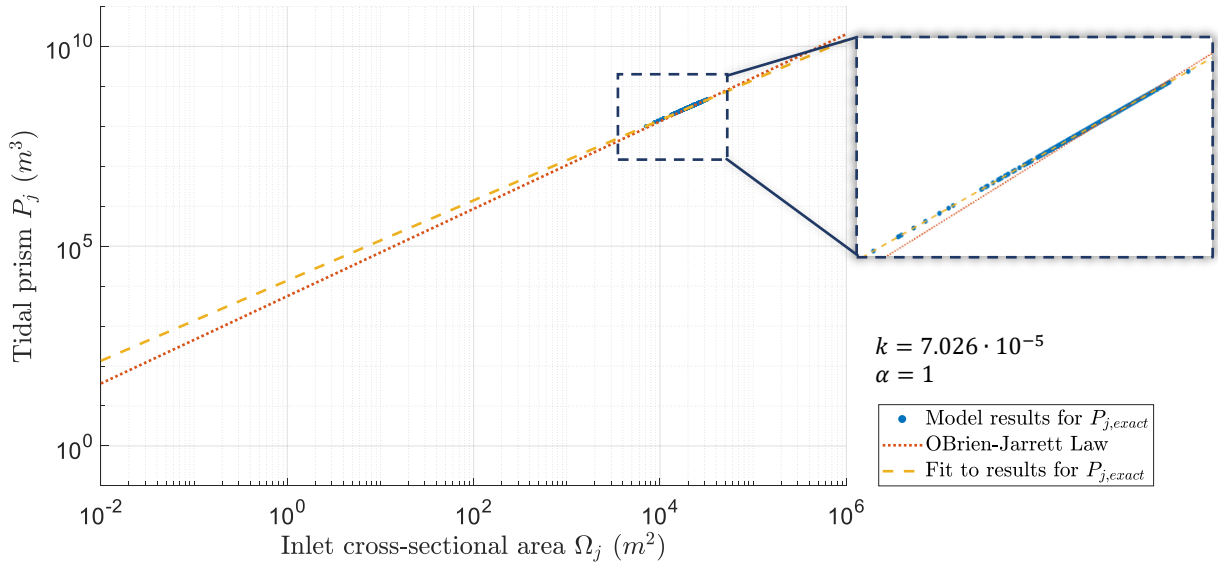


Fig. 4.2: Scatter plot of tidal prisms $P_{j,exact}$ vs. inlet areas Ω_j in equilibrium, with the O'Brien-Jarrett Law and the function that is fitted to the data (Wadden Sea).

The results show that a relationship of the form presented in Eq. (4.1) with coefficients k and α in Eq. (4.8) is indeed satisfied.

The same model runs that were used for Fig. 4.2, are also used to study the relation between the approximated tidal prism $P_{j,approx}$ (according to Eq. (4.6)), and the inlet's cross-sectional area. The results of this are shown in Fig. 4.3. The scatter in the results from $P_{j,approx}$ shown in Fig. 4.3 is so substantial that it is a challenging assignment to fit a first-degree polynomial of the form $\ln \Omega = \alpha \ln P + \ln k$ to the data. Nevertheless, such a fit results in $k = 970.9$ and $\alpha = 0.159$. Removing the significant outliers does not significantly change these coefficients, as the scatter in the results remains substantial. Comparing Fig. 4.3 to Fig. 4.2, we can deduce that the scatter in the model results depends on the accuracy of the tidal prism approximation. This will be quantified (using the coefficient of determination) and discussed in Section 4.3.

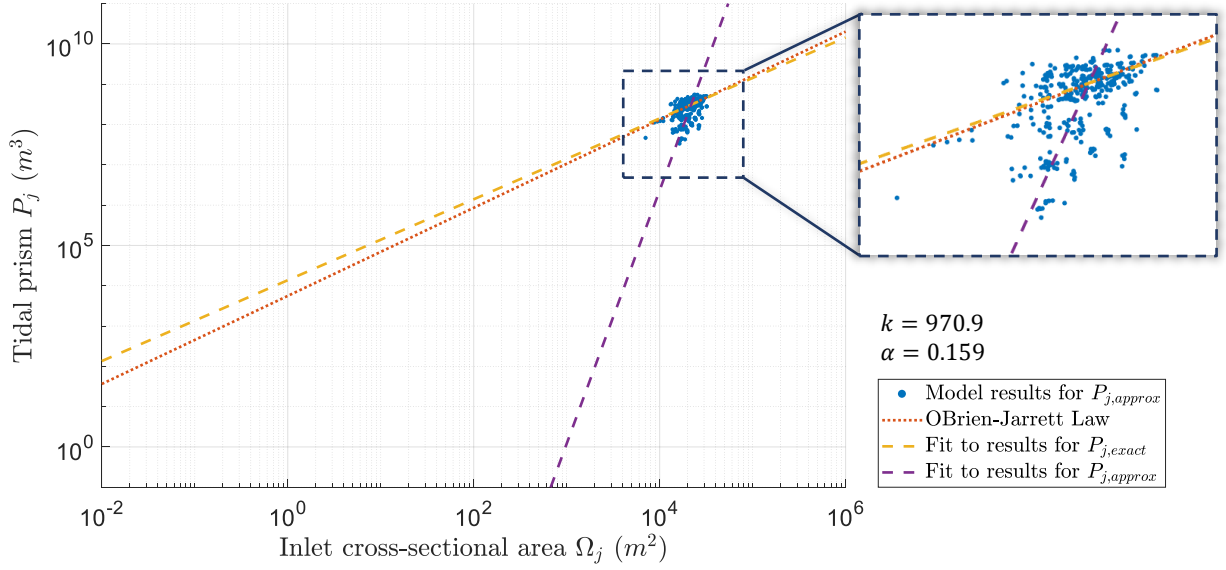


Fig. 4.3: Scatter plot of tidal prisms $P_{j,approx}$ vs. inlet areas Ω_j in equilibrium, with the O'Brien-Jarrett Law and the function that is fitted to the data (Wadden Sea).

4.2.2 Atlantic coast runs

The set of parameter values for the Georgia Bight on the Atlantic coast is presented in Table 2.1. The model again is run 50 times until it is in equilibrium each time. The results are shown in Fig. 4.4 and Fig. 4.5.

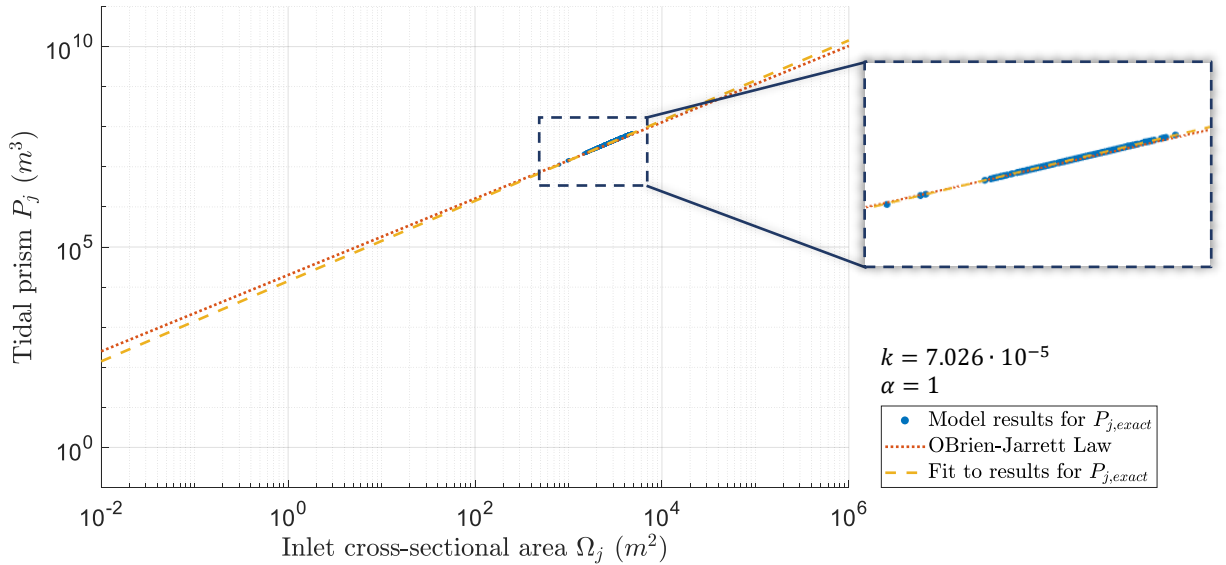


Fig. 4.4: Scatter plot of tidal prisms $P_{j,exact}$ vs. inlet areas Ω_j in equilibrium, with the O'Brien-Jarrett Law and the function that is fitted to the data (Georgia Bight).

The values of k and α resulting from $P_{j,exact}$ (shown in Fig. 4.4) are $k = 7.026 \cdot 10^{-5}$ and $\alpha = 1$. Hence, a tidal prism - inlet area relationship of the form in Eq. (4.1) with coefficients according to Eq. (4.8) is also satisfied by the model results that are obtained using the Georgia Bight parameter set.

For $P_{j,approx}$ (shown in Fig. 4.5), we obtain $k = 294.4$ and $\alpha = 0.146$. Fig. 4.5 shows a few outliers that largely influence the function that is fit to the data. Removing these outliers results in a different fit, as shown in Fig. 4.6.

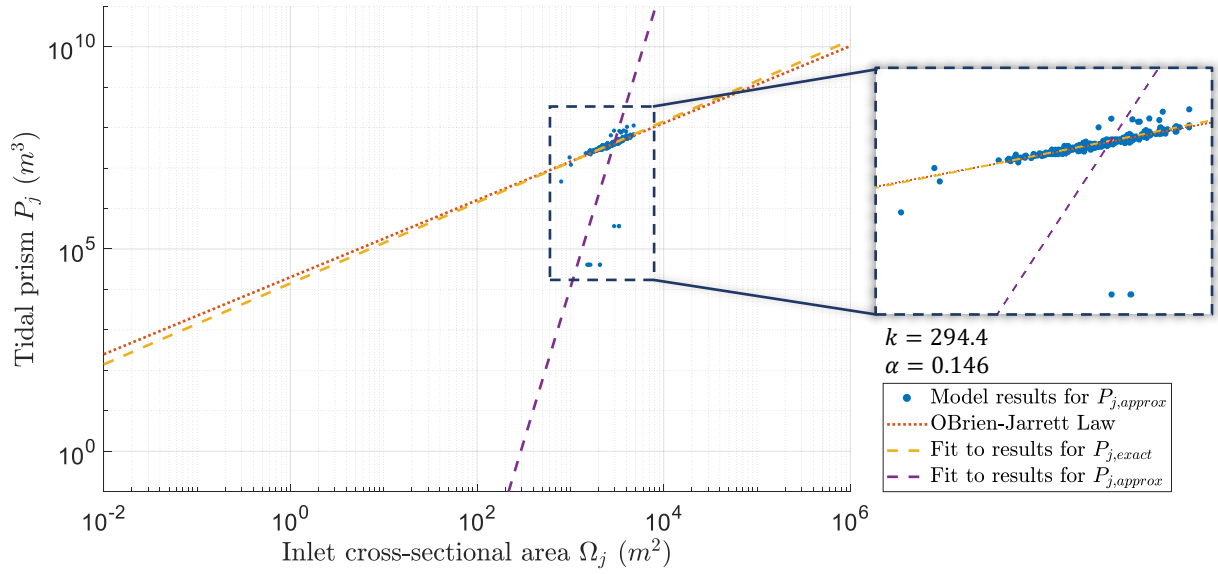


Fig. 4.5: Scatter plot of tidal prisms $P_{j,approx}$ vs. inlet areas Ω_j in equilibrium, with the O'Brien-Jarrett Law and the function that is fitted to the data (Georgia Bight).

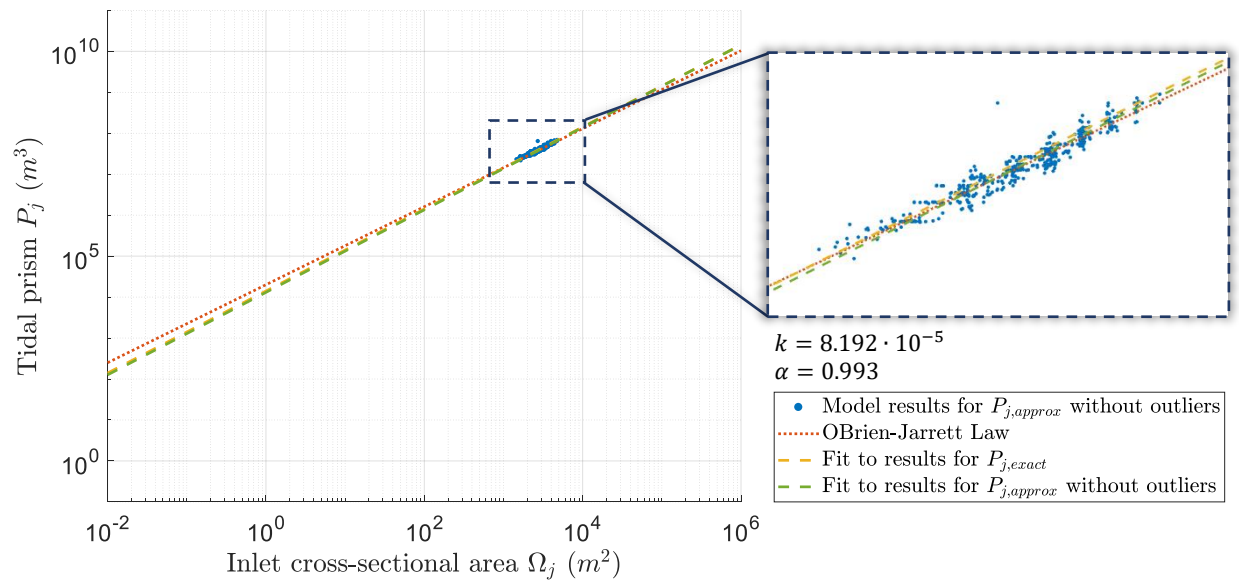


Fig. 4.6: Scatter plot of tidal prisms $P_{j,approx}$ vs. inlet areas Ω_j in equilibrium, with the O'Brien-Jarrett Law and the function that is fitted to the data without outliers (Georgia Bight).

The values of k and α resulting from the model results for $P_{j,approx}$ without outliers are $k = 8.192 \cdot 10^{-5}$ and $\alpha = 0.993$. As can be seen in Fig. 4.6, these results provide a fit that is remarkably close to the function that is fitted to the actual tidal prisms calculated from the model. Hence, for the Georgia Bight, using both tidal prism calculation methods, very similar tidal prism - inlet area relationships are obtained. The accuracy of the tidal prism approximation under different circumstances will be discussed in Section 4.3.

The functions that are fit to the model results for $P_{j,approx}$ and $P_{j,exact}$ using the Georgia Bight parameter set are both remarkably close to the O'Brien-Jarrett Law of the form $\Omega = kP^\alpha$ with empirical coefficients k and α determined by Jarrett (1976). They are not exactly equal, which is expected considering the relation between the tidal prism and the inlet area in the model.

4.3 Accuracy of tidal prism approximation

The scatter in the relationship between $P_{j,approx}$ and Ω_j is a result of the (in)accuracy of the tidal prism approximation. In Fig. 4.7, the tidal prism approximations $P_{j,approx}$ are plotted against the actual tidal prisms $P_{j,exact}$ for both the Wadden Sea runs (Fig. 4.7(a)) and the Georgia Bight runs (Fig. 4.7(b)). For both the Wadden Sea and the Georgia Bight, the same model data is used as for the O'Brien-Jarrett Law in the previous section where the model is run 50 times until the system is in equilibrium each time. The coefficient of determination R^2 is used to quantify the accuracy of the approximation.

R^2

The coefficient of determination R^2 is calculated as

$$R^2 = 1 - \frac{SS_{res}}{SS_{tot}}$$

where $SS_{res} = \sum (P_{j,approx} - P_{j,exact})^2$ and $SS_{tot} = \sum (P_{j,approx} - \text{mean}(P_{j,approx}))^2$ are the residual sum of squares and the total sum of squares, respectively.

The sum Σ is taken over all data points resulting from 50 model runs.

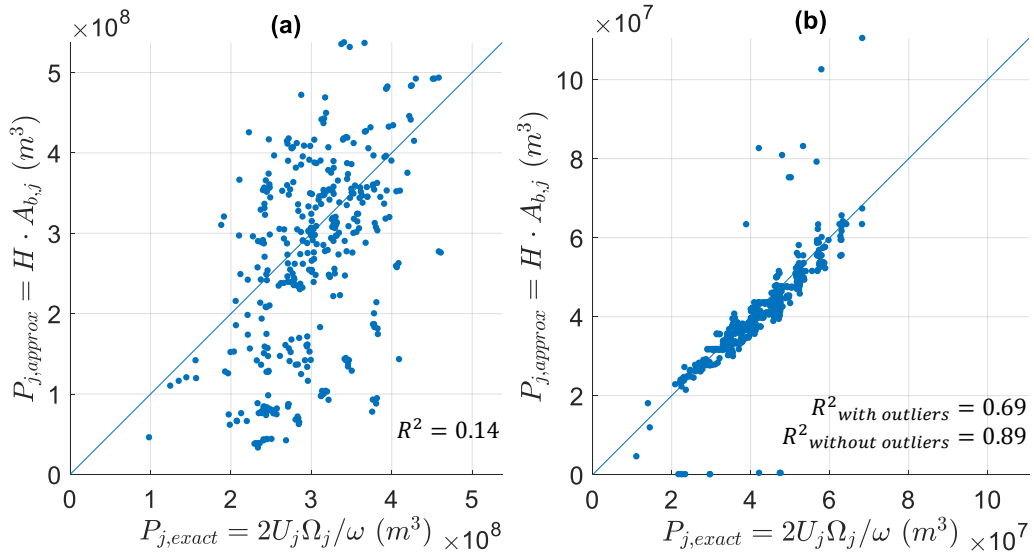


Fig. 4.7: Scatter plot of $P_{j,approx}$ vs. $P_{j,exact}$ for (a) the Wadden Sea parameter set and (b) the Georgia Bight parameter set (see Table 2.1), where R^2 is the coefficient of determination and the line represents the ideal situation in which the approximated and the actual tidal prisms are equal.

The scatter in the tidal prisms for the Wadden Sea parameter set, as shown in Fig. 4.7(a), is much more significant than the scatter for the Georgia Bight runs. For the Georgia Bight (see Fig. 4.7(b)), the approximated values are quite similar to the actual tidal prisms with a coefficient of determination of 0.69, but some outliers are present in the data. These outliers are caused by inlets that are small and close to the sides of the basin. The area of influence of these inlets is small, but their tidal subbasin areas are decreased even more by the edge of the basin. Consequently, $P_{j,approx}$ is significantly smaller than $P_{j,exact}$ for these inlets. An example of this effect can be seen in Fig. 3.7, where the inlet at the top of the figure is small and close to the edge of the basin. Without outliers, R^2 for the Georgia Bight tidal prisms is 0.89.

Comparing Fig. 4.7(a) to Fig. 4.7(b), the tidal prism approximation is more accurate for the Georgia Bight parameter set than for the Wadden Sea, with coefficients of determination of

0.14 for the Wadden Sea and 0.69 for the Georgia Bight. The most important difference between both parameter sets (see Table 2.1) is the basin length. The Wadden Sea basin has a length of 10 km, while for the Georgia Bight a basin length of 2 km is used. The increasing uncertainty in the tidal prism approximation $P_{j,approx}$ with the length of the tidal basin can be explained by (at least) two consequences of a larger basin length. Firstly, the uncertainty in the tidal divide identification method and hence in the tidal subbasin area calculation increases. The spatial differences between the (minimum) flow velocity amplitudes in the basin reduce with the distance away from the inlets, towards the back of the basin. This causes uncertainty in the tidal divide identification method (see Chapter 3), from which the tidal subbasin areas are calculated (see Section 4.1.2). The importance of this effect increases with basin length.

The second reason for more uncertainty in $P_{j,approx}$ is that the tidal prism approximation according to Eq. (4.6) is only valid when the surface area of the back-barrier basin is significantly small with respect to the tidal wave length (e.g. Kragtwijk, 2002). The spatial variations in the water level in the basin can then be neglected. According to Kragtwijk (2002), this is true for the Wadden Sea. Considering the parameter values for the Wadden Sea, the tidal wave length λ is

$$\lambda_{Wadden} = \frac{2\pi}{k_o} = \frac{2\pi}{\omega/\sqrt{gh_o}} = \frac{2\pi}{(2\pi/44712)/\sqrt{9.81 \cdot 20}} \approx 626 \text{ km} \quad (4.9)$$

Similarly, the tidal wave length at the Atlantic coast is, due to a different ocean water depth, equal to $\lambda_{Georgia} \approx 767 \text{ km}$.

To verify that the size of the basin indeed influences the accuracy of the tidal prism approximation, the basin length for the Wadden Sea is reduced from 10 km to 2 km (the same as Georgia Bight), of which the results are shown in Fig. 4.8(a). Decreasing the basin length reduces the scatter, which is confirmed by R^2 increasing from 0.14 to 0.72. Kragtwijk (2002) implies that the validity of the tidal prism approximation depends on the ratio between the surface area of the tidal basin and the tidal wave length. To study the influence of the basin width, the width of the basin is decreased from 100 km to 50 km (see Fig. 4.8(b)). From Fig. 4.8, it can be concluded that decreasing the basin width (alongshore) does not result in an increased accuracy of the approximation, while a decrease in basin length (cross-shore) does.

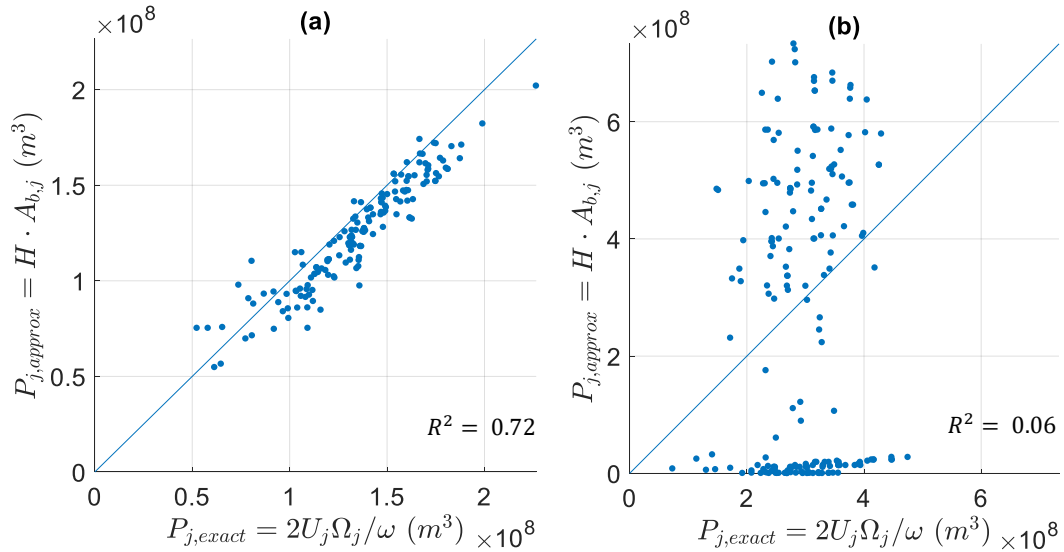


Fig. 4.8: Scatter plot of $P_{j,approx}$ vs. $P_{j,exact}$ for the Wadden Sea parameter set (see Table 2.1) with (a) a basin length of 2 km instead of 10 km and (b) a basin width of 50 km instead of 100 km, where R^2 is the coefficient of determination and the line represents the ideal situation in which the approximated and the actual tidal prisms are equal.

4.4 Development over time

The O'Brien-Jarrett Law is originally assumed to only be valid for tidal inlet systems that are in equilibrium, as it is determined empirically for systems that are assumed to be in equilibrium. Contrarily, according to Dieckmann et al. (1988), estimates may be made of the long-term changes in an inlet's cross-section up to the point at which a mean state of equilibrium is attained, on the basis of tidal prism cross-sectional area relationships. D'Alpaos et al. (2010) raised the question of whether the O'Brien-Jarrett Law is satisfied anywhere and at any time in a tidal inlet system, so also for a tidal system that is still evolving and not yet in equilibrium. To answer this, the development of the tidal prisms and the inlet areas over time will be studied. In this section, only the exact tidal prisms $P_{j,exact}$ will be considered.

While the system is still evolving, Ω_j, U_j and P_j vary over time, so they can be written as $\Omega_j(t), U_j(t)$ and $P_j(t)$ respectively. Note that here, t represents morphodynamic time in years. The tidal frequency ω remains constant. From Eq. (4.5), it follows that the relationship between tidal prism $P_j(t)$ and inlet area $\Omega_j(t)$ satisfies

$$\Omega_j(t) = \frac{\omega}{2U_j(t)} P_j(t) \quad (4.10)$$

where U_j is the flow velocity amplitude (m/s) in inlet j and ω is the tidal frequency (rad/s). We have already shown that when a system is in equilibrium, the relationship between P_j and Ω_j for each inlet j is of the form of Eq. (4.1) with coefficients k and α as given in Eq. (4.8). Substituting the expression for k presented in Eq. (4.8) into Eq. (4.10) gives

$$\Omega_j(t) = k \frac{U_{eq}}{U_j(t)} P_j(t) \quad (4.11)$$

where $k = \omega/2U_{eq}$ (rad/m) and the flow velocity amplitude U_j (m/s), cross-sectional area Ω_j (m^2) and tidal prism P_j (m^3) of inlet j all vary over time t (years). Hence, Ω_j and $P_{j,exact}$ of inlet j satisfy the relationship shown in Eq. (4.11) while the inlet evolves. It can easily be seen that as $U_j(t) \rightarrow U_{eq}$, the tidal prism - inlet area relationship of the evolving inlet system converges to the established relationship for the system in equilibrium.

The model is run once, until the system is in equilibrium, using the parameter set representing the Wadden Sea (see Table 2.1). The evolution of the inlets over time is presented in Fig. 4.9. It can be seen that eight inlets (inlets 4, 10, 17, 21, 26, 31, 35 and 40) remain open in the equilibrium state, which is reached after 2,814 years, while the other inlets close. In Fig. 4.11(a), (b) and (c), respectively the flow velocity amplitude U_j and the cumulative inlet areas $C\Omega_j$ and cumulative tidal prisms CP_j are plotted against the time, where $C\Omega_j$ and CP_j are calculated as

$$C\Omega_j = \sum_{j'=1}^j \Omega_{j'}, \quad CP_j = \sum_{j'=1}^j P_{j'} \quad (4.12)$$

for inlet j . The cumulative tidal prisms and inlet areas are used since they give a good overview of neighbouring inlets and also of the temporal development of the total tidal prisms and inlet areas for all open inlets in one system. Note that in the cumulative plots, the difference between two adjacent graphs in the plot actually gives the tidal prism or inlet area for one open inlet.

In Section 4.4.1, the temporal development of the P - Ω relationship for the inlets that remain open in equilibrium will be studied. Then, in Section 4.4.2, the same will be done for inlets that close during the evolution of the system.

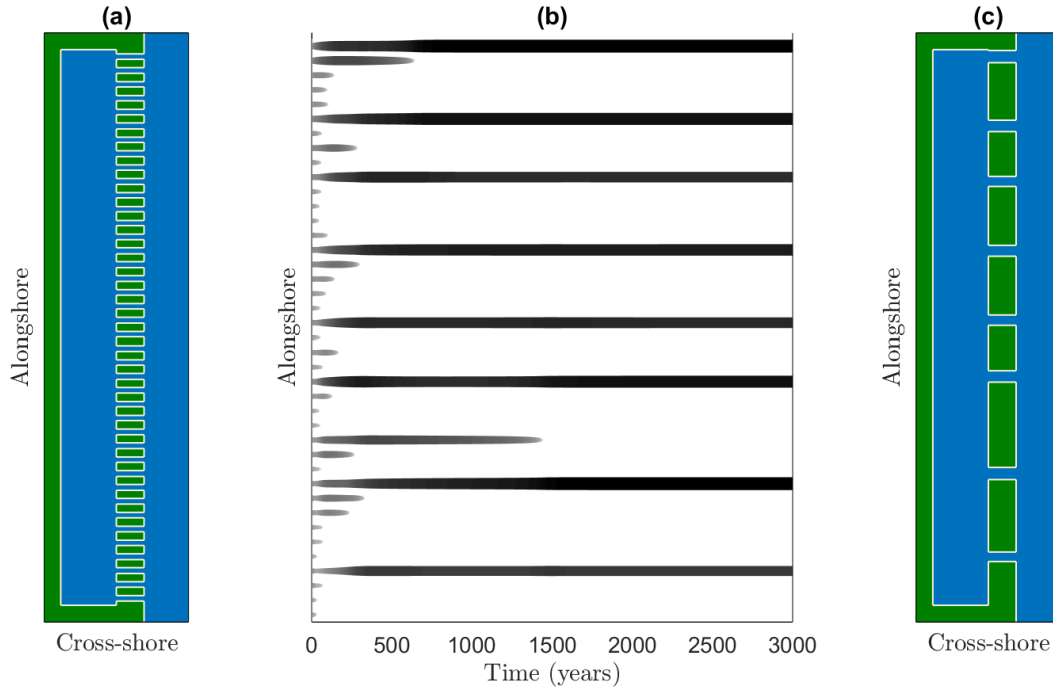


Fig. 4.9: Inlet evolution of model run using Wadden Sea parameter set (see Table 2.1), with (a) initial state with 40 inlets, (b) the evolution of the inlets over time in years, showing whether and when inlets close, (c) the equilibrium state.

4.4.1 Open inlets

To study the temporal development of P_j and Ω_j for the eight inlets that remain open, Ω_j is plotted against P_j for inlets 4, 10, 17, 21, 26, 31, 35 and 40 in a coloured scatter plot in Fig. 4.10. Furthermore, the empirical O'Brien-Jarrett Law (assumed to be valid in equilibrium) and the P - Ω relationship according to the model when the system is in equilibrium (Eq. (4.1) with coefficients according to Eq. (4.8)) are shown in Fig. 4.10.

From Fig. 4.10, it can be observed that the temporal development of the tidal prisms P_j and inlet areas Ω_j seems to closely resemble the P - Ω relationship in equilibrium. Considering Eq. (4.11), this suggests that the flow velocity amplitudes $U_j(t)$ in the inlets converge towards the equilibrium flow velocity amplitude U_{eq} relatively quickly, which is confirmed by the temporal development of $U_j(t)$ shown in Fig. 4.11(a).

As long as U_j in an inlet is close to U_{eq} , the temporal development of P_j and Ω_j will closely follow the P - Ω relationship that is satisfied in equilibrium. The relationship between P_j and Ω_j deviates from the expected P - Ω relationship when a neighbouring inlet closes. While an inlet is in the process of diminishing, U_j (see Fig. 4.11(a)) and Ω_j (see Fig. 4.11(b)) of the neighbouring inlets increase. Consequently, P_j also increases, where the increase in U_j amplifies the increase in P_j . This causes the deviations from the equilibrium P - Ω relationship that can be seen in Fig. 4.10. Once the diminishing inlet is actually closed, Ω_j in the adjacent open inlets remains at its adjusted value or still increases slightly, while U_j decreases again (towards the equilibrium value U_{eq}). Then, P_j and Ω_j have increased with respect to the situation before the closing of the inlet, but their relationship is again similar to the expected P - Ω relationship in equilibrium. Once the system is in a stable equilibrium, P_j and Ω_j will remain at their equilibrium values, satisfying the equilibrium P - Ω relationship. The U_j , Ω_j and P_j of an open inlet are more responsive to the closure of an inlet nearby than to an accretion of an inlet located farther away.

Legend — Empirical O'Brien-Jarrett Law

— Model $P - \Omega$ relationship in equilibrium

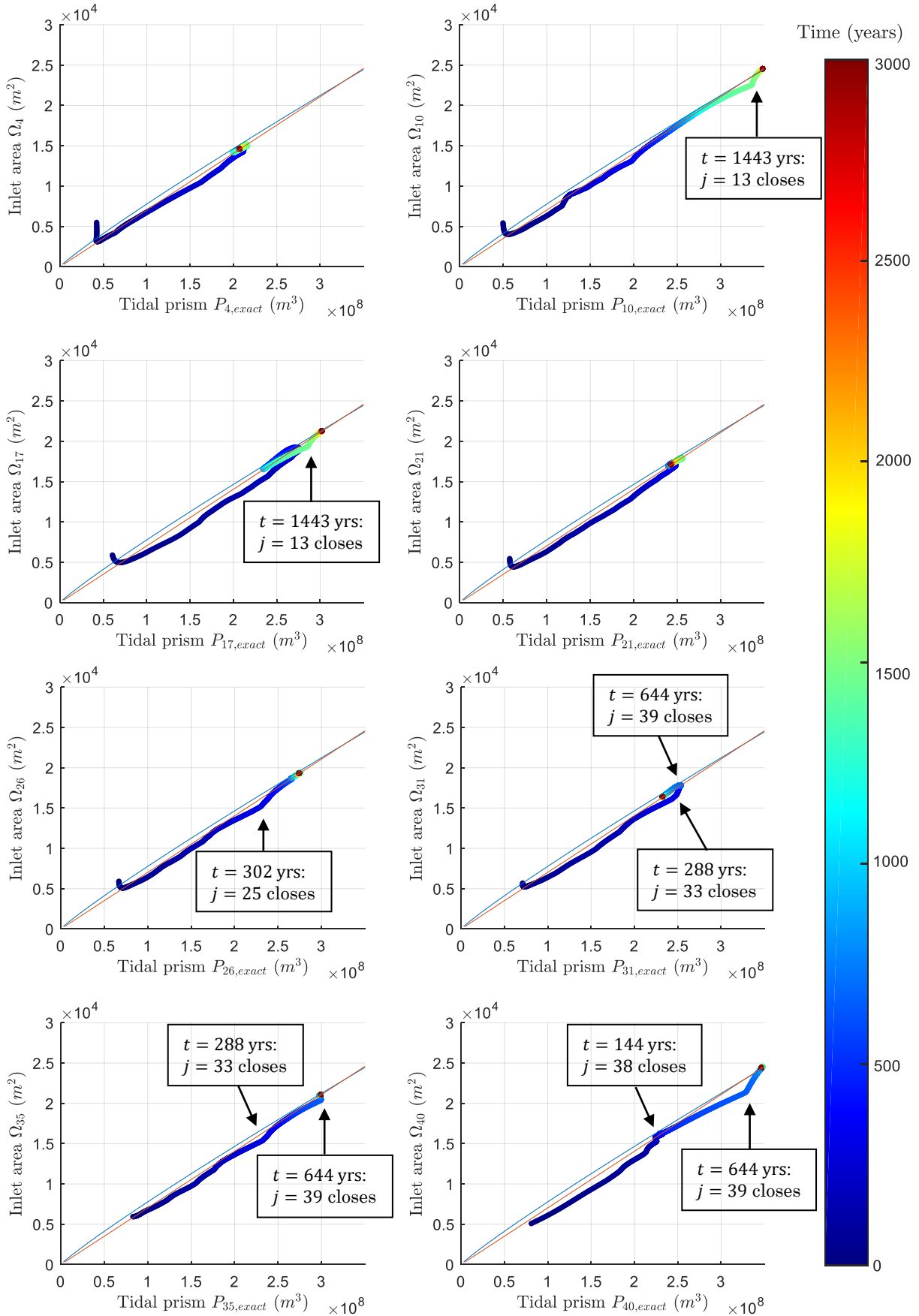


Fig. 4.10: The development of $P_{j,exact}$ and Ω_j over time t , for inlets $j = 4, 10, 17, 21, 26, 31, 35, 40$ (the inlets that remain open in equilibrium).

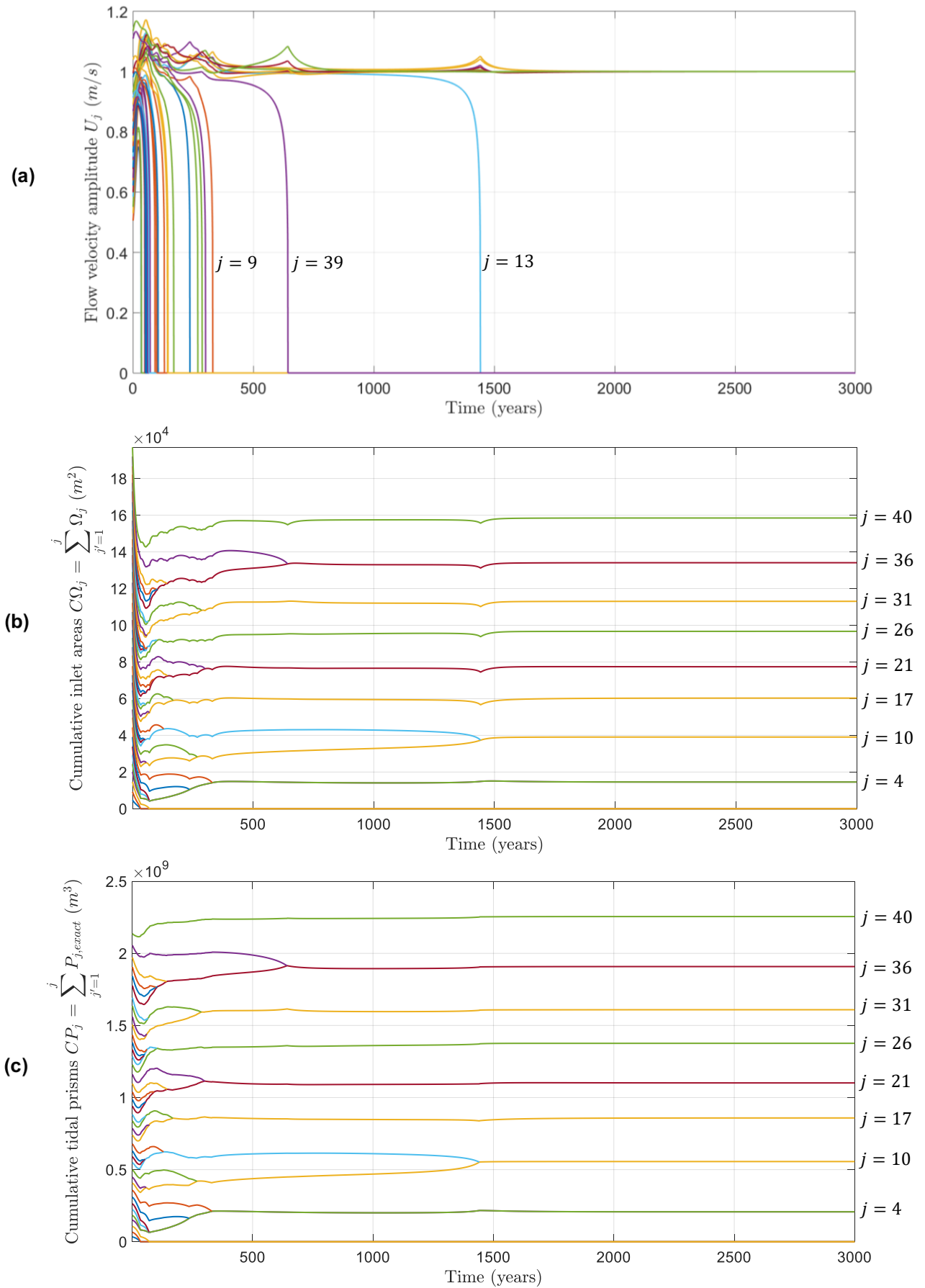


Fig. 4.11: The temporal development of (a) flow velocity amplitude U_j per inlet j , (b) cumulative inlet areas $C\Omega_j$ (see Eq. (4.12)) and (c) cumulative tidal prisms CP_j (see Eq. (4.12)).

4.4.2 Closing inlets

For completeness, we will also study the temporal development of P_j and Ω_j for inlets that do close during the system's evolution. We are mostly interested in the development of inlets that remain open for a while, but then close. To this end, we have chosen to study inlet 9 and inlet 13, which are also indicated in Fig. 4.11(a). For those inlets, it can be seen that initially, the P - Ω relationship does converge towards the expected relationship in equilibrium. This means that $U_j(t)$ converges towards U_{eq} . Then, P_j and Ω_j increase for a period of time, while other (neighbouring) inlets are accreting and closing. Hence, these inlets then display the same behaviour as the inlets that remain open in equilibrium. However, at some point the inlet starts accreting and Ω_j and P_j decrease until the inlet is fully closed and U_j, Ω_j and P_j are equal to zero. During the accretion, the decrease in U_j amplifies the decrease in P_j compared to Ω_j , which can also be seen in Fig. 4.12.

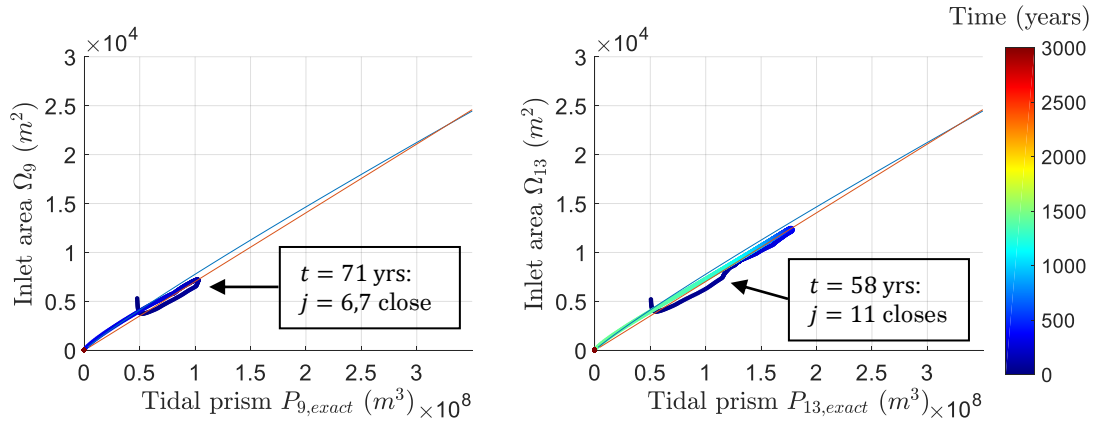


Fig. 4.12: The development of P_j and Ω_j over time t , for inlets $j = 9$ and 13 (two of the 32 inlets that are closed in equilibrium).

4.5 Subconclusions

The relationship between the exact tidal prisms $P_{j,exact}$ and inlet areas Ω_j in the model once the system is in equilibrium is of the form $\Omega = kP$ with $k = \omega/2U_{eq}$, where ω is the tidal frequency and U_{eq} is the equilibrium flow velocity amplitude in the inlet. Hence, the model satisfies a relationship of the form $\Omega = kP^\alpha$, with α equal to 1, for systems that are in equilibrium. Coefficients k and α in the empirical O'Brien-Jarrett Law are determined through regression analysis by Jarrett (1976) for North American inlets and by Dieckmann et al. (1988) for the Wadden Sea. The coefficients resulting from the model (see Table 4.3) for both the Wadden Sea and the Atlantic coast are not exactly equal to the empirical results due to the clear linear relationship between Ω_j and $P_{j,exact}$ in the model when the system is in equilibrium. However, the O'Brien-Jarrett Law also is a good representation of the model results that are obtained using $P_{j,exact}$, with coefficient of determination R^2 equal to 0.99 for the Wadden Sea and 0.96 for the Georgia Bight (see Table 4.3). The similarities between the empirical law and the P - Ω relationship in the model suggest that the relationship between P and Ω that is included in the model is indeed an acceptable representation of nature.

For the approximated tidal prisms $P_{j,approx}$ the results are a bit different as the relationship between $P_{j,approx}$ and Ω_j is less straightforward. For the parameter set representing the Wadden Sea, the resulting $k = 970.9$ and $\alpha = 0.159$ are far from the expected results. The coefficient of determination of that fit is 0.21 (see Table 4.3). There are no obvious outliers in the data that can be removed to obtain a better result. For the Georgia Bight runs however,

there are clear outliers. Removing these outliers results in $k = 8.192 \cdot 10^{-5}$ and $\alpha = 0.993$, which is similar to the expected results.

Location	Calculation tidal prism	Outliers included?	k_{fit}	α_{fit}	R_{fit}^2	k_{OBJL}	α_{OBJL}	R_{OBJL}^2
Wadden Sea	$P_{j,approx} = H \cdot A_{b,j}$	Not applicable	970.9	0.16	0.21	3.720×10^{-4}	0.915	-2.09
	$P_{j,exact} = 2\Omega_j U_j / \omega$	Not applicable	$7.026 \cdot 10^{-5}$	1	1			0.99
Georgia Bight (Atlantic coast)	$P_{j,approx} = H \cdot A_{b,j}$	Yes	294.4	0.15	0.23	3.039×10^{-5}	1.050	0.44
		No	$8.192 \cdot 10^{-5}$	0.99	0.92			0.91
	$P_{j,exact} = 2\Omega_j U_j / \omega$	Not applicable	$7.026 \cdot 10^{-5}$	1	1			0.96

Table 4.3: Results for the coefficients of $\Omega = kP^\alpha$, according to the model results and the empirical O'Brien-Jarrett Law. The coefficients of determination R_{fit}^2 and R_{OBJL}^2 are calculated as

$$R_{fit}^2 = 1 - \frac{SS_{res,fit}}{SS_{tot}} \quad R_{OBJL}^2 = 1 - \frac{SS_{res,OBJL}}{SS_{tot}}$$

where $SS_{res,fit} = \sum(\Omega_j - \Omega_{j,fit})^2$, $SS_{res,OBJL} = \sum(\Omega_j - \Omega_{j,OBJL})^2$ and $SS_{tot} = \sum(\Omega_j - \text{mean}(\Omega_j))^2$ are the residual sum of squares for the function that is fit to the model results, the residual sum of squares for the O'Brien-Jarrett Law and the total sum of squares, resp. Inlet areas Ω_j , $\Omega_{j,fit}$ and $\Omega_{j,OBJL}$ are the inlet areas according to the model results, the function that is fit to the model results and the O'Brien-Jarrett Law, resp. The sum Σ is taken over all data points resulting from 50 model runs.

The accuracy of the tidal prism approximation determines the extent to which $P_{j,approx}$ is similar to $P_{j,exact}$. This accuracy increases as the cross-shore basin length decreases. Therefore, the approximated tidal prisms $P_{j,approx}$ are more accurate for the Georgia parameter set than for the Wadden Sea parameter set.

For systems that are still evolving, the factor U_j/U_{eq} directly influences the relation between the exact tidal prisms $P_{j,exact}$ and inlet areas Ω_j . This results in a non-linear relationship between $P_{j,exact}$ and Ω_j when the system is not yet in equilibrium. The temporal development of the P - Ω relationship is different for every inlet, as U_j evolves differently for each inlet. However, the model results show that U_j converges towards U_{eq} relatively quickly during an inlet's evolution, such that U_j/U_{eq} is close to 1 for a significant part of the evolution. Consequently, the temporal development of the P - Ω relationship as P_j and Ω_j increase, due to the closing of other inlets, closely follows the equilibrium P - Ω relationship. The development (only) deviates from the equilibrium P - Ω relationship when a neighbouring inlet closes.

5. Sensitivity analysis

How will changes in ocean conditions affect the stability of multi-inlet tidal systems and the tidal prism - inlet area relationship?

The objective of the sensitivity analysis with respect to the outer sea or ocean conditions is to qualitatively study the system's response to changes in ocean parameters. Especially of interest are the resulting number of inlets, the tidal subbasin areas and the cross-sectional areas of the tidal inlets. Not only the inlet areas per inlet will be considered, but also the total inlet area for the entire system. Furthermore, the possible changes in the tidal prism - inlet area relationship as a consequence of changing ocean parameters will be studied. We will perform a sensitivity analysis with respect to the following parameters: water depth in Section 5.1, tidal amplitude in Section 5.2 and littoral drift in Section 5.3.

The initial parameter values used in the analysis are those representing the Wadden Sea (see Table 2.1). The model is run 25 times (see Appendix B) for every parameter value and each time for 1,000 timesteps. The flow velocity amplitudes in the open inlets are then generally between 0.98 m/s and 1.02 m/s, so the system is near equilibrium but not necessarily exactly in equilibrium yet. The number of inlets that remain open, the tidal subbasin areas and the inlets' cross-sectional areas are then extracted from the results and plotted in boxplots. Thus, each boxplot is plotted using the results of 25 model runs. For the number of inlets and the total inlet area, this means that 25 values are used per boxplot. For the tidal basin areas, tidal prisms and inlet areas per inlet, the number of values used for each boxplot is the total number of open inlets for the 25 runs.

Boxplots

The boxplots present the median of the data, the 25% and 75% quartiles, the “minimum”, the “maximum” and the outliers. The median is indicated by the red line, while the box shows the interquartile range between the 25% and 75% quartiles. The whiskers (dashed lines) extend to the most extreme data points (minimum and maximum) not considered outliers. The outliers are defined as the values that are above or below the edge of the box at a distance of at least 1.5 times the interquartile range. The notches in the box plots provide information about the statistical significance of the medians: if the notches of two boxes do not overlap, this offers evidence of a statistically significant difference between the medians.

Roos et al. (2013) explained their model results by considering the competition between a destabilizing and a stabilizing mechanism, that they identified, influencing the system. They concluded that bottom friction in the inlets acts as a destabilizing mechanism and the system's feedback on pressure gradients over the inlets forms a stabilizing mechanism. For further explanations regarding these mechanisms, we refer to Roos et al. (2013). The effects of the stabilizing and destabilizing mechanisms will be considered in the interpretation and explanation of the results of this sensitivity analysis.

5.1 Water depth

The water depth in a multi-inlet tidal system can increase as a consequence of a rising sea level. Van Goor et al. (2003) and Van der Spek (2018) state that a tidal inlet system can survive sea level rise (SLR) as long as the sediment demand is satisfied, so the probability that a tidal inlet system survives sea level rise depends on the sediment import into the system. The

sediment import is implemented in the model as a constant parameter value, which does not adapt to the new situation during a model run. Therefore, only the sensitivity of the system to an increase in water depth in the basin and ocean with a constant sediment import will be analysed in this research. Furthermore, only an instant sea level rise, so an increase in initial water depth at $t = 0$, is implemented in the model, whereas in reality the sea level rise would happen gradually over time. Note that the sensitivity to a change in sediment import will be analysed separately in Section 5.3.

The increased water depth values that will be studied are loosely based on the sea level rise predictions presented by Wang et al. (2018) for the Wadden Sea in the year 2100. Several scenarios for relative sea level rise will be considered, where relative means that both a rise in mean sea level and subsidence of the seabed are taken into account. Both of these components contribute to an increase in water depth. The scenarios that are considered are the RCP2.6, RCP4.5 and RCP8.5 climate scenarios (Wang et al., 2018). The corresponding water depth scenarios are presented in Table 5.1.

Parameter SLR	Initial value	Based on RCP2.6	Based on RCP4.5	Based on RCP8.5
Ocean water depth h_o (m)	$h_o = 20$	$h_o = 20.41$	$h_o = 20.54$	$h_o = 20.98$
Basin water depth h_b (m)	$h_b = 5$	$h_b = 5.41$	$h_b = 5.54$	$h_b = 5.98$

Table 5.1: Sea level rise scenarios used in the sensitivity analysis, based on climate change scenarios RCP 2.6, RCP 4.5 and RCP 8.5 (Wang et al., 2018).

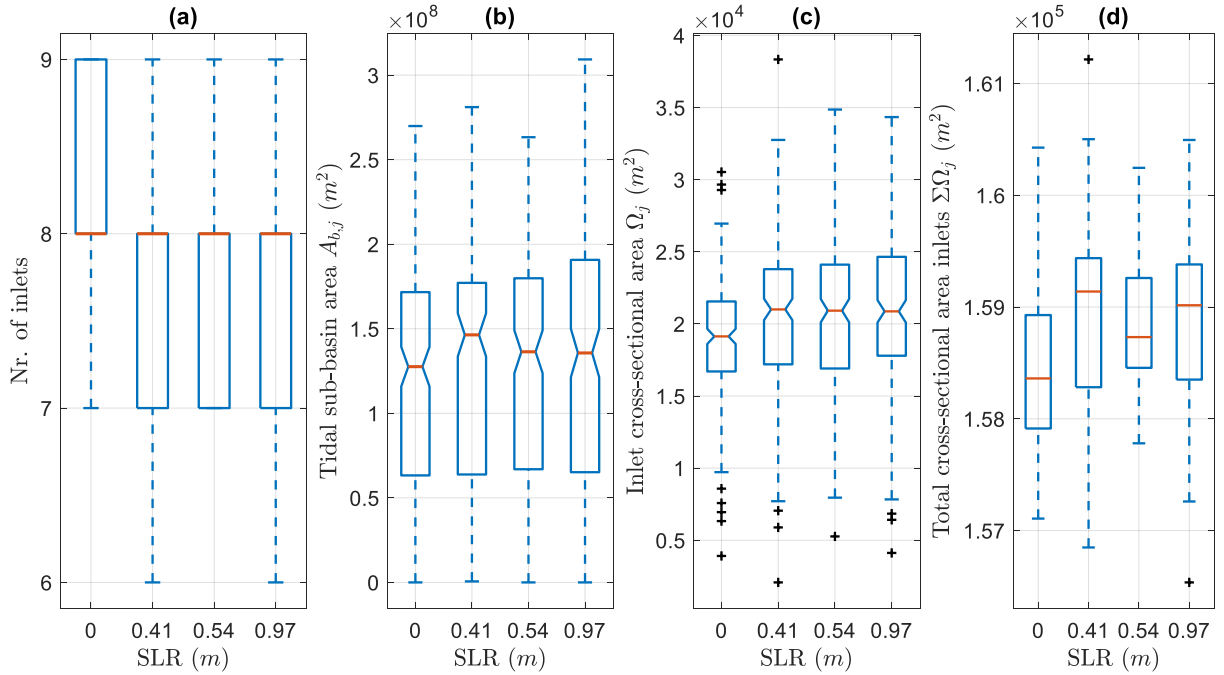


Fig. 5.1: The response of the (a) number of inlets, (b) tidal subbasin area, (c) inlet cross-sectional area per inlet and (d) total cross-sectional inlet area to the expected sea level rise until 2100.

As can be seen in Fig. 5.1, in water depth increase of less than a meter does not significantly influence the number of inlets, the surface areas of the tidal basins or the inlets' cross-sectional areas resulting from the model runs. However, the model is run for 1,000 years, while the water depth increase that is implemented in the model is the expected sea level rise in approximately 80 years (from 2018 until 2100). Hence, higher sea level rise values are expected on the timescale of the model. As these values are highly uncertain on such a timescale, assumptions have to be made. Levermann et al. (2013) predict a sea level rise of approximately 2.3 m with a temperature increase of 1°C in 2,000 years, which we will assume means a sea level rise of approximately 1.2 m in 1,000 years. For a temperature increase of 2, 3 or 4°C,

Levermann et al. (2013) predict approximately 4.8, 6.6 and 9.0 m sea level rise in 2,000 years, respectively. Hence, the sea level rise values that will be assessed in this analysis are a water depth increase of 1.2 m, 2.4 m, 3.3 m and 4.5 m. The results are shown in Fig. 5.2.

Parameter	Initial value	Based on +1°C in 2,000 years	Based on +2°C in 2,000 years	Based on +3°C in 2,000 years	Based on +4°C in 2,000 years
h_o (m)	$h_o = 20$	$h_o = 21.20$	$h_o = 22.40$	$h_o = 23.30$	$h_o = 24.50$
h_b (m)	$h_b = 5$	$h_b = 6.20$	$h_b = 7.40$	$h_b = 8.30$	$h_b = 9.50$

Table 5.2: Sea level rise scenarios used in the analysis, based on the predictions by Levermann et al. (2013).

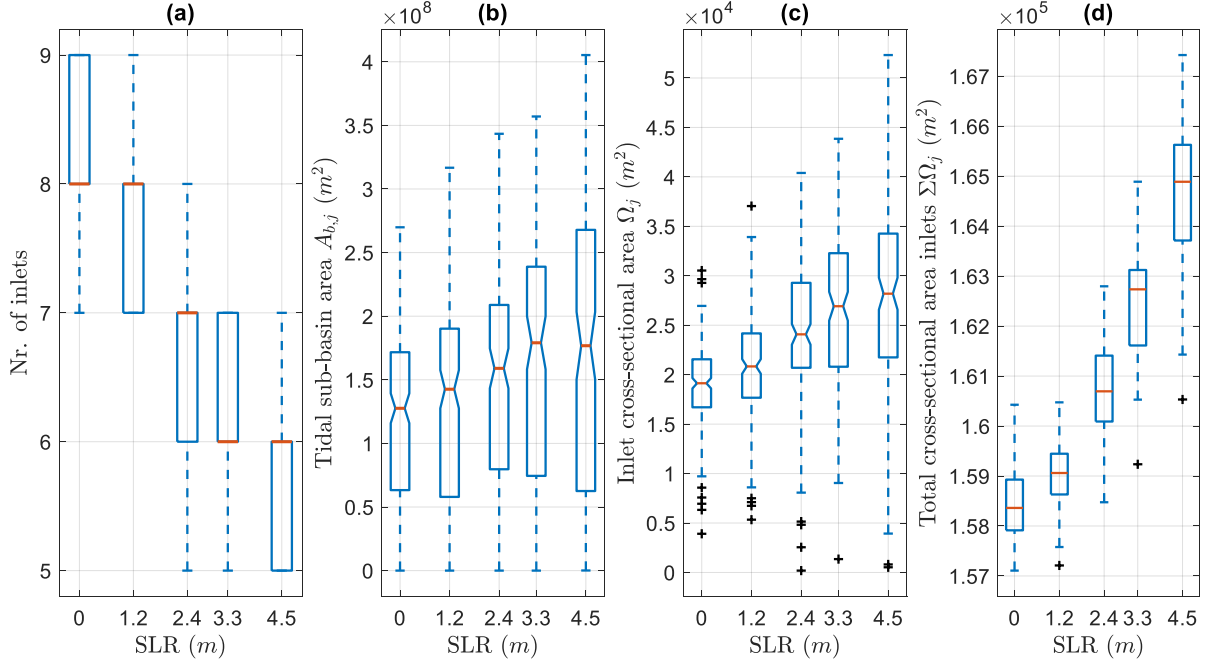


Fig. 5.2: The response of the (a) number of inlets, (b) tidal subbasin area, (c) inlet area per inlet and (d) total inlet area to sea level rise on a millennial scale.

As can be seen in Fig. 5.2(b), an increase in water depth in the outer sea and the basin causes a decrease in the number of inlets. Consequently, the tidal subbasin areas increase, but note that this increase might not be statistically significant in this case as the notched boxplots still overlap. Furthermore, the inlet areas of the separate inlets and the total inlet area increase as the sea level rise increases, which is expected since the water depth in the inlet and hence the equilibrium inlet area most likely increases as a consequence of sea level rise. Roos et al. (2013) state that the stabilizing mechanism that they identified gains relative importance for increasing cross-sectional area of the inlets. Consequently, for an increasing water depth, more inlets are expected to remain open in equilibrium. However, our sensitivity analysis suggests the opposite. The same was found by Roos et al. (2013), who concluded from their sensitivity analysis with respect to h_b and h_o that inlet spacing increases for increasing water depth. The inlet spacing is the alongshore basin width divided by the number of inlets, so an increase in inlet spacing for a constant basin width is equivalent to a decrease in number of inlets. The opposing trends in number of inlets and inlet areas might be explained by differing responses of the system to a water depth increase, depending on the resonance characteristics of the basin. However, this is beyond the scope of this research.

Van der Wegen et al. (2010) mention that the impact of sea level rise on the P - Ω relationship is not straightforward. Higher water levels increase the cross-sectional area of the inlet, but they may also increase the tidal prisms. Note that in this analysis a change in water depth in the inlet is not directly implemented, but only the water depth in the basin and ocean are modified in the model. Hence, the inlet areas Ω_j are not directly increased through increasing

the inlet depth, but according to Fig. 5.2(c) they do increase for increasing basin and ocean water depth. Based on the trends in Fig. 5.2(a) and (c), the tidal prisms $P_{j,approx}$ and $P_{j,exact}$ are expected to increase for increasing water depths in the basin and the ocean. However, considering the notches in the boxplots, these trends might not be statistically significant. This is indeed confirmed in Fig. 5.3(a) and (c). Considering the similar trends in tidal prisms and inlet areas, the coefficients k are expected to be independent of the water depth in the ocean and the basin, which is confirmed in Fig. 5.3(b) and (d).

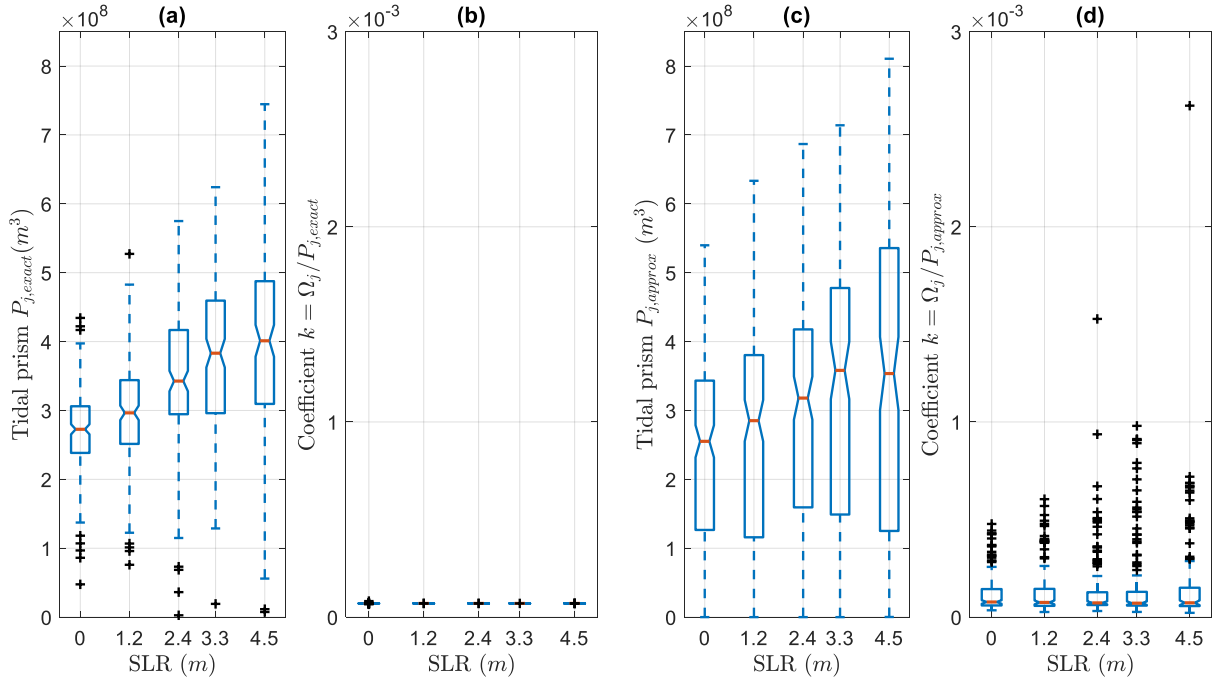


Fig. 5.3: The response of (a) tidal prism $P_{j,exact}$, (b) coefficient $k = \Omega_j / P_{j,exact}$, (c) tidal prism $P_{j,approx}$ and (d) coefficient $k = \Omega_j / P_{j,approx}$ to sea level rise (implemented as increased initial water depth in basin and ocean).

5.2 Tidal amplitude

Reise et al. (2010) state that the tides in the Wadden Sea have increased due to climate change and the rising sea level and the tidal range is currently between 1.5 m and 4 m (which is equivalent to a tidal amplitude between 0.75 m and 2 m). The initial value implemented in the model is a tidal amplitude Z of 1 m. To study what would happen for an increase and decrease of the tidal amplitude, the model is run for values of the tidal amplitude that are 20%, 50%, 150%, 200% and 250% of the initial value of $Z = 1$ m, as shown in Table 5.3.

Parameter	Initial value	Value 1	Value 2	Value 3	Value 4	Value 5
Tidal amplitude Z (m)	1	0.2 (20%)	0.5 (50%)	1.5 (150%)	2 (200%)	2.5 (250%)

Table 5.3: The parameter values of tidal amplitude Z that are used in the sensitivity analysis.

For the smallest tidal amplitude of 0.2 m, all inlets are closed after approximately 35 years, so the model runs will not give any results for the number of inlets, tidal basin areas or inlets' cross-sectional areas. For the five other values in Table 5.3, the results are shown in Fig. 5.4. In Fig. 5.4(a), it can be seen that the number of inlets increases as the tidal amplitude increases. Simultaneously, the surface areas of the tidal subbasins decrease (Fig. 5.4(b)). There is no obvious trend in the inlet area per inlet (Fig. 5.4(c)). Nevertheless, due to the significant increase in number of inlets, the total inlet area does increase as the tidal amplitude increases (Fig. 5.4(d)). By Escoffier's stability concept, increasing the tidal amplitude causes the

equilibrium (total) cross-sectional area to shift to a larger value (see Fig. 1.3). Hence, it is not surprising that more inlets will remain open in equilibrium when the tidal amplitude is increased. The same was concluded by Roos et al. (2013), who also found that the number of inlets in equilibrium increases with tidal range. They stated that for increasing cross-sectional area of the inlets, the stabilizing mechanism that they identified gains relative importance over the destabilizing mechanism. Consequently, the inlet spacing decreases and hence the number of inlets increases for an increasing tidal amplitude.

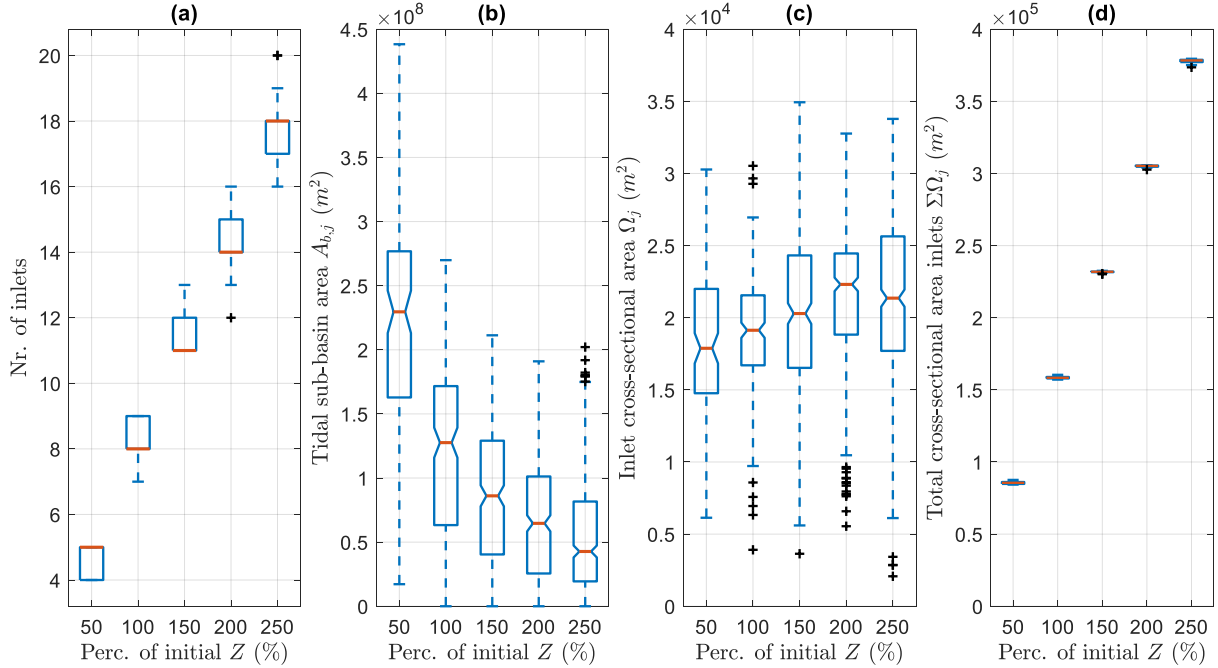


Fig. 5.4: The response of the (a) number of inlets, (b) tidal subbasin area, (c) inlet area per inlet and (d) total inlet area to changes in the tidal amplitude Z .

Now, we are interested in what a modification of the tidal amplitude means for the relationship between tidal prisms and inlets' cross-sectional areas. The total inlet area is (almost) directly proportional to the tidal amplitude Z : when the tidal amplitude is 200% of the original value, the total inlet area is also approximately two times as large, as can be seen in Fig. 5.4(d). However, there is no compelling trend in the response of the inlet area Ω_j per inlet to a change in tidal amplitude, so one would not expect a significant change in the tidal prism $P_{j,exact}$ as a consequence of changing the tidal amplitude. The tidal subbasin areas seem almost inversely proportional to the tidal amplitude, as the subbasin areas decrease by a factor two when the tidal amplitude increases by a factor two (see Fig. 5.4(b)). This is a direct consequence of the number of inlets increasing for increasing tidal amplitude, as the basin area then has to be “divided” over more open inlets. The opposite trends in tidal amplitude and subbasin areas should result in no change in tidal prism $P_{j,approx}$ for a changing tidal amplitude. This is indeed confirmed in Fig. 5.5(a) and (c), where there is no significant trend in the responses of both $P_{j,approx}$ and $P_{j,exact}$ to a change in tidal amplitude.

As both the tidal prisms and the inlet areas do not significantly respond to a modification of the tidal amplitude, the value of k also should not change, as confirmed in Fig. 5.5(b) and (d). This is in agreement with the expression for k in Eq. (4.8), which is independent of the tidal amplitude. The outliers in the values of k for $Z = 2.5$ m in Fig. 5.5(b) suggest that the system may not have been exactly in equilibrium yet after 1,000 timesteps for every model run, such that the flow velocity amplitude was not exactly equal to U_{eq} in all inlets.

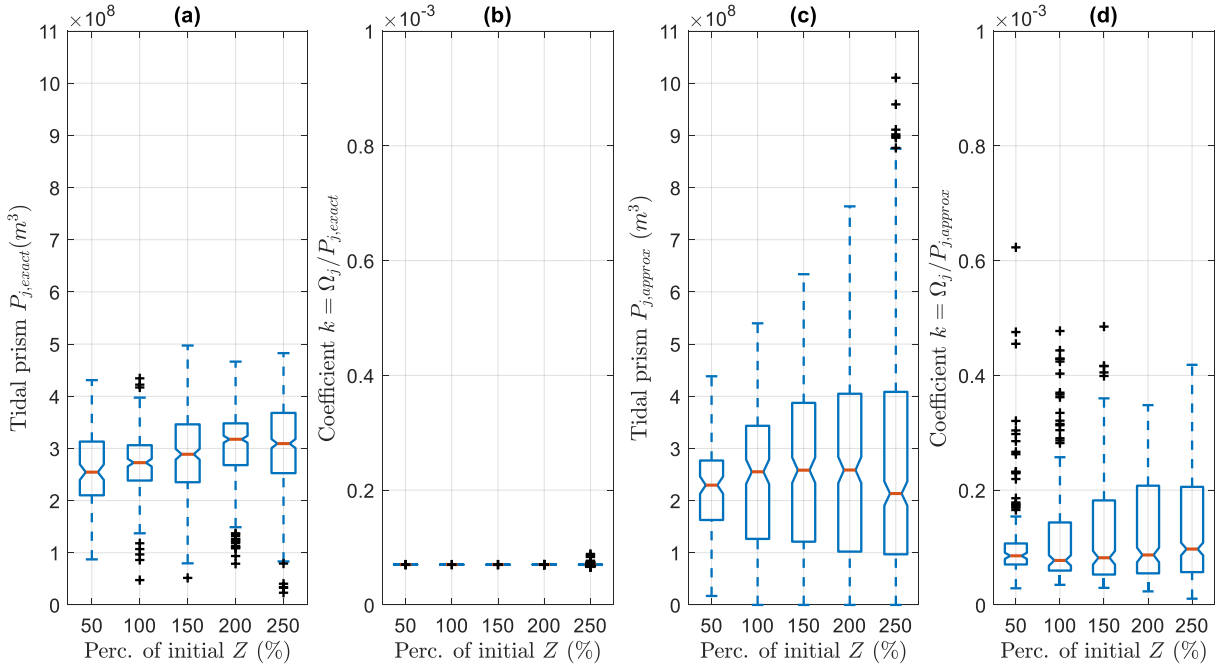


Fig. 5.5: The response of (a) tidal prism $P_{j,exact}$, (b) coefficient $k = \Omega/P_{j,exact}$, (c) tidal prism $P_{j,approx}$ and (d) coefficient $k = \Omega/P_{j,approx}$ to changes in tidal amplitude Z .

5.3 Littoral drift

The littoral drift into the inlets is the alongshore sediment transport, caused by waves and longshore currents. Part of this littoral drift is transported into the inlets (Section 1.1.1; De Swart and Zimmerman, 2009). The effect of wind waves and hence the littoral drift is parametrically included in the model through the equilibrium flow velocity U_{eq} and sediment import M . Changing the littoral drift will, because of the relationship $M = \kappa U_{eq}^3$, change both M and U_{eq} (Roos et al., 2013). To modify the littoral drift, M and U_{eq} should be changed in such a way that κ remains constant. As we are considering the parameter set representing the Wadden Sea (see Table 2.1), we have that

$$\kappa = \frac{M}{U_{eq}^3} = 1.0 \cdot 10^6 \text{ m}^3 \cdot \text{yr}^{-1} \cdot \text{s}^{-3}$$

The values of U_{eq} used in this analysis are 50%, 75%, 125% and 150% of the initial value of 1 m/s. The corresponding values of M are calculated by $M = \kappa U_{eq}^3$, where $\kappa = 1.0 \cdot 10^6$. Both parameters M and U_{eq} are included in the model equation in Eq. (2.2)). From that equation, it can be seen that M influences the time scale of the inlet evolution, while the ratio U_j/U_{eq} controls the inlet stability. A decrease of sediment import M increases the timescale of the system's evolution and therefore the model run durations are changed to the values presented in Table 5.4.

Parameter	Initial value	Value 1	Value 2	Value 3	Value 4
Equilibrium velocity U_{eq} (m/s)	1.0	0.5 (50%)	0.75 (75%)	1.25 (125%)	1.5 (150%)
Sediment import M (m^3/yr)	1,000,000	125,000	421,875	1,953,125	3,375,000
Timesteps needed until equilibrium	$\sim 2,000$	$\sim 20,000$	$\sim 15,000$	$\sim 1,500$	$\sim 1,000$

Table 5.4: The parameter values of the equilibrium velocity U_{eq} and the sediment import M that are used in the sensitivity analysis, where also the number of timesteps (years) for the model runs is modified.

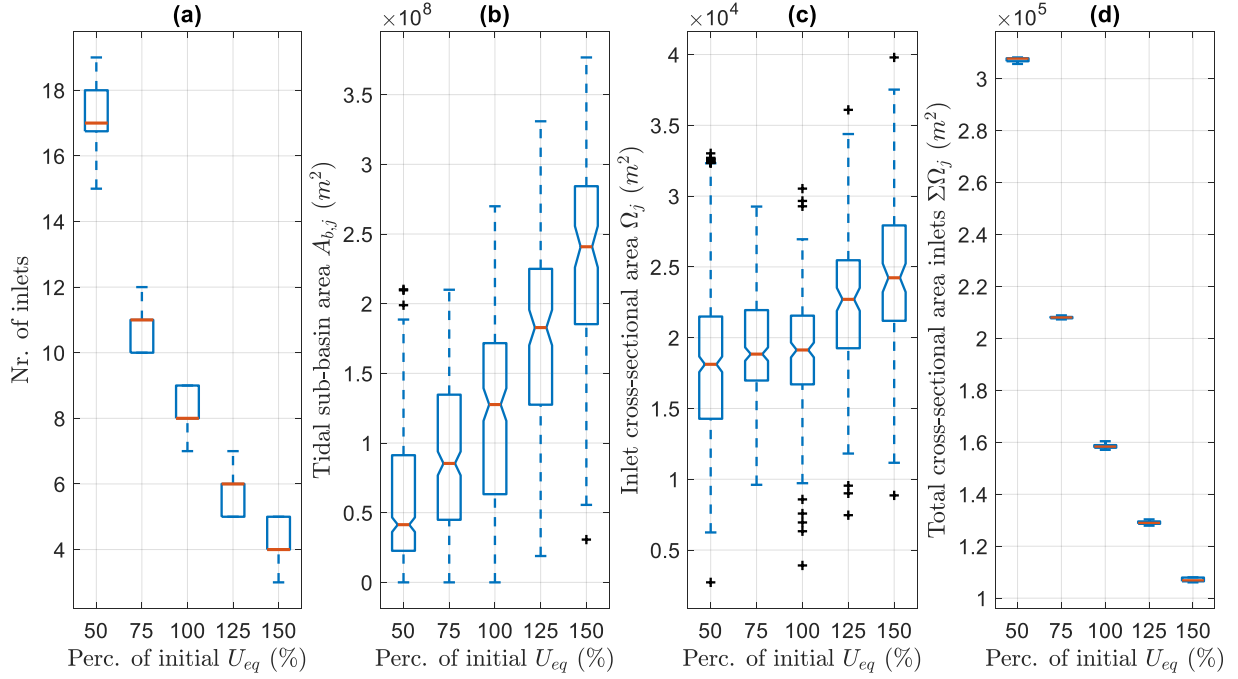


Fig. 5.6: The response of the (a) number of inlets, (b) tidal subbasin area, (c) inlet area per inlet and (d) total inlet area to changes in the equilibrium velocity U_{eq} (and corresponding sediment import M).

For an increasing equilibrium velocity U_{eq} , the number of inlets decreases and hence the tidal subbasin areas increase (Fig. 5.6(a)). Even though the inlet areas per inlet seem to slightly increase (Fig. 5.6(c)), the total inlet area decreases significantly due to the decrease in number of inlets (Fig. 5.6(d)). This is expected, as according to Escoffier's stability concept, an increase in U_{eq} means that the equilibrium (total) inlet cross-sectional area shifts to a smaller value (see Fig. 1.3). This also results in less inlets being open in equilibrium.

As mentioned, the ratio U_j/U_{eq} controls the inlet stability. Consequently, increasing U_{eq} while keeping U_j constant should have the same effect as decreasing U_j while keeping U_{eq} constant. We have already decreased U_j by decreasing the tidal amplitude Z in Section 5.2. Comparing Fig. 5.6 to Fig. 5.4, the trends in number of inlets, tidal subbasin areas and inlet areas in response to an increase in U_{eq} are indeed very similar to the trends for decreasing U_j .

In Section 5.2, we have found that modifying the tidal amplitude does not influence the tidal prism - inlet area relationship. Considering the results in Fig. 5.6, the tidal prisms $P_{j,approx}$ should increase for increasing U_{eq} as the subbasin areas increase while the tidal amplitude does not change. Furthermore, due to its direct relation to the equilibrium velocity, $P_{j,exact}$ in equilibrium should also increase as U_{eq} increases. Physically, as the flow discharge through inlets increases with increasing flow velocity, it is plausible that the tidal prism increases for increasing U_{eq} . The increase of $P_{j,approx}$ and $P_{j,exact}$ for increasing U_{eq} is confirmed in Fig. 5.7(a) and (c) In Fig. 5.6(c), it can be seen that the inlet areas slightly increase as U_{eq} increases. Nevertheless, the value of coefficient k still decreases for increasing U_{eq} , which can be seen in Fig. 5.7(b) and (d). This is expected considering the expression for k in Eq. (4.8), where k is inversely proportional to U_{eq} . In Fig. 5.7(d), it can be seen that the accuracy of k according to $\Omega/P_{j,approx}$ increases as U_{eq} increases. This can be explained by the fact that when there are many open inlets, the calculated subbasin areas $A_{b,j}$ and hence tidal prisms $P_{j,approx}$ can become very small. Consequently, k will be very large, which is the case for $U_{eq} = 0.5$ m/s in Fig. 5.7(d).

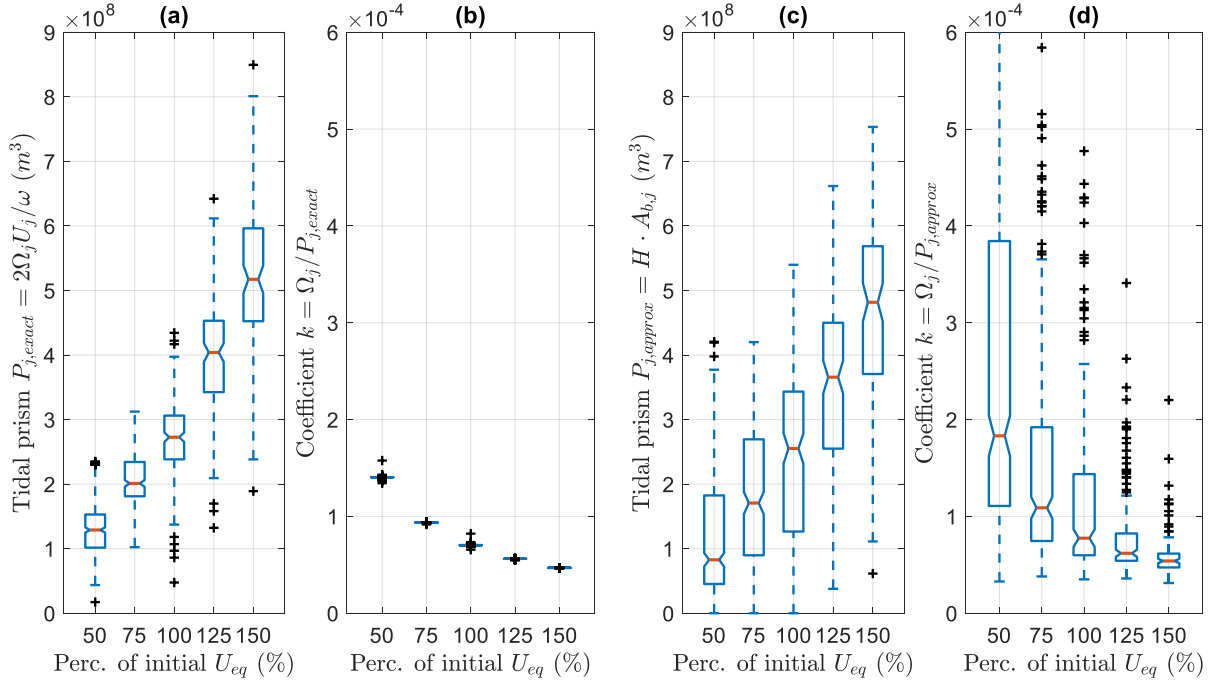


Fig. 5.7: The response of (a) tidal prism $P_{j,exact}$, (b) coefficient $k = \Omega_j / P_{j,exact}$, (c) tidal prism $P_{j,approx}$ and (d) coefficient $k = \Omega_j / P_{j,approx}$ to changes in the equilibrium velocity U_{eq} (and corresponding sediment import M).

5.4 Subconclusions

Only instant sea level rise is modelled in this analysis, where the water depth in the basin and the ocean at $t = 0$ are modified. The results suggest that the number of inlets decreases for a larger water depth in basin and ocean. Logically, a decrease in number of inlets goes hand in hand with an increase of the surface area per tidal subbasin. The inlet areas per inlet and the total inlet areas for the entire system seem to increase as the water depths in the basin and ocean increase. However, according to Roos et al. (2013), an increase in cross-sectional inlet area should result in the “stabilizing mechanism” gaining relative importance over the “destabilizing mechanism” that they have identified. Consequently, the inlet spacing should decrease and hence the number of inlets should increase. However, even though the inlet areas increase, the number of inlets decreases with increasing water depth. This effect cannot be explained using the results from the sensitivity analysis that is conducted in this study and hence requires further research.

The results of the sensitivity analysis suggest that the number of inlets increases for an increasing tidal amplitude. Moreover, the number of inlets and the total cross-sectional area of the inlets are directly proportional to the tidal amplitude. This is plausible, as an increase in tidal amplitude causes an increase in the flow velocities in the inlets. Consequently, according to Escoffier’s concept (see Section 1.1.1), the (total) cross-sectional areas of the inlets in equilibrium will increase. This is indeed the case for an increase in tidal amplitude, for which the total inlet area in equilibrium increases. Consequently, the number of inlets increases. This was also concluded by Roos et al. (2013), who found that inlet spacing decreases for increasing tidal amplitude. The sensitivity analysis with respect to the tidal amplitude also has confirmed that the tidal prism - inlet area relationship in the model for systems in equilibrium does not depend on the tidal amplitude, which was expected considering the expression for k in Eq. (4.8).

Decreasing the littoral drift will reduce both M and U_{eq} due to the relationship $M = \kappa U_{eq}^3$ in the model (see Section 2.1.1), so they are modified simultaneously. The sediment import M influences the timescale of the system's evolution, while its equilibrium state depends on the equilibrium flow velocity amplitude U_{eq} . As U_{eq} increases, the number of inlets decreases and the tidal subbasin areas increase, while the total inlet areas decrease. The inlet areas per inlet show no significant trend in response to a change in littoral drift. The increase in number of inlets and total inlet area can be explained by the increasing dominance of the waves with increasing U_{eq} and M , which are the parameters representing wave activity. As waves tend to close the inlets by transporting sediment into the inlets, less inlets will remain open when U_{eq} and M are increased. The tidal prisms show an upward trend for increasing U_{eq} , while the inlet areas per inlet show no significant trend. Therefore, the value of coefficient k in the tidal prism - inlet area relationship decreases for increasing U_{eq} , which is in agreement with the expression for k in Eq. (4.8).

The wave activity is parametrized in the model through sediment import M and equilibrium flow velocity U_{eq} . The tidal amplitude Z influences the flow velocity amplitude U_j and hence increasing these parameters increases the dominance of the tides. From the equation that describes the development of the inlet areas over time (Eq. (2.2)), it can be deduced that the ratio U_j/U_{eq} controls the inlet stability. The results of the sensitivity analysis indeed confirm that increasing U_j while keeping U_{eq} constant has a similar effect on the equilibrium state of the system as decreasing U_{eq} while keeping U_j constant. However, this does not hold for the effect on the tidal prism - inlet area relationship in equilibrium. Modifying Z and hence U_j does not change that relationship, while changing U_{eq} does result in a different equilibrium P - Ω relationship. This is expected, as coefficient k in the P - Ω relationship in equilibrium directly depends on the equilibrium velocity U_{eq} , while it does not depend on the tidal amplitude Z or flow velocity U_j .

6. Discussion

In Section 6.1, the results of the tidal divide identification methods will be interpreted and their reliability will be discussed. Then, the similarities and differences between the empirical O'Brien-Jarrett Law and the relationship between tidal prisms and inlet areas that we identified for the model in this study are discussed in Section 6.2. For the applicability of these P - Ω relationships, distinctions are made between single-inlet and multi-inlet tidal systems and systems that are in equilibrium and systems that are still evolving. Lastly, in Section 6.3, the relation between tidal subbasin areas that are calculated after identifying the tidal divides and inlet areas is discussed.

6.1 Interpretation of tidal divides

The results of the tidal divide identification methods developed in this study suggest that hydraulic tidal divides occur closer to smaller inlets, two tidal divides can converge into one, a tidal divide appears behind every barrier island and the hydraulic tidal divides might have a width. The tidal divides that are identified using the method based on the minimum flow velocity amplitudes also suggest that tidal divides are continuous all the way from an island to the main land, but that is an assumption that is included in that identification method.

The tidal divides form the boundaries between tidal subbasins, which are also referred to as the “areas of influence” of their corresponding inlets. A smaller inlet would have a smaller area of influence than a larger inlet, so it is plausible that tidal divides occur closer to smaller inlets and even show a slight deflection towards those smaller inlets. A consequence of this deflection is that the tidal divides can converge into one when an inlet is significantly smaller compared to its adjacent inlets. Being able to identify such tidal divides in models is important as they also occur in nature, for example the divide between the Marsdiep and Vlie basins in the Wadden Sea (Dastgheib et al., 2008; Elias et al., 2003).

The results of both identification methods suggest that tidal divides appear behind every barrier island. This is explicitly imposed in the method based on the minimum flow velocity amplitudes, as the assumption is made that a tidal divide starts behind every barrier island. It seems to be a reasonable assumption since the tidal divides mark the locations where tidal waves through adjacent open inlets “meet” each other and hence one can imagine that this would naturally happen between every adjacent pair of open inlets. Such an assumption is not implemented in the second method based on the large phase differences, but nevertheless the tidal divides still appear behind every island. However, Elias et al. (2003) observed that the Marsdiep and Vlie basins in the Wadden Sea used to form one basin with two inlets. Only after the construction of the Afsluitdijk that closed off the Zuiderzee from the Wadden Sea, a tidal divide was formed between the two basins. Such a transition can most likely not be simulated using the identification methods in this study as one tidal subbasin with two open inlets is not identified. However, note that Elias et al. (2003) observed morphological tidal divides and not hydraulic tidal divides, the locations of which do not necessarily coincide.

The surface plots showing the locations of the tidal divides suggest that the hydraulic tidal divides might have a width, as the method can only mark the location in which the tidal divide is located on a discretized “spatial grid”. The flow velocity amplitudes in the back-barrier basin have been discretized spatially and, in this study, each “grid cell” has a width of 1 km. The spatial resolution can be increased, such that the locations of the tidal divides can be identified more precisely. Hydraulic tidal divides are defined as the location where two tidal waves meet and hence their width is typically infinitesimal. However, hydraulic tidal divides can instigate

the development of a morphological tidal divide, i.e. topographic high, that can occur over a certain width. Such a morphological high also developed at the tidal divide between the Marsdiep and Vlie tidal basins (Elias et al., 2003). Morphological tidal divides cannot be identified in this model, as the bed level in the basin is assumed to be uniform.

In the tidal divide identification method based on locating minimum flow velocity amplitudes, the assumption is included that the tidal divides are lines over the entire distance from the barrier islands to the main land, while no such assumption is made for the method based on large phase differences. One of the objectives of identifying tidal divides in this model is being able to divide the back-barrier basin into tidal subbasins, such that every location in the back-barrier basin can be assigned to a tidal subbasin of which the area can be calculated. Therefore, the method that identifies “continuous” tidal divides is considered more valuable. However, there can be some discussion about the reliability of these tidal divides close to the main land, as some show zigzagging behaviour. This can be explained by the low flow velocity amplitudes in that part of the basin, such that the differences between the minima and the surrounding flow velocity amplitudes are so small that they might be negligible. These zigzagging patterns in the tidal divides probably have to be accepted in order to divide the entire back-barrier basin into tidal subbasins, but they will decrease as the spatial resolution of the basin is increased.

Being able to identify realistic tidal divides in the exploratory model will increase the understanding of how the movement and location of a tidal divide and hence the tidal basin areas depend on the characteristics of the tidal system. The locations of tidal divides are influenced by natural processes, but also by human interventions such as the aforementioned construction of the Afsluitdijk. The morphology of tidal basins responds to the existence and movement of hydraulic tidal divides and hence the equilibrium state of multi-inlet tidal systems is largely influenced by the movement of tidal divides (Wang et al., 2011).

6.2 Applicability of tidal prism - inlet area relationship

In this section, the applicability of the empirical O’Brien-Jarrett Law and the model’s tidal prism - inlet area relationship to single-inlet and multi-inlet tidal systems, as well as systems in equilibrium and evolving systems, is discussed. Herein, relevant outcomes of the sensitivity analysis are also taken into account. In this section, the exact tidal prisms will be considered. The results for the approximated tidal prisms will be discussed implicitly in Section 6.3.

6.2.1 Single inlet vs. multiple inlets

Several previous studies, e.g. Dongfeng et al. (2010) and Van der Wegen et al. (2010), confirmed the resemblance between empirical tidal prism - inlet area relationships and modelled and observed P - Ω relationships. However, these studies only considered single-inlet tidal systems. Tidal inlet systems with multiple inlets have of course also been studied in previous research, e.g. by Van de Kreeke et al. (2008) and Roos et al. (2013). In their study, Van de Kreeke et al. (2008) did relate the P - Ω relationship to double-inlet tidal systems, but they concluded that a topographic high forming a morphological tidal divide between tidal subbasins was necessary in order to obtain a stable system. Contrarily, Roos et al. (2013) did not study the tidal prism - inlet area relationships for multiple inlets, but they were able to model a stable multi-inlet tidal system without topographic highs. The model by Roos et al. (2013) is used in this study and the tidal prism - inlet area relationship in that model is studied. Thus, models that closely resemble and satisfy the empirical relationship between tidal prism and inlet area are not new, but in this study we have considered the P - Ω relationship for multi-inlet tidal systems without topographic highs.

For the model that is used in this study, the number of inlets included in the tidal system does not influence the relationship between the exact tidal prism and the inlet area. That relationship only depends directly on the tidal frequency and the flow velocity amplitude in the inlet. Therefore, it is plausible that the applicability of the empirical O'Brien-Jarrett Law is not restricted to single-inlet systems, but it also holds for multi-inlet tidal systems. The results of this study indeed show that the O'Brien-Jarrett Law or similar tidal prism - inlet area relationships are applicable to multi-inlet tidal systems, even without topographic highs. Furthermore, the similarity of the P - Ω relationship in the model compared to the empirical O'Brien-Jarrett Law confirms that the physical-mathematical formulations of the model describing the hydrodynamic and morphodynamic processes in multi-inlet tidal systems are a respectable representation of the reality.

6.2.2 Systems in equilibrium

The expression for the exact tidal prisms in the model, $P_{j,exact} = 2\Omega_j U_j / \omega$, suggests that the relationship between the tidal prisms P and the inlet areas Ω only depends on the tidal frequency ω and the flow velocity U_j in the inlet. Indeed, for a multi-inlet tidal system that is in equilibrium, a relationship of the form $\Omega = kP$ with $k = \omega / 2U_{eq}$ is satisfied by the model results. A relationship of this form was also obtained by Krishnamurthy (1977). He calculated the tidal prism by integrating a given velocity profile across the inlet's cross-section to obtain the flow discharge through the inlet and eventually the tidal prism. The same holds for the calculation of the exact tidal prism in the model. Thus, it would make sense that the model results agree with the relation found by Krishnamurthy (1977). At the same time, this means that coefficients k and α according to the model are not exactly equal to the coefficients k and α that are empirically determined by Jarrett (1976) and Dieckmann et al. (1988) for the O'Brien-Jarrett Law of the form $\Omega = kP^\alpha$. However, the empirical O'Brien-Jarrett Law and the model's P - Ω relationship are almost indistinguishable, especially in the range of values of P and Ω that are studied in this research, representing the Wadden Sea and the Georgia Bight.

The sensitivity analysis that we have performed confirms that coefficient k for systems in equilibrium is inversely proportional to the equilibrium flow velocity amplitude. Besides that, it also depends on the tidal frequency. Accordingly, D'Alpaos et al. (2009) observed that k increases with the tidal frequency and decreases with the critical velocity for sediment transport. The critical flow velocity is directly related to the equilibrium flow velocity, as the equilibrium flow velocity depends on the flow velocity for which the sediment in the inlet can be transported by the tides and waves (Escoffier, 1940). According to D'Alpaos et al. (2009), the value of coefficient k is fully independent of the tidal amplitude when the system is in equilibrium. The same is found in this study, as the inlet areas Ω and tidal prisms P respond to a change in tidal amplitude in exactly the same manner, such that k in $\Omega = kP$ does not change.

6.2.3 Prediction of system's evolution

Until now, it is assumed that the O'Brien-Jarrett Law is valid for systems that are in equilibrium, because the assumption is made that the inlet systems for which the coefficients were determined empirically were in equilibrium (e.g. Hinwood and McLean, 2018). Nevertheless, Dieckmann et al. (1988) suggested that estimates of the long-term changes in the inlets' cross-sections until the system is in equilibrium may be based on relationships between tidal prisms and inlet areas such as the O'Brien-Jarrett Law. In this study, we have found that the P - Ω relationship for an inlet that is still evolving is very similar to the relationship for a system in equilibrium. The actual resemblance between the P - Ω relationship

that holds at a certain time t and the relationship in the equilibrium situation directly depends on the ratio between $U_j(t)$, where t represents the morphological time in years, and U_{eq} . Therefore, these two relationships are only very close together when $U_j(t)$ has converged towards U_{eq} . It turns out that generally, $U_j(t)$ in an inlet that remains open in equilibrium converges towards U_{eq} relatively quickly during the inlet's evolution.

The results of this study suggest that the flow velocity amplitude $U_j(t)$ initially converges towards U_{eq} for inlets that remain open in equilibrium. However, during the first years of a system's evolution this also happens for inlets that will eventually close. Thereafter, both accreting and eroding inlets may closely follow the P - Ω relationship that is expected in equilibrium. Hence, a prediction of whether an inlet remains open or will close cannot be based on the temporal development of the P - Ω relationship. The relationship between P_j and Ω_j of an inlet at a certain time t solely depends on ω , U_{eq} and $U_j(t)$. As long as the tidal frequency ω and equilibrium velocity amplitude U_{eq} remain constant during a model simulation, only $U_j(t)$ influences the actual P - Ω relationship. Therefore, studying the development of the relationship between P_j and Ω_j during the system's evolution does not provide any extra information that can help predict whether the inlet closes or remains open than the flow velocity amplitude $U_j(t)$ already does. However, if it is known or assumed that an inlet will remain open in equilibrium, then the P - Ω relationship or O'Brien-Jarrett Law can be used for predicting the development of an inlet. For example, for a perturbation in the tidal prism, the adjusted inlet area can be determined as it will approximately satisfy the equilibrium P - Ω relationship, and vice versa.

The findings of this study with regards to the applicability of the O'Brien-Jarrett Law to a system that is not yet in equilibrium are in accordance with the conclusions of D'Alpaos et al. (2010), who studied whether one relationship of the form $\Omega = kP^\alpha$ with the same coefficients could hold during the entire evolution of a single-inlet system. They modelled the time evolution of Ω and P for an accreting tidal inlet and showed that Ω is related to P through a relationship of the form $\Omega = kP^\alpha$, but the values of k and α depend on the particular phase of the evolutionary process. Furthermore, they also state that the equilibrium state of a tidal inlet system is reached relatively early during its evolution, which is also found in this study. The conclusions of D'Alpaos et al. (2010) are based on numerical modelling, as well as observations in the Venice lagoon.

6.3 Relation between subbasin areas and inlet areas

The results of the tidal divide identification (larger areas of influence for larger inlets) and the sensitivity analysis (tidal subbasin areas and inlet areas show the same trend, except when the tidal amplitude changes) suggest that there should be a relation between the inlets' cross-sectional areas and their corresponding tidal subbasins. This is not yet proven by the tidal prism - inlet area relationship discussed in Section 6.2, as the basin area is not included in that relation.

The relation between the basin areas and inlet areas has been quantified empirically by O'Brien (1966) as $\Omega = 6.65 \cdot 10^{-5}P$ for the Pacific coast. He based his derivation on the tidal prism approximation $P_{j,approx} = H \cdot A_{b,j}$, so he used exactly the same approximation of the tidal prism as we did in this study. The approximation of the tidal prism that depends on the tidal range and the (sub)basin area is widely used in research and modelling of tidal inlet systems, e.g. in the ASMITA model used by Kragtwijk (2002). Hinwood and McLean (2018) state that most of the power laws of the form $\Omega = kP^\alpha$ that were proposed throughout the years, even

when tidal prisms were calculated using more involved models, are fitted almost as well by this linear equation determined by O'Brien (1966). From this, it could be concluded that the tidal prism is quite accurately approximated by $P_{j,approx} = H \cdot A_{b,j}$. Nevertheless, e.g. Kragtwijk (2002) states that this tidal prism approximation is only valid when the tidal wave length is significantly large compared to the tidal basin area, where they only consider single-inlet systems. We have confirmed in this study that the tidal prism approximation is indeed more accurate for larger basins, also in multi-inlet tidal systems, but the results suggest that only the basin dimension in the direction of the tidal wave influences the accuracy.

The relationship between tidal prisms and inlet areas in the model can be combined with the expression for the approximated tidal prism, which depends on the tidal subbasin areas. This results in a relationship between the tidal subbasin areas and the inlet areas, assuming that the tidal prism approximation $P_{j,approx} = H \cdot A_{b,j}$ is significantly accurate. Hence, for systems where the basin length is significantly small with respect to the tidal wave length, the subbasin area $A_{b,j}$ in equilibrium can be calculated by

$$A_{b,j} \approx \frac{2U_{eq}}{\omega H} \Omega \quad (6.1)$$

where Ω is the cross-sectional area (m²) of the inlet in equilibrium, U_{eq} is the equilibrium flow velocity amplitude (m/s), ω is the tidal frequency (rad/s) and H is the tidal range (m). The sensitivity analysis with respect to the equilibrium velocity indeed shows that the tidal subbasin areas are proportional to the equilibrium velocity and inversely proportional to the tidal amplitude. Furthermore, the boxplots of $A_{b,j}/\Omega$ in Appendix C show that Eq. (6.1) is indeed an acceptable approximation of the relation between subbasin areas and inlet areas in the model, in this case for the Wadden Sea parameter set. Meanwhile, it should be noted that we have already concluded in this study that the tidal prism approximation is not highly accurate for the parameter set representing the Wadden Sea. This leads us to expect that the relation in Eq. (6.1) will be even more accurate for systems with shorter back-barrier basins, such as the Georgia Bight.

7. Conclusion

The objective of this research was to identify tidal divides in the model of multi-inlet tidal systems by Roos et al. (2013), to compare the model results to the empirical O'Brien-Jarrett Law relating tidal prisms to inlet areas and to study the effect of changing ocean conditions.

We have identified tidal divides in the model by Roos et al. (2013) using two different methods, both based on the complex flow velocity amplitude in the back-barrier basin: (1) locating the continuous lines of minimum flow velocity amplitude in the basin and (2) locating large phase differences in the alongshore flow velocity in the basin. The first method proves to be suitable for dividing the entire back-barrier basin into several tidal subbasins corresponding to the open inlets, which is one of the objectives of identifying tidal divides. This is not the case for the tidal divides resulting from the second method, as they do not form boundaries between the subbasins over the entire distance from the barrier islands to the main land. It is concluded that the first method can be used for identifying tidal divides and hence tidal subbasins in the exploratory model. The identification method works qualitatively for reproducing a situation where two tidal divides converge into one, which also occurs in nature. On the other hand, it cannot simulate a single tidal subbasin with two tidal inlets since it is assumed that a tidal divide appears between every pair of adjacent open inlets.

The empirical O'Brien-Jarrett Law of the form $\Omega = kP^\alpha$, relating inlet areas Ω to tidal prisms P , is compared to the tidal prism - inlet area (P - Ω) relationship in the model. We have calculated the tidal prism for the model in two different ways, of which one gives the exact tidal prism based on the flow discharge through the inlet and the other is an approximation, depending on the tidal range and the subbasin areas. The accuracy of the tidal prism approximation increases with decreasing basin length in the cross-shore direction. For multi-inlet tidal systems that are in equilibrium, we have found that the relationship between the exact tidal prisms and the inlet areas in the model is linear, such that it is very similar to the empirical law and α is 1 regardless of the location characteristics. Coefficient k is inversely proportional to the flow velocity in the inlet, such that the P - Ω relationship while a system is still evolving directly depends on the flow velocity in the inlet. Using the tidal prism approximation, we have related the tidal subbasin areas to the inlet areas in equilibrium, under the condition that the tidal wave length is significantly small compared to the cross-shore basin length. It is found that the relation between subbasin areas and inlet areas depends on the equilibrium velocity, the tidal amplitude and the tidal frequency.

The sensitivity analysis that we conducted confirms that tidal amplitude and equilibrium flow velocity amplitude influence the stable equilibrium state of multi-inlet tidal systems in the model, where the tidal subbasin areas indeed increase with equilibrium velocity and decrease with tidal amplitude. An increase in water depth in the basin and ocean increases both the basin areas and the inlet areas, but it slightly decreases the number of inlets. These opposing trends cannot be explained using the results of this research, so the response of multi-inlet tidal systems to changing water depths and hence sea level rise requires further research. The P - Ω relationship in equilibrium changes for changing equilibrium flow velocity, but it is independent of the tidal amplitude and the water depth.

In conclusion, we have identified hydraulic tidal divides and thus tidal subbasins, as well as the relationship between tidal prisms and inlet areas in the exploratory model by Roos et al. (2013) for multi-inlet tidal systems in equilibrium and also evolving systems. From this, we have derived a relationship between tidal subbasin areas and inlet areas in equilibrium, which is confirmed by analysing the sensitivity of the subbasin and inlet areas to changes in the equilibrium flow velocity amplitude and tidal amplitude.

8. Recommendations

To improve the tidal divide identification method, especially for systems with more open inlets, it is recommended to use a higher grid resolution in the basin. This was not possible in the current research due to the limited timespan available and the high number of model runs that needed to be executed. However, when more time is available and a more precise outcome is desired, the grid resolution might be increased and the consequential increase in computational time should be accepted.

Tidal basins are defined as the “area of influence” of a certain open tidal inlet. An alternative identification method of tidal divides can be based on this definition, as the influence of the tidal flow through a certain inlet can be quantified for each location in the back-barrier basin. This can be done using Eq. (2.17), which gives the surface elevation due to a certain inlet at each location in the basin. Developing and studying this alternative identification method might be an interesting topic for future research.

Only hydraulic tidal divides have been identified in this study, but it would be valuable to also be able to identify morphological tidal divides. Currently, the model is unable to identify bed level variations in the basins and the bed level is assumed to be uniform. For future research, it would be interesting to add a morphodynamic model that also models the morphology in the basin. In that way, the interaction between hydraulic and morphological tidal divides can be examined.

Until now, we have only identified tidal divides in rectangular back-barrier basins. It is expected that the tidal divide identification method that is developed in this study also works for differently, e.g. conically, shaped basins, as long as the flow velocity amplitudes in the basin can be calculated. However, this has not yet been assessed in the current research.

For a high tidal amplitude and a low equilibrium velocity, resulting in an equilibrium state with a large number of inlets, the results of the sensitivity analysis seem to deviate from the trend. Therefore, it is recommended to (re)validate the model for systems with many inlets, or at least study such situations in more detail.

In this study, we have performed a sensitivity analysis using the Wadden Sea parameter set. However, it is also concluded that the tidal prism approximation is more accurate for a smaller back-barrier basin, which occurs in the parameter set representing the Georgia Bight. Therefore, it is interesting to do the sensitivity analysis and especially study the relation between basin areas and inlet areas for that parameter set.

In the sensitivity analysis that is conducted in this study, sea level rise is simulated by increasing the initial water depth in the basin and the ocean. In reality, sea level rise happens gradually and the sediment import may adapt to the rising sea level. To study this, the sea level rise should be increased gradually during a model run.

Appendices

A. Example model run

An example of a model run and its results are shown in Fig. A1 and A2.

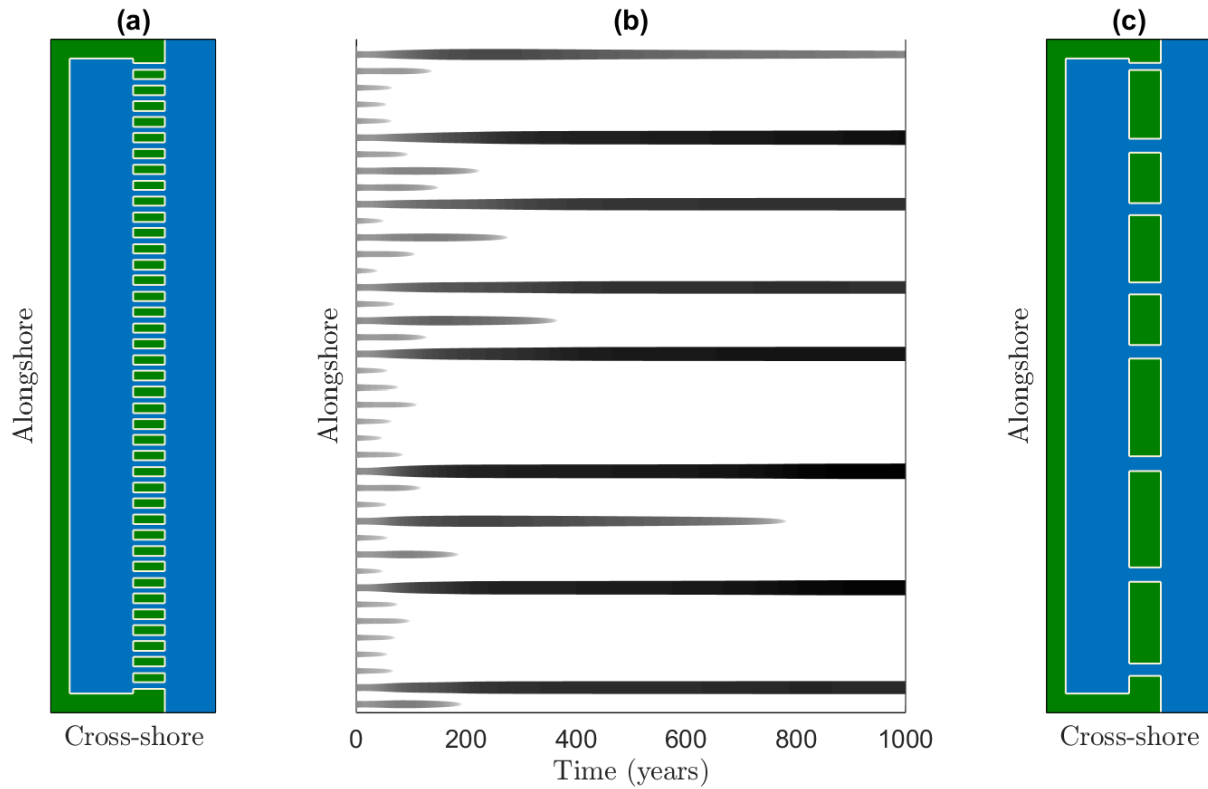


Fig. A1: Model geometry and example of a simulation, using parameter values for the Wadden Sea: (a) the initial state, shown as a plan view of the geometry with a prescribed number of 40 inlets, (b) the inlet evolution over time, showing that 32 inlets close and 8 remain open, (c) the state after 1,000 timesteps, shown as a plan view of the geometry with 8 open inlets.

Fig. A1 shows the evolution of the inlets, from the initial state, over time, to the equilibrium state. It can be seen that some inlets close and some inlets grow. While the initial state is a multi-inlet tidal system with 40 inlets, after 1,000 timesteps there are only 8 open inlets. In Fig. A2, the amplitude of the flow velocity vector $\hat{\mathbf{u}}_b = (\hat{u}_b, \hat{v}_b)$ is shown. Note that actually the magnitude of these complex amplitudes is plotted.

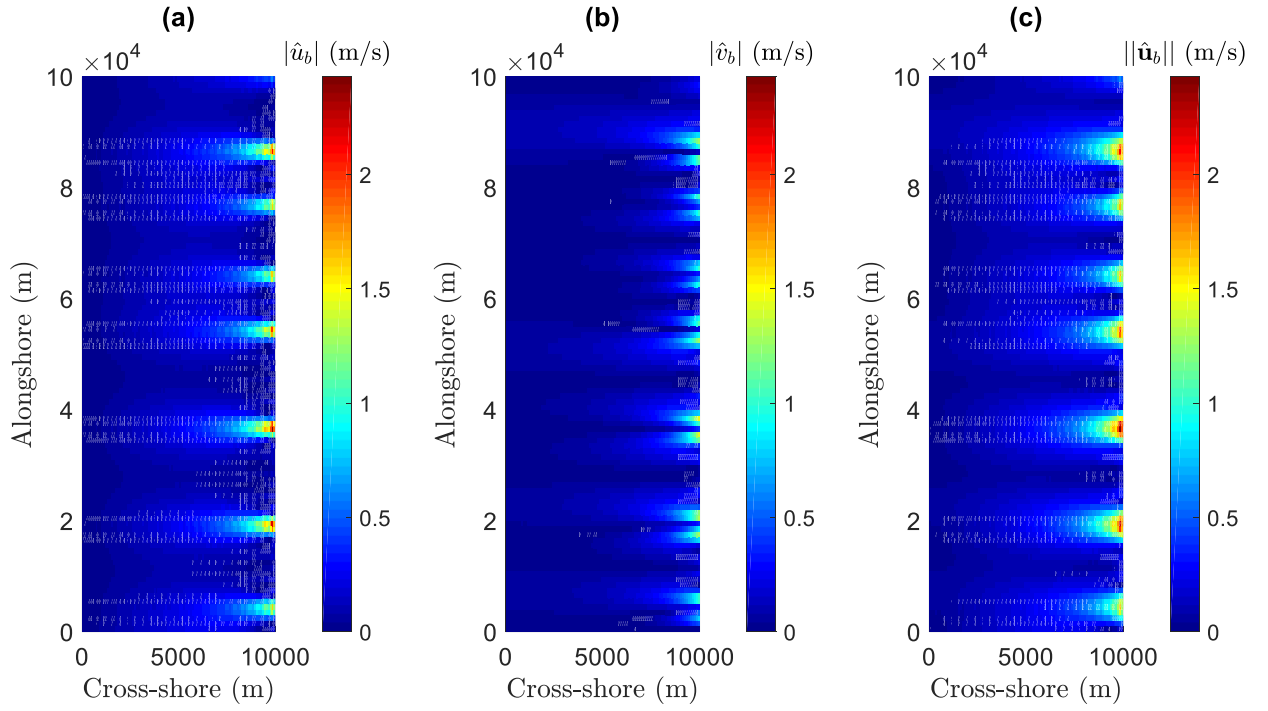


Fig. A2: Surface plot of the flow velocity amplitudes in the basin: (a) the magnitude of the complex flow velocity amplitude in the cross-shore x -direction, $|\hat{u}_b|$ (see Eq. (2.21)) (b) the magnitude of the complex flow velocity amplitude in the alongshore y -direction, $|\hat{v}_b|$ (see Eq. (2.21)) (c) The complex norm of the complex flow velocity amplitude vector, $||\hat{\mathbf{u}}_b||$ (see Eq. (3.1)).

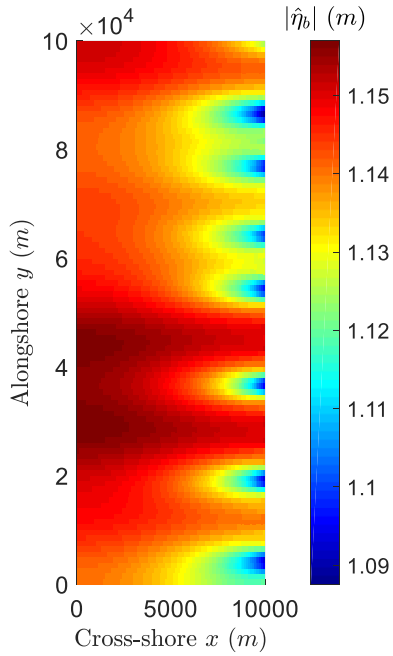


Fig. A3: Surface plot of the magnitude of the complex elevation amplitude in the basin, $|\hat{\eta}_b|$.

B. Number of model runs for sensitivity analysis

To determine how many model runs should be used in the sensitivity analysis, the model is run 10, 20, 25, 30, 40, 50, 60, 70, 80, 90 and 100 times and the boxplots of the number of inlets, tidal basin areas and cross-sectional areas of the inlets are considered. The notches in the boxplots of the basin areas and inlet areas decrease as the number of runs increases. However, also considering the computational time, it is decided to use 25 model runs per modified parameter value in the analysis.

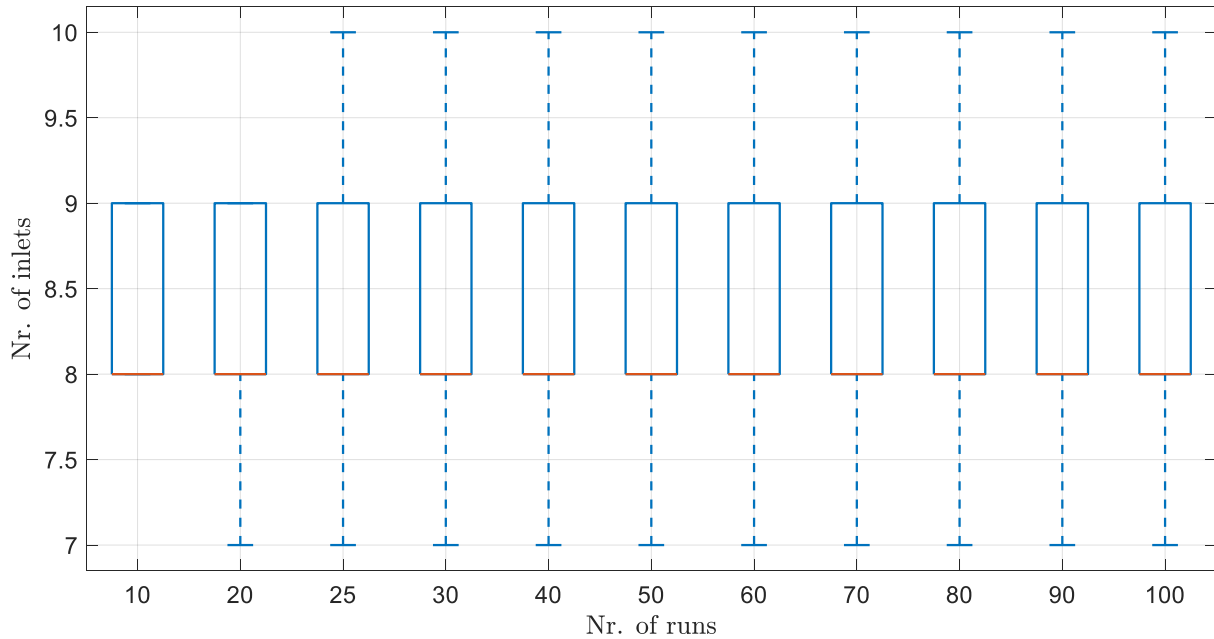


Fig. B1: Boxplots of the number of inlets resulting from 10, 20, 25, 30, 40, 50, 60, 70, 80, 90 and 100 model runs.

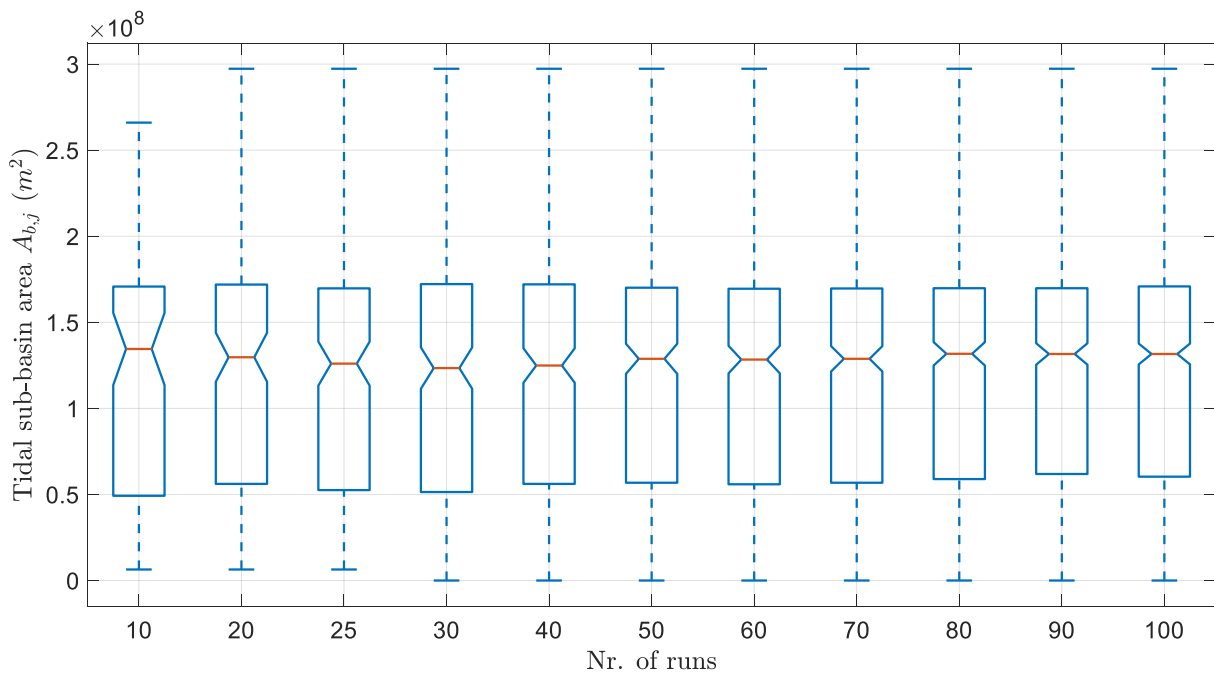


Fig. B2: Boxplots of the tidal subbasin areas resulting from 10, 20, 25, 30, 40, 50, 60, 70, 80, 90 and 100 model runs.

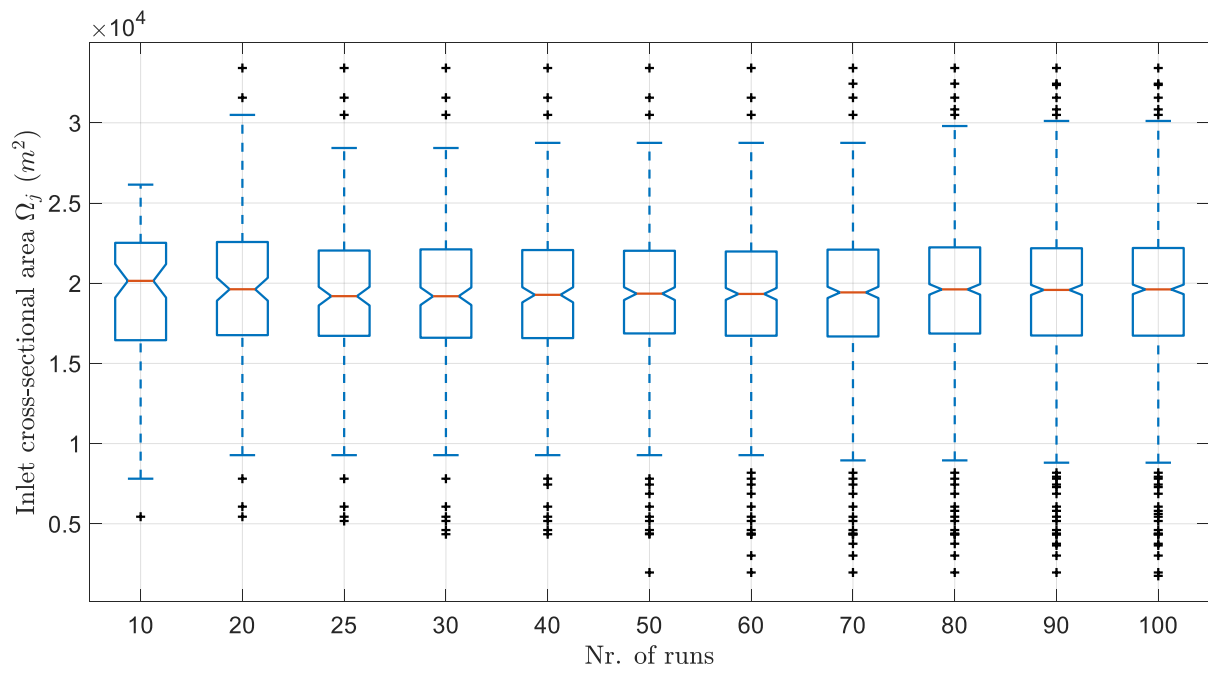


Fig. B3: Boxplots of the cross-sectional areas per inlet resulting from 10, 20, 25, 30, 40, 50, 60, 70, 80, 90 and 100 model runs.

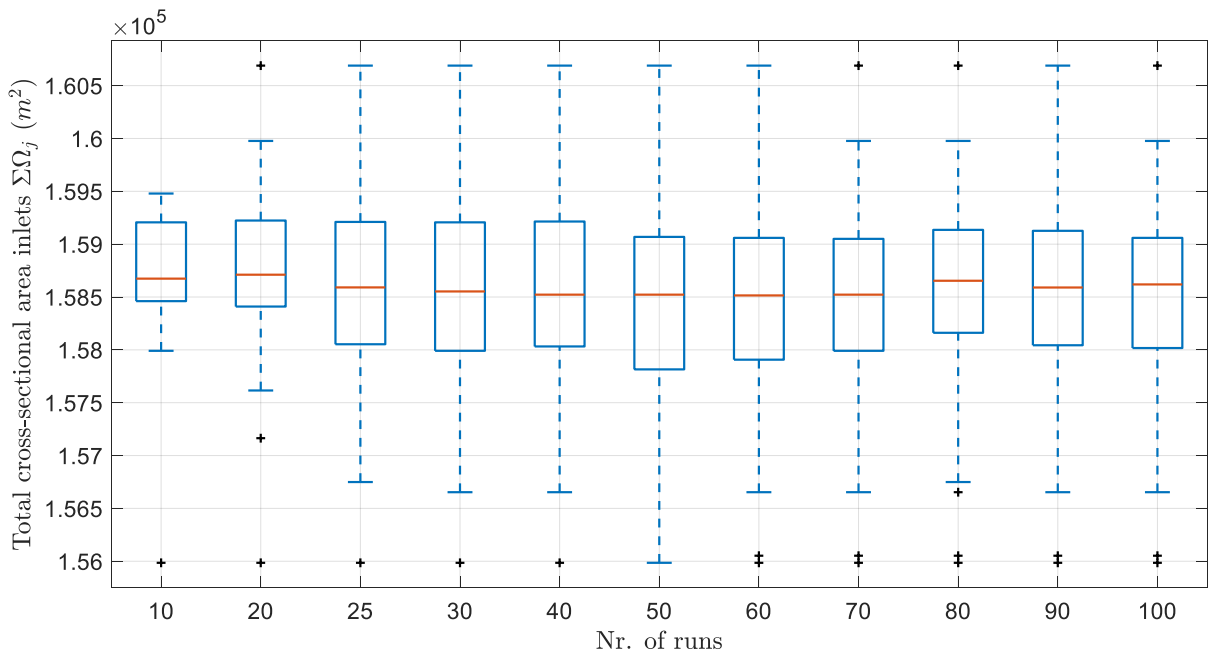


Fig. B4: Boxplots of the total cross-sectional areas per run resulting from 10, 20, 25, 30, 40, 50, 60, 70, 80, 90 and 100 model runs.

C. Basin areas and inlet areas

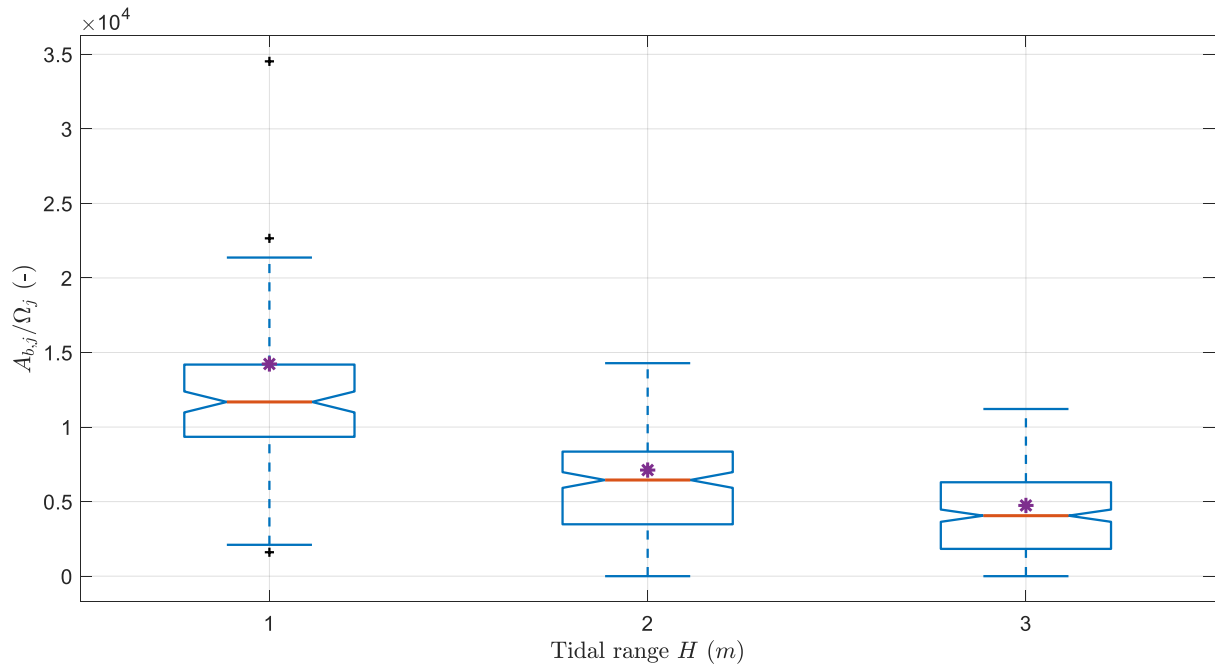


Fig. C1: The basin area $A_{b,j}$ divided by the inlet area Ω_j for varying tidal range H (where $H = 2Z$ for tidal amplitude Z), where the purple asterisk represents the expected value of $2U_{eq}/\omega H$.

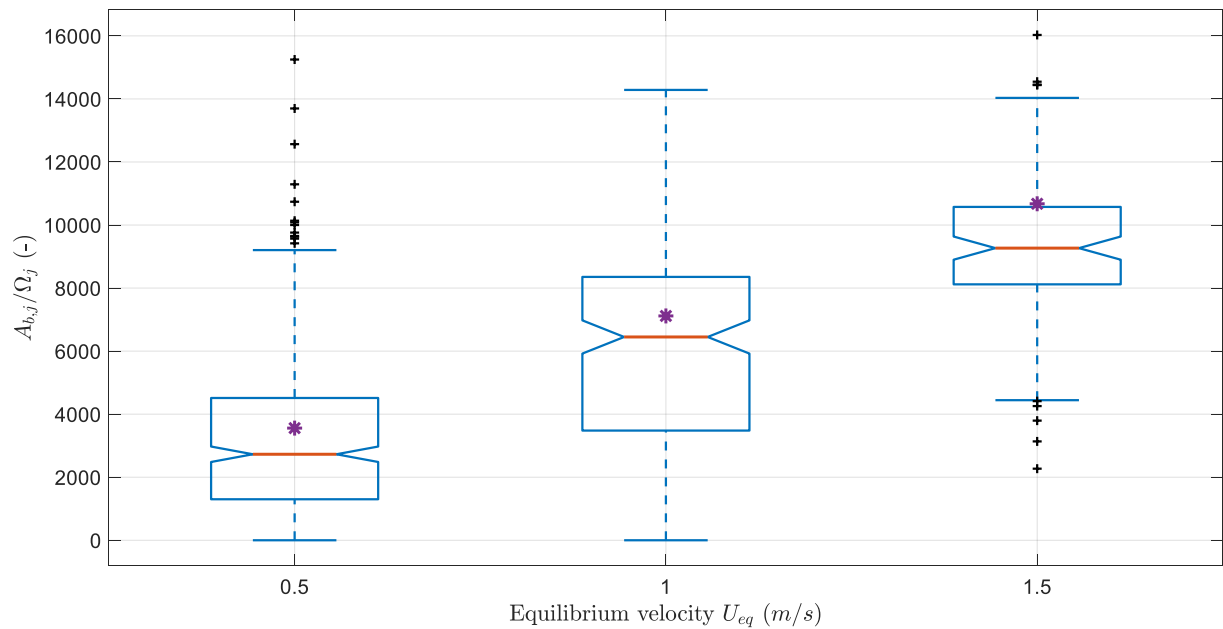


Fig. C2: The basin area $A_{b,j}$ divided by the inlet area Ω_j for varying equilibrium velocity U_{eq} (and corresponding sediment import M), where the purple asterisk represents the expected value of $2U_{eq}/\omega H$.

References

- Brouwer, R.L., Zitman, T.J., Schuttelaars, H.M., Van de Kreeke, J. (2008). *Effects of amplitude differences on equilibrium and stability of a two-inlet bay system*. River, Coastal and Estuarine Morphodynamics, RCEM 2007 at Enschede, Volume 1, Taylor & Francis Group, London, doi:10.1201/NOE0415453639-c5.
- Brouwer, R.L., Van de Kreeke, J., Schuttelaars, H.M. (2012). *Entrance/exit losses and cross-sectional stability of double inlet systems*. Estuarine, Coastal and Shelf Science, 107, 69-80, doi:10.1016/j.ecss.2012.04.033.
- Brouwer, R.L., Schuttelaars, H.M., Roos, P.C. (2013). *Modelling the influence of spatially varying hydrodynamics on the cross-sectional stability of double inlet systems*. Ocean dynamics: Theoretical, Computational and Observational Oceanography, ISSN 1616-7341, doi:10.1007/s10236-013-0657-6.
- Bruun P., Mehta A.J., Johnsson I.G. (1978). *Stability of Tidal Inlets*. Theory and Engineering. Elsevier Scientific, Amsterdam, The Netherlands p. 506
- Byrne, R.J., Gammisch, R.A., Thomas, G.R. (1981). *Tidal prism-inlet area relations for small tidal inlets*. Proceedings of the 17th international conference on coastal engineering. ASCE, New York, pp 2517–2533.
- D’Alpaos, A., Lanzoni, S., Marani, M., Rinaldo, A. (2009). *On the O’Brien-Jarrett-Marchi Law*. Rend. Fis. Acc. Lincei (2009), 20:25-236, doi:10.1007/s12210-009-0052-x.
- D’Alpaos, A., Lanzoni, S., Marani, M., Rinaldo, A. (2010). *On the tidal prism–channel area relations*. Journal of Geophysical Research, 115, F01002, doi:10.1029/2008JF001243.
- Dastgheib, A., Roelvink, J.A., Wang, Z.B. (2008). *Long-term process-based morphological modeling of the Marsdiep Tidal Basin*. Marine Geology, 256(1-4), 90-100, ISSN: 00253227, doi:10.1016/j.margeo.2008.10.003.
- De Swart, H.E. and Zimmerman, J.T.F. (2009). *Morphodynamics of tidal inlet systems*. Annu. Rev. Fluid Mech., 41(7), 203–229, doi:10.1146/annurev.fluid.010908.165159.
- Dieckmann, R., Osterthun, M., Partenscky, H.W. (1988). *A comparison between German and North American tidal inlets*. Coastal Engineering Proceedings [S.I.], 21, p.199, ISSN: 2156-1028, doi: 10.9753/icce.v21.199.
- Dongfeng, X., Shu, G., Cunhong, P. (2010). *Process-based modeling of morphodynamics of a tidal inlet system*. Acta Oceanol. Sin., 29 (6), p. 51-61. doi: 10.1007/s13131-010-0076-1
- Elias, E.P.L., Stive, M.J.F., Bonekamp, J.G., Cleveringa, J. (2003). *Tidal inlet dynamics in response to human intervention*. Coastal Engineering Journal, 45(4), p 629-658. doi: 10.1142/S0578563403000932
- Elias, E.P.L., Van der Spek, A.J.F., Wang, Z.B., De Ronde, J. (2014). *Morphodynamic development and sediment budget of the Dutch Wadden Sea over the last century*. Netherlands Journal of Geosciences Foundation – Geologie en Mijnbouw, 91, 3, 2012, ISSN:00167746.
- Escoffier, F.F. (1940). *The stability of tidal inlets*. Shore Beach, 8(4), 114–115.
- Hayes, M.O. (1979). *Barrier island morphology as a function of tidal and wave regime*. In: Leatherman, S. (ed.), Barrier Islands, from the Gulf of St. Lawrence to the Gulf of Mexico. New York: Academic, pp. 1–27.

- Hinwood, J.B., McLean, E.J. (2018). *Tidal inlets and estuaries: Comparison of Bruun, Escoffier, O'Brien and attractors*. Coastal Engineering, 133, p.92-105. doi: 10.1016/j.coastaleng.2017.12.008.
- Hughes, S.A. (2002). *Equilibrium cross-sectional area at tidal inlets*. Journal of Coastal Research, 18(1), p. 160–174.
- Jarrett, J.T. (1976). *Tidal prism–inlet area relationships*. Gen. Invest. Tidal Inlets, Tech. Rep. 3, 59.
- Kragtwijk, N.G. (2002). *Aggregated Scale Modelling of Tidal Inlets of the Wadden Sea*. Report Z2822/DC03.01.03b. Delft, The Netherlands: WL I Delft Hydraulics/Delft Cluster.
- Kragtwijk, N.G., Zitman, T.J., Stive, M.J.F., Wang, Z.B. (2004). Morphological response of tidal basins to human interventions. Coastal Engineering, 51, p.207-221. doi:10.1016/j.coastaleng.2003.12.008.
- Krishnamurthy, M. (1977). *Tidal prism of equilibrium inlets*. ASCE J Waterway Port Coast Ocean Div 103 (WW4), p. 423–432.
- Levermann, A., Clark, P.U., Marzeion, B., Milne, G.A., Pollard, D., Radic, V., Robinson, A. (2013). *The multimillennial sea-level commitment of global warming*. Proceedings of the National Academy of Sciences (PNAS), Environmental Sciences. doi:10.1073/pnas.1219414110.
- Mayor-Mora, R.E. (1973). *Hydraulics of tidal inlets on sandy coast*. Hydraulic Engineering Laboratory, Report HLL 24–16. University of California, Berkeley.
- Murray, A.B. (2003). *Contrasting the Goals, Strategies, and Predictions Associated With Simplified Numerical Models and Detailed Simulations*. In Prediction in Geomorphology (eds P. R. Wilcock and R. M. Iverson), doi:10.1029/135GM11.
- O'Brien, M.P. (1931). *Estuary and tidal prisms related to entrance areas*. Civil Eng., 1(8), 738–739.
- O'Brien, M.P. (1966). *Equilibrium flow areas of tidal inlets on sandy coasts*. Proc. 10th Conf. Coastal Eng. Amer. Soc. Civil. Eng., Tokyo, p. 676-686.
- O'Brien, M.P. (1969). *Equilibrium flow areas of inlets in sandy coasts*. ASCE J Waterways Harbors Div, 95, p. 43–52.
- Reise, K., Baptist, M., Burbridge, P., Dankers, N., Fischer, L., Flemming, B., Oost, A.P., Smit, C. (2010). *The Wadden Sea – A Universally Outstanding Tidal Wetland*. Wadden Sea Ecosystem No. 29. Common Wadden Sea Secretariat, Wilhelmshaven, Germany, page 7 -24. ISSN 0946 – 896X.
- Roos, P.C., Schuttelaars, H.M., Brouwer, R.L. (2013). *Observations of barrier island length explained using an exploratory morphodynamic model*. Geophysical Research Letters, 40 (16), 1-6, doi:0.1002/grl.50843.
- Salles, P., Voulgaris, G., Aubrey, D.G. (2005). *Contribution of nonlinear mechanisms in the persistence of multiple inlet systems*. Estuarine Coastal and Shelf Science, 65 (3), 475–491, doi:10.1016/j.ecss.2005.06.018.
- Seabergh, W.C., King, D.B., Stephens, B.E. (2001). *Tidal inlet equilibrium area experiments, inlet laboratory investigations*. Engineer Research and Development Center, Vicksburg, MS Coastal and Hydraulics Laboratory, Vicksburg.
- Stive, M.J.F., Wang, Z.B. (2003). *Morphodynamic Modeling of Tidal Basins and Coastal Inlets*. Advances in Coastal Modeling, Elsevier Science B.V., edited by V.C. Lakhan, p. 367-392.
- Van Goor, M.A., Zitman, T.J., Wang, Z.B., Stive, M.J.F. (2003). *Impact of sea-level rise on the morphological equilibrium state of tidal inlets*. Marine Geology, 202, 211-227, doi:10.1016/S00253227(03)00262-7.

- Van de Kreeke, J. (1990). *Can multiple inlets be stable?* Estuarine Coastal and Shelf Science, 30 (3), 261-273, doi:10.1016/0272-7714(90)90051-R.
- Van de Kreeke, J., Brouwer, R.L., Zitman, T.J., Schuttelaars, H.M. (2008). *The effect of a topographic high on the morphological stability of a two-inlet bay system.* Coastal Engineering, 55 (4), 319–332, doi:10.1016/j.coastaleng.2007.11.010.
- Van der Spek, A.J.F. (2018). *The development of the tidal basins in the Dutch Wadden Sea until 2100: the impact of accelerated sea-level rise and subsidence on their sediment budget – a synthesis.* Netherlands Journal of Geosciences - Geologie en Mijnbouw, 97 (SI 3), p. 71–78, doi:10.1017/njg.2018.10.
- Wang, P. and Roberts Briggs, T.M. (2015). *Storm-Induced Morphology Changes along Barrier Islands and Poststorm Recovery.* In J. F. Shroder, J. T. Ellis, & D. J. Sherman (Eds.), Coastal and Marine Hazards, Risks, and Disasters, pp. 271–306
- Wang, Z.B., Vroom, J., Van Prooijen, B.C., Labeur, R.J., Stive, M.J.F., Jansen, M.H.P. (2011). *Development of tidal watersheds in the Wadden Sea.* RCEM 2011: Proceedings of the 7th IAHR Symposium of River, Coastal and Estuarine Morphodynamics, Beijing, China, 6-8 September 2011, Tsingua University Press
- Wang, Z.B., Hoekstra, P., Burchard, H., Ridderinkhof, H., De Swart, H.E., Stive, M.J.F. (2012). *Morphodynamics of the Wadden Sea and its barrier island system.* Ocean & Coastal Management, 68 (SI), 39-57, doi:10.1016/j.ocecoaman.2011.12.022.
- Wang, Z.B., Elias, E.P.L., Van der Spek, A.J.F., Lodder, Q.J. (2018). *Sediment budget and morphological development of the Dutch Wadden Sea: impact of accelerated sea-level rise and subsidence until 2100.* Netherlands Journal of Geosciences – Geologie en Mijnbouw, 97(3), p.183-214, doi: 10.1017/njg.2018.8